All-optical Soliton Control
in Photonic Lattices

Zhiyong Xu

Supervisor:

Professor Lluis Torner
Director
The Institute of Photonic Sciences

Control Óptico de Solitones Ópticos en Mallas Fotónicas

Memoria de la tesis presentada
por Zhiyong Xu para optar
al grado de Doctor

Director de la tesis: Dr. Lluis Torner
Catedrático de Universidad i Director del ICFO

This dissertation is to my mother, father, two sisters and brother with deep respect and love.

Everyday is a new day.
It is better to be lucky.
But I would rather be exact.
Then when luck comes you are ready.
– from The Old Man and the Sea by Ernest Hemingway

Abstract

Optical solitons are light packets (beams and/or pulses) that do not broaden because of the balance between diffraction/dispersion and nonlinearity. They propagate and interact with one another while displaying properties that are normally associated with real particles. The properties of optical solitons in optical fibers and crystals have been investigated comprehensively during the last two decades. However, solitons in optical lattices, which might be used for all-optical signal processing and routing, have recently emerged a new area of research. The main objective of this thesis is the investigation of new techniques for soliton control in nonlinear media with/without an imprinted optical lattice.

Chapter 2 focuses on properties of optical solitons in quadratic nonlinear media. The first section presents in detail the existence and stability of three representative families of two-dimensional spatiotemporal solitons in quadratic nonlinear waveguide arrays. It is assumed, in addition to the temporal dispersion of the pulse, the combination of discrete diffraction that arises because of the weak coupling between neighboring waveguides. The other section reports on the existence and stability of multicolor lattice vortex solitons, which comprise four main humps arranged in a square configuration. It is also investigated the possibility of their dynamical generation from Gaussian-type input beams with nested vortices.

Solitons in cubic nonlinear media are the topic in Chapter 3. The chapter puts forward the concept of reconfigurable structures optically induced by mutually incoherent nondiffracting Bessel beams in Kerr-type nonlinear media. Two-core couplers are introduced and it is shown how to tune the switching properties of such structures by varying the intensity of the Bessel beams. The chapter also discusses various switching scenarios for solitons launched into multi-core directional couplers optically-induced by suitable arrays of Bessel beams. Furthermore, propagation of solitons is investigated

in reconfigurable two-dimensional networks induced optically by arrays of nondiffracting Bessel beams. It is shown that broad soliton beams can move across networks with different topologies almost without radiation losses. Finally, properties of X-junctions are studied, which are created with two intersecting Bessel beams.

Chapter 4 treats the impact of nonlocality in the physical features exhibited by solitons supported by Kerr-type nonliner media with an imprinted optical lattice. The chapter investigates properties of different families of lattice solitons in nonlocal nonlinear media. It is shown that the nonlocality of the nonlinear response can profoundly affect the soliton mobility. The properties of gap solitons are also discussed for photorefractive crystals with an asymmetric nonlocal diffusion response and in the presence of an imprinted optical lattice.

Chapter 5 is devoted to the impact of nonlocality on the stability of soliton complexes in uniform nonlocal Kerr-type nonlinear media. First, it is shown that the different nonlocal response of materials has different influence on the stability of soliton complexes in scalar case. Second, experimental work is reported on scalar multi-pole solitons in 2D highly nonlocal nonlinear media, including dipole, tripole, and necklace-type solitons, organized as arrays of out-of-phase bright spots. Finally, the chapter addresses the stabilization of vector effects on soliton complexes in nonlocal nonlinear media.

Finally, Chapter 6 summarizes the main results obtained in the thesis and discusses some open prospects.

Thesis Publications

Most results obtained in the thesis have been presented at international conferences and have been published in international journals. The salient publications include:

- **Zhiyong Xu**, Yaroslav V. Kartashov, and Lluis Torner, *Soliton mobility in nonlocal optical lattices*, Physical Review Letters, **95**, 113901 (2005).

- **Zhiyong Xu**, Yaroslav V. Kartashov, and Lluis Torner, *Gap solitons supported by optical lattices in photorefractive crystals with asymmetric nonlocality*, Optics Letters, **31**, 2027 (2006).

- **Zhiyong Xu**, Yaroslav V. Kartashov, and Lluis Torner, *Upper threshold for stability of multipole-mode solitons in nonlocal nonlinear media*, Optics Letters, **30**, 3171 (2005).

- **Zhiyong Xu**, Yaroslav V. Kartashov, Lluis Torner, and Victor. A. Vysloukh, *Reconfigurable directional couplers and junctions optically induced by nondiffracting Bessel beams*, Optics Letters, **30**, 1180 (2005).

- **Zhiyong Xu**, Yaroslav V. Kartashov, and Lluis Torner, *Reconfigurable soliton networks optically-induced by arrays of nondiffracting Bessel beams*, Optics Express, **13**, 1774 (2005).

- **Zhiyong Xu**, Yaroslav V. Kartashov, and Lluis Torner, *Stabilization of vector soliton complexes in nonlocal nonlinear media*, Physical Review E, **73**, 055601(R) (2006).

- **Zhiyong Xu**, Yaroslav V. Kartashov, Lucian-Cornel Crasovan, Dumitru. Mihalache, and Lluis Torner, *Multicolor vortex solitons in two-dimensional photonic lattices*, Physical Review E, **71**, 016616 (2005).

- **Zhiyong Xu**, Yaroslav V. Kartashov, Lucian-Cornel Crasovan, Dumitru. Mihalache, and Lluis Torner, *Spatiotemporal discrete multicolor solitons*, Physical Review E, **70**, 066618 (2004).

- Carmel Rotschild, Mordechai Segev, **Zhiyong Xu**, Yaroslav V. Kartashov, Lluis Torner, and Oren Cohen *Two-dimensional multipole solitons in nonlocal nonlinear media*, Optics Letters, **31**, 3312 (2006).

Acknowledgements

First of all, I would like to express my gratitude to my PhD advisor, Prof. Lluis Torner, who provided me the invaluable opportunity to work in one of the most modern and excellent scientific centers. You will always be a role model to me, a great advisor, researcher, leader and human being. Thank you for inspiring me, guiding me and caring for me throughout all these years.

I have been privileged to work with the most intuitive and smart advisor, Dr. Yaroslav.V. Kartashov, who deserves specific thanks. His clarity, persistence and ability to write one or two new publications every month, has taught me a lot. I have been stimulated and excited by his constant flow of good ideas. He has also known when and how to give me a little push in the forward direction when I needed it.

I would like to thank Dr. Lucian.-Cornel. Crasovan for the help in many aspects of academic life and Prof. Dumitru Mihalache for the guidance during the initial stage of my research, and having good conversation on life.

I would also like to thank Prof. Juan Perez Torres, Dr. David Artigas, and Dra. Silvia Carrasco for professional help and advices.

With most respect I thank Prof. Mordechai Segev for inviting me to work in his group in Israel Institute of Technology (Technion), Israel for about one month. Special thanks to Dr. Carmel Rotschild who conducted our experiments.

I would like to specially thank Prof. Marin Soljacic for allowing me to work in RLE at the Massachussetts Institute of Technology (MIT), US for about 7 months. I also would like to thank Dr. Bjorn Maes for discussing and guiding the work related to photonic crystals.

My very sincere and special thanks to Sergi Vicente for his warm invitation to spend Christmas and New Year holidays with his family in Ex-

tremadura. I also would like to thank Juan and Paca every year to host me to take fresh air and relax in Planoles. Because of them, I had never felt home-sick in Spain.

I am grateful to all the secretaries at ICFO (specially Esther Pujol, Laia Miralles, Manuela Furkert, and Eulalia Ossul) who help me with various official paper works, which made my study go smoothly.

I would like to thank all colleagues and friends at ICFO for creating an exciting and fun environment to study. I am specially grateful to all the present and former fellow graduate students.

I am grateful to Generalitat de Catalunya for supporting me with AGAUR fellowship. I appreciate the Chinese Government to give me the Chinese Government Award for Outstanding Self-financed Students Abroad.

I am fortunate to have Ma Hui, Liang Quanwei, Shi Xiaojuan and Zhao Bingfeng as the company, with whom I share much of my spare time.

Most importantly and specially, my career would not have been possible without the love, understanding and supporting from my parents (Xu Hen and Dou Yunhua), two sisters (Xu Shuqing and Xu Shufang), and my elder brother (Xu Zhiqing). I hope I make you proud.

Contents

Chapter 1

Introduction

1.1 Historical background

Nonlinearity permeates our physical world. The evidence for nonlinear behaviors is present in so many aspects of physics, chemistry, biology, economics, etc., that it is not possible to mention them all in here. Among the most striking and aesthetically appealing manifestations of nonlinearity is the propagation of solitons or, more generally, solitary waves. Strictly speaking, solitons differ from solitary waves because of the remarkable property of integrability of the governing models and its consequence. However, such a property is scarcely relevant to the physics discussed in the thesis. Therefore through the whole thesis, the term "soliton", in its broader sense, is used to mean a wavepacket held together by the interplay of mutually counterbalancing linear and nonlinear effects.

The history of solitons, dates back to 1834, the year in which Mr. John Scott Russell [left panel in Fig.1.1] observed that a heap of water in a canal propagated undistorted over several kilometers [a soliton reproduced experiment shown in right panel of Fig.1.1]. His report, published in 1844 and reproduced extensively in soliton literature, includes the following text [1]:

I was observing the motion of a boat which was rapidly drawn along a narrow channel by a pair of horses, when the boat suddenly stopped-not so the mass of water in the channel which it had put in motion; it accumulated round the prow of the vessel in a state of violent agitation, then suddenly leaving it behind, rolled forward with great velocity, assuming the form of a large solitary elevation, a rounded, smooth and well-defined heap of water, which continued its course along the channel apparently without change of

form or diminution of speed. I followed it on horse-back, and overlook it still rolling on at a state of some eight or nine miles an hour, preserving its original figure some thirty feet long and a foot to a foot and a half in height. Its height gradually diminished, and after a chase of one or two miles. I lost it in the windings of the channel. Such, in the month of August 1834, was my first chance interview with that singular and beautiful phenomenon which I have called the Wave of Translation.
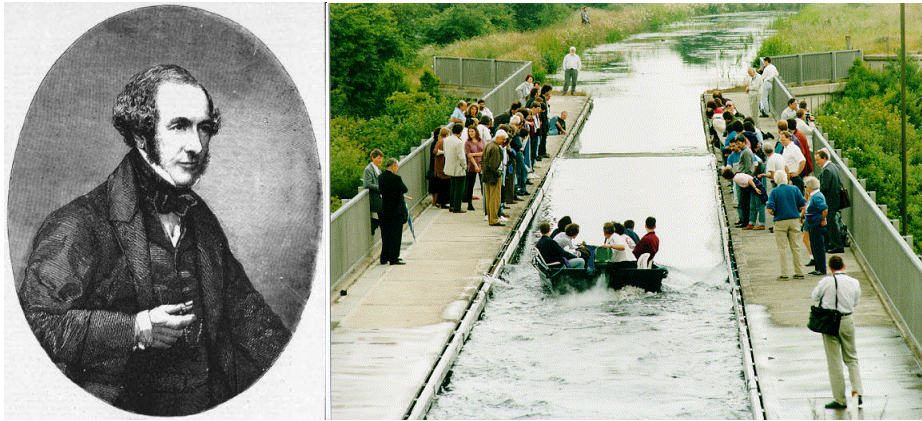

Figure 1.1: Left panel: John Scott Russell (1808-1882); right panel: Soliton recreated on the John Scott Russell aqueduct on the Union Canal near Heriot-Watt University, 12 July, 1995.

It took more than fifty years for two Dutchmen, Korteweg and de Vries (Fig. 1.2), to realize that for this phenomenon to occur the "solitary wave" must have an unusually large amplitude. This means that the medium in which the wave propagates (water, in this case) must behave in a fundamentally different manner of waves of different amplitudes, that is, its behavior is *nonlinear*. During the following seventy years similar phenomena have been observed in many other systems in which waves propagate, such as charge density waves in plasma and phonons in solids, but they were considered little more than a curiosity. Until 1965, however, Zabusky and Kruskal [2] realized that localized wave-packets (self-trapped pulses), under certain assumptions about the form of the nonlinearity, maintain their identities even when they undergo collisions with each other, and that each one of them conserves its power and initial velocity. They concluded that these pulses behave and interact with each other like particles do, and named them "solitons". Soon thereafter an immense amount of theoretical and experimental

work followed and the general features of solitons were observed in many different branches of science including hydrodynamics, nonlinear optics, plasma physics, biology, Bose-Einstein-Condensates, etc [3, 4, 5, 6, 7, 8, 9, 10].

Figure 1.2: Left panel: Diederik Johannes Korteweg (1848-1941); right panel: Gustav de Vries (1866-1934).

In the context of nonlinear optics, solitons are classified as being either *temporal* or *spatial* or both *temporal* and *spatial* depending on whether the confinement of light occurs in time or/and space during the wave propagation. Temporal solitons represent optical pulses that maintain their shape, whereas spatial solitons represent self-guided beams that remain confined in the transverse directions orthogonal to the direction of propagation. In other words, temporal solitons do not disperse, and spatial solitons do not diffract. In the simplest cases, both types of solitons evolve from a nonlinear change in the refractive index of an optical materials induced by the light intensity-a phenomenon known as the optical Kerr effect in the field of nonlinear optics [11, 12, 13]. The intensity dependence of the refractive index leads to spatial self-focusing (or self-defocusing) and temporal self-phase modulation (SPM), the two major nonlinear effects that are responsible for the formation of most optical solitons. Much more complicated nonlinear mechanisms may lead to the formation of solitons, as described below, but the physical insight is most easily grasped for the Kerr case. A spatial soliton is formed when the self-focusing of an optical beam balances its natural diffraction-induced spreading. In contrast, it is SPM that counteracts the natural dispersion-induced broadening of an optical pulse and leads to the formation of a temporal soliton [14]. Temporal solitons were first predicted

by Hasegawa and Tappert [15] in 1973 and first observed experimentally by Mollenauer *et al.* [16] in 1980. Temporal optical solitons have generated great interest during the last few decades and are being used for actual long distance optical communication systems [14, 17, 18]. If the self-tapping occurs both in a spatial and the temporal domains, such kind of beam is called spatiotemporal solitons or light bullets (for a comprehensive review see ref. [19]).
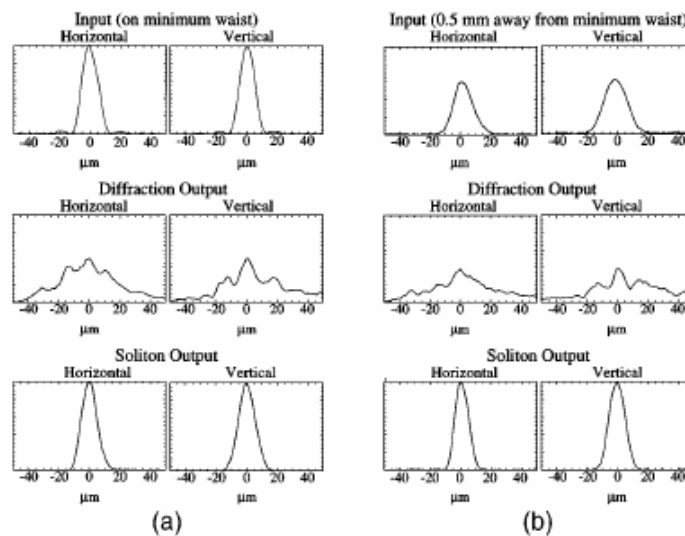

Figure 1.3: Horizontal and vertical profiles of the input (upper traces), diffracted output (middle traces), and soliton output (lower traces) beams when the input face of the crystal is (a) at the minimum waist of the input beam and (b) 500 μm away from the minimum waist (After ref. [22]).

1.2   Optical spatial solitons

The background of spatial soliton arose already in 1964 in the discovery of the nonlinear phenomenon of self-trapping of continuous-wave (CW) optical beams in a bulk nonlinear medium [20]. Self-trapping was not linked to the concept of spatial solitons immediately because of its unstable nature. During the 1980s, stable spatial solitons were observed using nonlinear media in which diffraction spreading was limited to only one transverse dimension [21]. Later on, spatial solitons in two-transverse dimensions have been observed, for example, as shown in Fig. 1.3, steady-state photorefractive screening solitons have been demonstrated [22].

Over the past several decades, the existence and unique properties of spatial optical solitons in homogeneous cubic, cubic-like, photorefractive and quadratic nonlinear media, among others and discrete systems have been studied extensively both theoretically and experimentally (for detailed reviews, see refs[23, 24, 25, 26, 27]). This section describes the basic physics and concepts required for studying spatial solitons.

1.2.1   Basic concepts

To understand why spatial solitons can form in a self-focusing nonlinear medium, consider first how light is confined by optical waveguides. Optical beams have an innate tendency to spread (diffract) as they propagate in homogeneous media. However, diffraction can be compensated by using refraction if the material refractive index is increased in the transverse region occupied by the beam. Such a structure becomes an optical waveguide and confines light to the high-index region by providing a balance between diffraction and refraction. The propagation of light in an optical waveguide is described by a linear but inhomogeneous wave equation whose solution provides a set of guided modes that are spatially localized eigenmodes of the optical field in the waveguide that preserve their shape and satisfy all boundary conditions.

As early as 1964 [20], it was discovered that the same effect-suppression of diffraction through a local change of the refractive index-can be produced solely by the nonlinear effects if they lead to a change in the refractive index of the medium in such a way that it is larger in the region where the beam intensity is large. In essence, an optical beam can create its own waveguide and be trapped by this self-induced waveguide. Thus, the basic scheme as follows: when one launches a beam onto a nonlinear medium, at low power the input beam diffracts but forms a spatial soliton when its intensity is large enough to create a self-induced waveguide by changing the refractive index. This change is largest at the beam center and gradually reduces to zero near the beam edges, resulting in a graded-index waveguide. The spatial soliton can be thought of as the fundamental mode of this waveguide. Such a nonlinear waveguide can even guide a weak probe beam of a different frequency or polarization [28].

One can also understand the formation of spatial solitons through a lens analogy. Diffraction creates a curved wavefront similar to that produced by a concave lens and spreads the beam to a wider region. The index gradient created by the self-focusing effect, in contrast, acts like a convex lens that tries to focus the beam towards the beam center. In essence, a Kerr medium acts as a convex lens in such a way that the beam can become self-trapped and propagate without any change in its shape if the two lensing effects cancel each other [20]. Of course, the intensity profile of the beam should have a specific shape for a perfect cancelation of the two effects. These specific beam profiles associated with spatial solitons are the nonlinear analog of the modes of the linear waveguide formed by the self-induced index gradient. Similar, albeit more elaborate intuitive pictures, may be drawn for other types of nonlinearities which are not so simple as Kerr media.

1.2.2   Nonlinear response

Kerr and Kerr-like solitons rely primarily on a physical effect which produces an intensity-dependent change in refractive index. The origin can be electronic or due to carrier generation, thermal, etc. In general, Kerr solitons form in materials which have a local response. However, recently spatial solitons have been reported in nonlinear materials whose response is nonlocal due to thermal or molecular reorientation effects. Photorefractive solitons utilize materials where a light-induced change of refractive index also occurs. However, in this case it is a DC electric-field distribution in a crystal that is affected by the optical field, and this in turn changes the refractive index via the electro-optic effect. Quadratic solitons depend on second-order nonlinearities. In this case the response involves energy exchange between different frequency components of the optical field. This section offers an opportunity to review the rich physics of spatial solitons due to the different nonlinearities.

Third-order Kerr nonlinearities

The simplest type of nonlinearity for solitons to occur is related to the linear dependence of the refractive index of materials on the light beam intensity, namely $n = n_0 + \Delta n$ ($\Delta n = n_2|E|^2$ is much smaller than n_0), where n_0 is the background refractive index, $E(r,t)$ is the electric field amplitude, and $n_2 = 12\pi^2\chi^{(3)}/n_0^2 c$ is an optical constant whose sign depends on the

actual anharmonicity, $\chi^{(3)}$ is the third-order susceptibility tensor. The nonlinear effect involving $n_2|E|^2$ is called optical Kerr effect, which produces the self-focusing effect needed for spatial solitons.

In nonlinear Kerr media self-focusing was suggested in the 1960s [20]. Soon after, it became clear that in bulk Kerr media the beam undergoes catastrophic self-focusing and eventually breaks up [29]. Indeed, many early experiments in nonlinear optics showed this catastrophic self-focusing, frequently leading to damage [30]. It was not until the mid 1980s that Barthelemey *et al.* were able to observe spatial Kerr solitons in liquid CS_2 [21]. Several years later, Aitchison *et al* observed Kerr solitons in a single-mode glass waveguide [31]. All these experiments were performed in planar waveguides, which are inherently one-dimensional systems, i.e. one longitudinal dimension along which the beam propagates and one transverse dimension in which the beam diffracts or self-traps.

Saturable nonlinearities

Kerr nonlinearity is one of the many different types of nonlinearities known today. As the intensity of the beam increases, the change of refractive index tends to saturate, so that, $\Delta n = \Delta n_s/[1+I/I_s] = \Delta n_s + n_2 I - n_4 I^2 + ...$ ($I = |E|^2$ is the intensity of beam), which is applicable, e.g. in a homogeneous broadened 2-level system. As early as 1969, Dawes and Marburger [32] found numerically that saturable nonlinearities are able to arrest the catastrophic collapse and lead to stable self-trapping of two-dimensional beams. Other authors have reached similar conclusions in several other forms of saturable nonlinearities (related to solitons in plasmas) [33, 34, 35]. In 1974 Bjorkholm and Ashin [36] of Bell labs observed the saturable effects in propagating beams in bulk media (saturable), in the close vicinity of an electronic resonant transition of atomic (sodium) vapor. To date, solitons in saturable nonlinear media have been investigated extensively.

The nonlinearities discussed above feature *local* response, namely, the change of refractive index in the particular point is determined by the intensity of beam in that point. However, in some cases, the response of nonlinear media also depends on the intensity of beam in its vicinity, which is so called *nonlocality*. In nonlinear optics, it occurs in thermal nonlinear media, liquid crystals and photorefractive media.

Thermal nonlinearities

Thermal processes can lead to large nonlinear optical effects. The origin of the thermal nonlinearity is that some fraction of the incident laser power is absorbed in passing through an optical material. The temperature of the illuminated portion of the material consequently increases, which leads to a change in the refractive index of the material. For gases, the refractive index typically decreases with increasing temperature (at constant pressure), but for condensed matter the refractive index can either increase or decrease with changes in temperature, depending upon details of the internal structure of the materials.

Thermal effects can be described mathematically by assuming that the refractive index n varies with temperature according to $n = n_0 + (\mathrm{d}n/\mathrm{d}T)T_1$ under steady-state conditions, where the quantity $(\mathrm{d}n/\mathrm{d}T)$ describes the temperature dependence of the refractive index of a given material and where T_1 designates the laser-induced change in temperature [13]. Notice that the time scale for changes in the temperature of the materials can be quite long (of the order of seconds), and consequently thermal effects often lead to strongly time-dependent nonlinear optical phenomena. Under steady-state conditions, in the case of continuous-wave radiation, the temperature change T_1 obeys the heat-transport equation:

$$\kappa\nabla^2 T_1 = -\alpha I(r). \tag{1.1}$$

where κ stands for the thermal conductivity, and α denotes the linear absorption coefficient of the material. Eq. (1.1) can be solved as a boundary value problem, and hence the refractive index at any point in space can be found from the relation $n = n_0 + (\mathrm{d}n/\mathrm{d}T)T_1$. Note that thermal nonlinearity is nonlocal, because the change in refractive index at some given point generally depends on the laser intensity at other nearby points.

In nonlinear optics thermal nonlinearities have been reported in different materials, such as self-trapping of bell-shaped beams in lead glass [37], formation of steady-state cylindrical thermal lenses in an ethanol-dye solution [38], and thermal nonlinear effects in gases [39]. Thermal nonlinearity introduces remarkable features in solitons. Recently, stable vortex-ring solitons [40], and multi-pole mode solitons [41] have been demonstrated in bulk lead glass [namely, (2+1)D geometry]. Very recently, long-range interactions between solitons were demonstrated in thermal nonlinear media [42].

More interesting, surface solitons have been demonstrated at the interface between a dielectric medium (air) and a thermal nonlinear media with a very long-range nonlocal response [43].

Reorientation nonlinearities

Similar to thermal nonlinearities, reorientation nonlinearities also feature a nonlocal response. The orientation effect is a unique characteristic of the liquid-crystalline phase. Liquid crystals are fascinating materials with many unique properties and applications [44]. The cubic, Kerr-like nonlinearity induced by the orientation effect in the nematic phase of liquid crystals is responsible for numerous nonlinear effects that are not observed in other materials. Not only does the reorientation nonlinearity induce extremely large intensity-dependent changes in the refractive index at relatively low power levels, but also such changes can be modified by external optical or electrical fields. Moreover, the nonlinearity depends on light polarization but is independent of light wavelength within a wide range. The nonlinear optics of liquid crystals has been of interest for many years, and the experimental and theoretical studies on self-focusing in such materials date back to the early 1990s [45, 46, 47].

Liquid crystals are composed of anisotropic molecules, i.e. molecules having an anisotropic polarizability tensor. The origin of their nonlinearity is the tendency of molecules to become aligned in the electric field of an applied optical wave. The optical wave then experiences a modified value of the refractive index because the average polarizability per molecule has been changed by the molecular alignment. The anisotropy of liquid crystals manifest itself in various properties, such as electrical permittivity, magnetic permeability, conductivity, and optical birefringence. As a result, an external electric field $\mathbf{E}$ induces an electrical dipole with moment $\mathbf{p}$ that is not parallel to $\mathbf{E}$. Consequently, the torque $\mathbf{p} \times \mathbf{E}$ tends to rotate the molecules into alignment with the applied electrical field. This reorientation does not depend on the sign of the electric field and occurs for time-varying fields as well, including optical fields. A similar behavior is observed for magnetic fields, but magnetic anisotropy is usually smaller than the electric one. At optical frequencies, the interaction with the magnetic field can be neglected, and the interaction between light and a liquid crystal is described by the electrical dipole. The rotation induced by the electric dipole is opposed by the elastic forces that maintain the long-range order with a liquid-crystalline

cell. The orientation of each molecule is determined by those two oppos-
ing forces. Because the birefringence of liquid crystal is connected with the
orientation of molecules, changes in orientation cause the rotation of the
optical birefringence axis. Physically speaking, the light incident on a liquid
crystal modifies the electric permittivity tensor, leading to the reorientation
nonlinearity. Because the anisotropy for a liquid crystal is relatively large,
the orientation nonlinearity can create large changes in the refractive index
at relatively low intensity levels (~ 1 `kW/cm`^{2}).

The orientation nonlinearity can be calculated by minimizing the total
free-energy density, which induces the deformation energy, the energy of
interaction with the external field, and the effects of boundaries. The key
variable that governs the orientation problem is the angle θ between the
director **n** and the axis along which the input light is polarized. The mag-
nitude of the orientation nonlinearities depends on the initial orientation
n, and therefore the liquid-crystal configuration. The nonlinear response
due to reorientation nonlinearities is highly nonlocal, in the sense that the
director distortion spreads from the excitation owing to the intermolecular
links.

As an example of the reorientation nonlinearities, nematic liquid crystals
have offered an ideal workbench for the study of light localization, because
they conjugate a giant molecular nonlinearity with a large electro-optic re-
sponse, a mature technology and extended spectral transparency, allowing
for the demonstration and the understanding of fundamental effects at rel-
atively low powers [48]. Almost a decade ago, the self-focusing phenomena
was observed in nematic liquid crystal waveguides [49]. As mentioned before,
being highly nonlocal anisotropic dielectrics, nematic liquid crystals not only
support stable spatial solitons in two transverse dimensions [(2+1)D] [50, 51]
but they also allow to take full advantage of their inherent birefringence and
walk-off to control the direction of energy flux, i.e. their Poynting vector,
by acting on an external polarization (voltage) to reorient the constituent
molecules [198]. Very recently, tunable refraction and reflection of optical
spatial solitons beam have been demonstrated at the interface between two
regions of a nematic liquid crystal [53].

Photorefractive nonlinearities

Photorefractive materials have been known for many years [54, 55], in
which the change in refractive index results from the optically induced re-

distribution of electrons and holes. Typically, these are dielectric (or semi-insulating) single crystals that are noncentrosymmetric and give rise to $\chi^{(2)}$ nonlinearities.

The origin of photorefractive effect is illustrated as follows. Photorefractive materials always have some dopants hosted in the crystalline matrix, with energy levels deep inside the forbidden gap. These dopants are in the form of donors and acceptors, i.e. they can contribute (or trap) free charges. Let us consider now an optical beam incident upon such a crystal, with optical photons that are not energetic enough to cause valence-to-conduction band excitation, but can excite charges (assumed electrons here) from the deep dopant levels. Once excited into the conduction band, the electrons are free to move. If the intensity of the optical beam is not uniform in space, these photo-excited electrons experience transport: they diffuse from high concentrations to lower ones and they can drift if an external bias field is applied. At the same time, the donor dopants which are now positively charged are localized immobile ions. Eventually, after some characteristic time (dielectric relaxation time), the electrons are re-trapped either by acceptors or by ionized donors at locations that are different from their original donor ions. The resulting charge separation establishes an electric filed within the medium, which varies in space (e.g. the field in an illuminated spot is different from that in a dark spot). Through the electro-optic effect, the internal space charge field $E_{sc}^{(0)}$ gives rise to a change in the refractive index (Δn). Thus nonuniform illumination incident upon a photorefractive medium results in nonuniform change in the refractive index.

Photorefractive solitons were first predicted in 1992 [56] and observed experimentally a year later [57]. Since then on, several different types of photorefractive solitons have been discovered, each resulting from a different nonlinear mechanism which is inherently saturable (there always exists a limit to the number of carries), and each exhibiting a different dependence of Δn on the optical intensity $I = |E|^2$. Amongst all types of photorefractive solitons, the *photorefractive screening soliton* has become the most commonly used in experiments since it is the easiest to understand intuitively in (1+1) dimensions and hence it is worth dwelling on the physical process to the formation of this particular soliton. A strong external electric field is applied to the photorefractive crystal (usually strontium barium titanate) using electrodes attached to opposing crystal faces. In the absence

of illumination, the field is distributed uniformly across the crystal, lowering (or raising) its average index of distributed uniformly via the Pockels effect. When a narrow light beam propagates through the crystal in a direction normal to the field, electric charges are excited from traps within the bandgap, increasing the charge density in the illuminated region. The presence of these charges modifies the conductivity of the crystal, and as a consequence the local field (space charge field) is screened. This modifies the local refractive index via the Pockels effect and can create the conditions for solitons to form. The actual dependence of Δn on the optical intensity for (1+1)D screening solitons is $\Delta n = (V/L)(n^3 r_{\mathtt{eff}}/2)[1/(|E|^2 + I_{dark})]$, where $r_{\mathtt{eff}}$ depends on the direction of the applied field and the polarization of the beam, V is the voltage applied between electrodes separated by distance L ($L \gg$ soliton width), and I_{dark} is the so-called 'dark irradiance', which is a material parameter that is proportional to the conductivity of the crystal in the dark. Photorefractive screening solitons were first predicted in 1990s [58, 59], and shortly after observed experimentally [60, 61, 62].

As noted above, several other kinds of photorefractive solitons have been found so far. *Quasi-steady-state* solitons, which exist during a finite window in time (never surviving to steady state), were observed [57]. They occur when an external applied field is slowly being screened by the space charge field. Another kind is *photovoltaic* solitons. They do not require an external bias field but instead rely on the bulk photovoltaic effect to create the space charge field, which in turn, modifies the refractive index and leads to a soliton. The nonlinearity supporting (1+1)D photovoltaic solitons is of the form $\Delta n \propto [|E|^2/(|E|^2 + I_{dark})]$. Photovoltaic solitons were predicted theoretically in 1994 [63, 64] and first observed a year later [65, 66]. A fourth type of photorefractive solitons exist in biased photorefractive semiconductors, such as InP, in which both electrons and holes participate in the formation of the space charge field. Interestingly enough, the self-focusing effects supporting these solitons undergo a large enhancement when the rate of optical excitation of holes is close to (but smaller than) the thermal excitation rate of electrons, self-focusing turns into self-defocusing, i.e. the sign of the optical nonlinearity can be reversed by all optical means. These solitons were demonstrated experimentally in 1996 [67, 68]. Finally, it was predicted theoretically that solitons exist in centrosymmetric photorefractive media, which fundamentally do not possess quadratic nonlinearities [69]. The change in

the refractive index giving rise to these solitons is driven by the dc Kerr effect, which is similar to Pockels effect but Δn is now proportional to $(E_{sc})^2$ and thus to $1/(|E|^2 + I_{dark})^2$. These solitons were demonstrated experimentally in 1988 [70].

It is worth noting two additional properties that are common to all photorefractive solitons. The first is the ability to generate solitons with optical power levels of $1\mu W$ or lower [61, 62]. This occurs because the refractive index change Δn depends on the ratio $|E|^2/I_{dark}$ rather than on the absolute value of the optical intensity $|E|^2$, and I_{dark} is typically very low in photorefractive materials (the dark current is very low). The drawback is that the response time (dielectric relaxation time) scales as the inverse of the optical intensity, and can be long (seconds) for these power levels in $10\mu m$ wide soliton. The other property is that the response of materials is wavelength-dependent. Thus one can generate solitons with microwatts power and use the waveguides induced by these solitons to guide, steer and control powerful beams at wavelengths for which the material is less photosensitive [71, 72].

Quadratic nonlinearities

Solitons in quadratic nonlinear media are a quite different breed of solitons from those discussed previously. These solitons rely solely on the second-order nonlinearities $\chi^{(2)}$. The self-trapping exists by virtue of the strong interaction and energy exchange between two or more beams at different frequencies. Because of these constraints, quadratic solitons can only be launched in a limited class of materials, namely non-centrosymmetric media in which phase matching is possible, i.e. they only exist at reasonable powers over a narrow range of directions. Although it is now clear that quadratic solitons exist for different parametric mixing process involving $\chi^{(2)}$, and indeed they have been observed in optical parametric generators and amplifiers, to date they have been studied primarily during second harmonic generation.

Quadratic solitons consist of beams at two or more frequencies which are strongly coupled by second order nonlinearities under conditions of wavevector conservation. Here I discuss the self-trapping mechanism for quadratic solitons generation for the simplest case of Type I second harmonic generation (a single input fundamental beam) in a (1+1)D slab waveguide with diffraction along the x axis and waveguide confinement along the

y axis. From standard textbooks in nonlinear optics, the coupled mode equations which describe the parametric interaction between a fundamental ($E_1(r,t) = A_1(x,z)\texttt{exp}(i\omega t - ik_1 z)/2 + c.c.$) and second harmonic ($E_2(r,t) = A_2(x,z)\texttt{exp}(i2\omega t - ik_2 z)/2 + c.c.$) beams propagating along the z direction as follows:

$$-2ik_1 \frac{\partial A_1(z,x)}{\partial z} + \frac{\partial^2 A_1(z,x)}{\partial x^2} = -\Gamma A_1^*(z,x) A_2(z,x) \texttt{exp}(i\Delta k z)$$

$$-2ik_2 \frac{\partial A_2(z,x)}{\partial z} + \frac{\partial^2 A_2(z,x)}{\partial x^2} = -\Gamma A_1^2(z,x) \texttt{exp}(-i\Delta k z), \qquad (1.2)$$

where $\Delta k = k_2 - 2k_1$ is the wavevector mismatch, Γ is the nonlinear coupling coefficient which is proportional to $\chi^{(2)}$, $A_{1,2}(z,x)$ are complex, slowly varying amplitudes, the second term in the left-hand side in each case describes diffraction and the source term on the right-hand side. The key to self-trapping is the structure of the source terms which consist of the product of the two fields of finite spatial extent. Consider first the generation of second harmonic driven by the term $A_1^2(z,x)$ so that the generated second harmonic is initially narrower along x-axis than the fundamental. Furthermore, the generated fundamental via the product $A_1(z,x)A_2(z,x)$ is also narrower than the original fundamental. The robust balance between this mutual beam narrowing and diffraction leads to a mutually locked soliton.

Quadratic solitons were first predicted in the mid 1970s by Karamzin and Sukhorukov [73], and it was not until 1996 that their experimental observation was reported [74]. The main reason behind such a delay was the lack of high-quality materials. Moreover, the advantages offered by quadratic solitons for practical applications were not obvious. The situation changed in the 1990s with the rediscovery of the self-action effect in $\chi^{(2)}$ media and with the appearance of high-damage optical materials with long enough propagation lengths [23]. Since then the area of quadratic solitons has been rapidly advancing in many interesting directions, including quadratic solitons in resonators [75], beam steering and control with quadratic solitons [76, 77], reshaping [78] and transverse instabilities of (1+1)D quadratic solitons propagating in a bulk medium [79, 80, 81, 82]. With the advent of quasi-phase matching and the expected advances in the growth and engineering of $\chi^{(2)}$ materials, parametric solitons may find practical applications in frequency converters and generators (for a comprehensive review on quadratic solitons, see ref [26]).

1.2.3   Optically induced lattices

All materials discussed in Sec. 1.2.2 are homogenous. However, the propagation of nonlinear waves in periodic structures exhibits different behavior fundamentally from that of their homogeneous counterparts. The physics of nonlinear waves in periodic structures is common for a variety of systems, including excitations in biological molecules [83], electrons in solid-state systems [84], ultracold atoms in optical standing waves [85], and light waves in nonlinear media with periodic modulation of the refractive index [86]. In optics the effects associated with this phenomenon can be easily observed and examined in close detail. A strong motivation for the work in the field of photonics comes from the analogy between the behavior of light in periodic photonic structures and electrons in superconductors. This analogy suggests the possibility of replacing electronic components with novel types of photonic devices where light propagation is fully controlled in engineered micro-structures. Nonlinearity adds a possibility to control propagation of light purely optically, i.e. with light itself. Such all-optical devices may form foundation of future high-bandwidth, ultrafast communications and computing technologies.
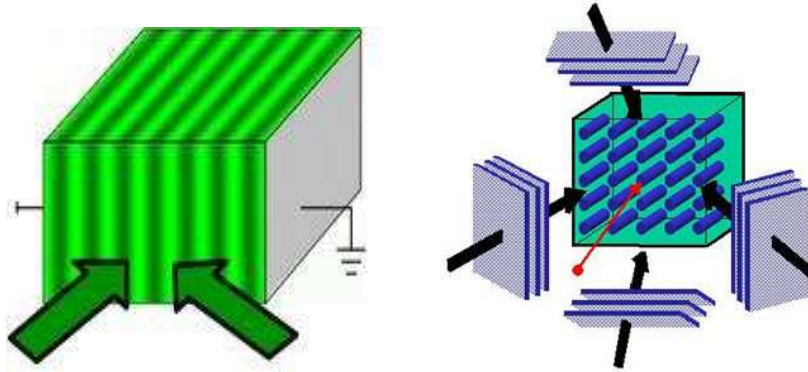
Figure 1.4: Intensity pattern of optically induced lattices.

In practice, for the development of new schemes to control light in periodic systems although there are difficulties that arise in fabrication of materials with both periodicity on the optical wavelength scale and strong nonlinearity accessible at low laser powers, such kind of periodic structure is achieved with current available materials and technology. An example is shown in Fig. 1.4 on optically induced lattices in a highly nonlinear

photorefractive crystal. Such a lattice can be photoinduced by periodic diffraction-free intensity patterns that result from plane-wave superposition (provided that the system is linear for the interfering waves). As shown in Fig. 1.4, a one-dimensional lattice can be generated from the interference of two plane waves (left one in Fig. 1.4). More complicated lattices can be generated by superimposing two or more mutually incoherent plane wave pairs at different angles, one example, two dimensional lattices is generated by four beams (right one in Fig. 1.4). What makes possible the nonlinear waves propagating in such lattices is the large electro-optic anistropy of the photorefractive crystal. This allows almost diffraction-free periodic patterns polarized in a nonlinear electro-optic direction, whereas at the same time the signal beam is polarized in the crystalline orientation that yields the highest possible nonlinearity.

An optical lattice induces a band-gap structure for the propagating optical waves. The existence of gaps implies that optical waves with certain wave-vectors cannot propagate through the structure due to either total internal or Bragg reflection. The dynamics of the probe laser beam propagation in a nonlinear optically induced lattice is therefore dominated by an interplay between nonlinearity of the medium and scattering from the periodic structure. For example, self-localized states in such kind of lattices, named *lattice solitons* were predicted in 2002 [87], and demonstrated experimentally in 1D [88] and 2D [89] lattices. Later on, a variety of fascinating phenomena due to lattices have been reported, such as, formation and steering of gap solitons [88, 90], and trapping and stabilization of discrete vortices [91, 92, 93, 94]. Interesting, note that soliton dynamics can be made richer with different lattice symmetry, for example, solitons can be set rotating in a ring-shaped (Bessel-type) photonic lattices [95, 96]. Very recently, surface solitons were reported in optically induced lattices and laser-written waveguide arrays [97, 98, 99, 100, 101, 102].

1.2.4 Soliton topologies

As discussed in the preceding sections, spatial solitons can exist in a broad branch of nonlinear materials, such as cubic Kerr, saturable, thermal, reorientation, photorefractive, and quadratic media, and periodic systems. Furthermore, the existence of solitons varies in topologies and dimensions.
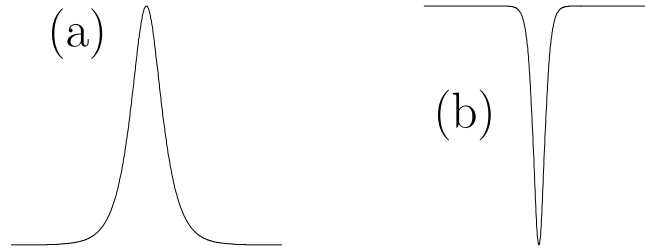
Figure 1.5: Intensity profiles for bright (a), and dark (b) solitons.

In (1+1)D systems, namely one transverse coordinate and one longitudinal propagation direction, one of the fundamental formation of solitons are *bright solitons*, which are formed due to the diffraction or dispersion compensated by self-focusing nonlinearity. Bright solitons appear as intensity hump in a zero background as shown in Fig. 1.5(a), which can exist in all the materials discussed above. The other kind of fundamental solitons which appear as intensity dips with a CW background are called *dark solitons* as shown in Fig. 1.5(b). Dark solitons exist in self-defocusing nonlinear media and feature a π-phase jump, for a comprehensive review see ref. [103]. Both bright and dark solitons in one dimension are stable in the reported materials.
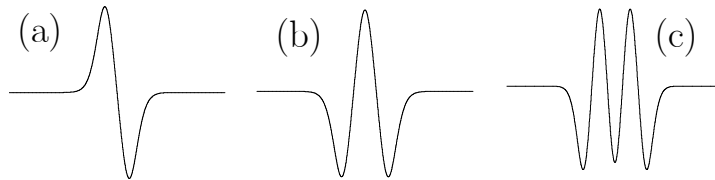
Figure 1.6: Amplitude profiles for dipole-mode (a), triple-mode (b) and five-hump (c) solitons.

The fundamental bright and dark solitons feature only one hump or dip. However, more complex structures can also occur to solitons. As shown in Fig. 1.6, the intensity of complex multihump solitons features more peaks. Intuitively, such multipole-mode solitons can be viewed as nonlinear combinations of fundamental solitons with alternating phases, named *bound states*. Such bound states cannot exist in local Kerr-type medium in the scalar case, in which a π phase difference between solitons causes a local decrease of re-

fractive index in the overlap region and results in repulsion. By contrast, in nonlocal media, such as lead glass with thermal nonlinearities, and liquid crystals with reorientation nonlinearities, the refractive index change in the overlap region depends on the whole intensity distribution in the transverse direction, and under appropriate conditions the nonlocality can lead to an increase in the refractive index and to attraction between solitons. The proper choice of separation between solitons results in such kind of bound states. Multipole mode solitons have been reported in local saturable media in vector case [104, 105], and quadratic media [106, 107, 108]. Very recently, the stability of multipole mode solitons has been reported in nonlocal media for both scalar and vector cases [109, 110].
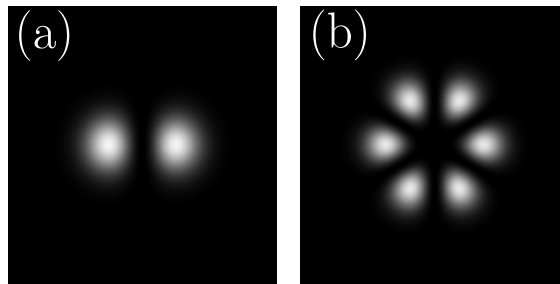
Figure 1.7: Intensity distributions for dipole-mode (a), and hexapole (b) solitons in two dimension systems.

One natural question is whether spatial (1+1)D solitons can be extended to (2+1)D systems, namely, two transverse coordinates and one longitudinal propagation direction. It turns out that bell-shaped solitons are unstable in bulk Kerr media, in which they suffer catastrophic collapse. A few different mechanisms have been found to arrest collapse, such as, saturable nonlinearity, photorefractive and nonlocal effects, therefore, spatial solitons in (2+1)D have become an active topic. Solitons can take on more complex configurations, such as dipole [Fig. 1.7(a)] and multihump solitons, solitons organized as necklaces [Fig. 1.7(b)], which are composed of several bright spots out-of phase. More complex beams carrying angular momentum, such as vortex solitons [Fig. 1.8], whose intensity distribution features a *donut* shape, have been demonstrated (for a comprehensive review see ref. [111]). In contrast, another important example of a (2+1)D spatial soliton is the *dark* type soliton, which exists in self-defocusing media in the form of a

"hole" in an extended backgroud, which is supported by a vortex phase
pattern imprinted onto the background [112, 113, 114]. As the transverse
plane is two dimensional, solitons can be set into rotation. For example,
a rotating propeller soliton has been demonstrated [115], which is a com-
posite soliton made of a rotating dipole component jointly trapped with a
bell-shaped component.
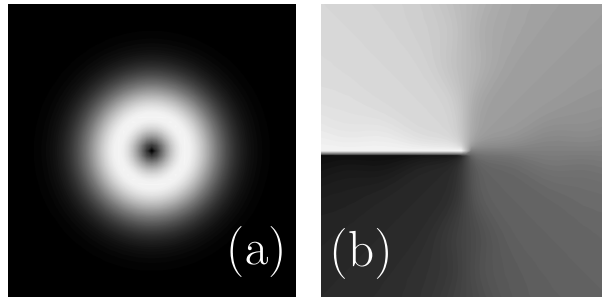
Figure 1.8: The field (a), and phase (b) distributions of vortex solitons

One of the major goals in the study of nonlinear optics is the generation
of light packets that are localized in all transverse dimensions of space, as
well as in time. Such kind of localized objects are termed (3+1)D solitons,
known as *spatiotemporal solitons* or *light bullets*, where there are two trans-
verse coordinates, one temporal variable, and one longitudinal propagation
direction. The search for the generation of such objects dates back to the
early days of the field. In particular, such pulses in Kerr media were con-
sidered by Silberberg in 1990 [116], who coined the term *light bullets* for
them, which stresses their particle-like nature. In contrast to the extensive
developments in the studies of temporal and spatial solitons in one and two
dimensions, experimental progress towards to the production of spatiotem-
poral solitons in three-dimensional case has been slow. To date, (3+1)D
spatiotemporal solitons have not been observed yet.

The formation of (3+1)D solitons involves the same mechanism as for
their (1+1)D and (2+1)D counterparts, which provide for the proper balance
between linear spreading and a suitable nonlinearity. Thus spatiotemporal
solitons may be understood as the result of the simultaneous balance of
diffraction and dispersion by the transverse self-focusing and nonlinear phase
modulation in the longitudinal direction, respectively. A comprehensive
review on spatiotemporal solitons can be found in ref. [19].

The realization of spatiotemporal solitons faces two challenges: first, physically relevant models of nonlinear optical systems, based on evolution equations that allow stable three-dimensional propagation, ought to be identified; second, suitable materials should be found where such models can be implemented.

1.3   Overview of thesis

After this introductory chapter, Chapter 2 addresses properties of optical solitons in quadratic nonlinear media. The first section presents in detail the existence and stability of three representative families of two-dimensional spatiotemporal solitons in quadratic nonlinear waveguide arrays. It is assumed, in addition to the temporal dispersion of the pulse, the combination of discrete diffraction that arises because of the weak coupling between neighboring waveguides. The other section reports on the existence and stability of multicolor lattice vortex solitons, which comprise four main humps arranged in a square configuration. It is also investigated the possibility of their dynamical generation from Gaussian-type input beams with nested vortices.

Solitons in cubic nonlinear media are the topic in Chapter 3. The chapter puts forward the concept of reconfigurable structures optically induced by mutually incoherent nondiffracting Bessel beams in Kerr-type nonlinear media. Two-core couplers are introduced and it is shown how to tune the switching properties of such structures by varying the intensity of the Bessel beams. The chapter also discusses various switching scenarios for solitons launched into multi-core directional couplers optically-induced by suitable arrays of Bessel beams. Furthermore, propagation of solitons is investigated in reconfigurable two-dimensional networks induced optically by arrays of nondiffracting Bessel beams. It is shown that broad soliton beams can move across networks with different topologies almost without radiation losses. Finally, the properties of X-junctions are studied, which are created with two intersecting Bessel beams.

Chapter 4 treats the impact of nonlocality in the physical features exhibited by solitons supported by Kerr-type nonliner media with an imprinted optical lattice. The chapter investigates properties of different families of lattice solitons in nonlocal nonlinear media. It is shown that the nonlo-

cality of the nonlinear response can profoundly affect the soliton mobility. The properties of gap solitons are also discussed for photorefractive crystals with an asymmetric nonlocal diffusion response and in the presence of an imprinted optical lattice.

Chapter 5 is devoted to the impact of nonlocality on the stability of soliton complexes in uniform nonlocal Kerr-type nonlinear media. First, it is shown that the different nonlocal response of materials has different influence on the stability of soliton complexes in scalar case. Second, experimental work is reported on scalar multi-pole solitons in 2D highly nonlocal nonlinear media, including dipole, tripole, and necklace-type solitons, organized as arrays of out-of-phase bright spots. Finally, the chapter addresses the stabilization of vector effects on soliton complexes in nonlocal nonlinear media.

Finally, Chapter 6 presents a summary of the main results and discusses open prospects.

Chapter 2

Localized Modes in Discrete Quadratic Media

2.1 Overview

In this chapter, we will study localized modes (discrete or lattice solitons) in quadratic nonlinear media. Since their first experimental observation [74], quadratic solitons have been demonstrated in a variety of materials and geometries. Spatial, temporal, and spatiotemporal solitons in quadratic media have been extensively investigated both experimentally and theoretically (for detailed reviews, see [23, 26, 117, 118]). Recently, it is noted that propagation of optical radiation in media with transverse refractive index modulation differs considerably from the propagation in uniform media. Localized structures in such periodic media, termed discrete or lattice solitons, do exist and exhibit a rich variety of topologies.

Since their theoretical prediction in 1988 in cubic nonlinear media [86], discrete optical solitons have attracted a steadily growing interest because of their potential applications in switching and routing devices [119, 120, 121]. The discrete solitons that form in tight-coupled waveguide arrays made of quadratic nonlinear media have been comprehensively investigated [122, 123, 124, 125, 126, 127] due to the rich variety of effects that are possible with them. It is noted that recently discrete quadratic solitons have been experimentally observed in arrays of waveguides made in lithium niobate [128]. On the other hand, the intermediate regime between continuous and discrete solitons [129, 130] constituted by continuous nonlinear media

with an imprinted transverse modulation of the refractive index, has been shown recently to offer a variety of new opportunities. The concept behind this regime might be termed *tunable discreteness*, the strength of modulation being the parameter that tunes the system properties from continuous to discrete. In this context, wave dynamics is governed by the interplay between optical tunnelling to adjacent sites and nonlinearity. This kind of lattice solitons have been observed recently in two-dimensional (2D) photorefractive optical lattices [87, 88, 89, 131, 132].

In section 2.2, we will study in detail the existence and stability of three representative families of two-dimensional spatiotemporal solitons in quadratic nonlinear waveguide arrays. In section 2.3, we will report on the existence and stability of multicolor lattice vortex solitons, which comprise four main humps arranged in a square configuration. We also investigate the possibility of their dynamical generation from Gaussian-type input beams with nested vortices.

2.2 Spatiotemporal discrete multicolor solitons

2.2.1 Introduction

In this section, we will study spatiotemporal discrete solitons in quadratic nonlinear media. In the last two decades, the concept of optical spatiotemporal solitons (STS's), referred as light bullets in the three-dimensional case [116], has been attracting attention as a unique opportunity to create a self-supporting fully localized object (for detailed reviews, see [133]). The existence of STS's in quadratic nonlinear materials was theoretically predicted [134] and thereafter experimentally realized in a two-dimensional geometry involving one temporal and one spatial coordinate [135]. The existence and properties of continuous-discrete spatiotemporal solitons has been extensively investigated in cubic nonlinear media and stable odd solitons have been shown to exist [136, 137, 138, 139, 140]. It was shown that the cubic weakly-coupled waveguide arrays act as collapse compressors [136, 137, 138]. In contrast with the cubic spatiotemporal solitons, the quadratic ones do not display collapse in both two- and three-dimensional geometries [141].

Discrete soliton solutions were classified as *staggered* and *unstaggered* ones (see, for example, Ref. [142]). The staggered solutions display out-of-phase fields between the neighbor noncentral waveguides whereas the un-

staggered ones display in-phase fields in these noncentral waveguides. Inside each of these classes of solitons (staggered and unstaggered) one can find solutions with different topologies, dictated mainly by the energy and phase distribution in the central waveguides. Thus, one can have (i): *odd* solitons, for which most part of the energy is located in one central waveguide and the energy distribution across the waveguide array is symmetric with respect to this central waveguide, (ii): *even* solitons, for which most part of the energy is equally distributed in the two central waveguides, the fields in these central waveguides being in-phase and of equal amplitudes, and (iii): *twisted* solitons, for which most part of the energy is equally distributed in the two central waveguides, but the fields in the two central waveguides are out-of-phase.

2.2.2 Model and stationary solutions

Here we assume, in addition to the temporal dispersion of the pulse, the contribution of the discrete diffraction, that arises because of the weak coupling between neighboring waveguides. The evolution of the spatiotemporal two-component field in quadratic nonlinear waveguide arrays in a degenerate second-harmonic generation geometry may be described by the following set of nonlinearly coupled reduced differential equations:

$$i\frac{\partial u_n}{\partial \xi} = -c_u \left(u_{n-1} + u_{n+1}\right) + \frac{g_1}{2}\frac{\partial^2 u_n}{\partial \tau^2} - u_n^* v_n \exp\left(-i\beta\xi\right),$$

$$i\frac{\partial v_n}{\partial \xi} = -c_v \left(v_{n-1} + v_{n+1}\right) + \frac{g_2}{2}\frac{\partial^2 v_n}{\partial \tau^2} - u_n^2 \exp\left(i\beta\xi\right)\ , \qquad (2.1)$$

where u_n and v_n represent the normalized amplitudes of the fundamental frequency (FF) and second-harmonic (SH) fields in the nth waveguide, with $n = -N, ... -1, 0, 1, ..., N$, $2N + 1$ being the number of waveguides, * means complex conjugation, $c_{u,v}$ and $g_{1,2}$ are the linear coupling coefficients and group-velocity dispersion (GVD) coefficients, respectively, and β is the wave-vector mismatch. The evolution variable ξ denotes the normalized propagation distance along the waveguides. The dynamical system (2.1) admits several conserved quantities including the energy flow and Hamiltonian which read

$$I = \sum_n \int \left(|A_n|^2 + |B_n|^2\right) d\tau\,, \qquad (2.2)$$

$$H = -\sum_n \int \left[\frac{g_1}{2} \left| \frac{\partial A_n}{\partial \tau} \right|^2 + c_u \left(A_n A_{n+1}^* + A_n^* A_{n+1} \right) \right.$$

$$+ \frac{1}{2}(A_n^2)^* B_n + \frac{g_2}{4} \left| \frac{\partial B_n}{\partial \tau} \right|^2 + \frac{c_v}{2} \left(B_n B_{n+1}^* + B_n^* B_{n+1} \right)$$

$$\left. - \frac{\beta}{2} |B_n|^2 + \frac{1}{2} A_n^2 B_n^* \right] d\tau \, , \tag{2.3}$$

where we have defined $A_n \equiv u_n$, and $B_n \equiv v_n \exp\left(-i\beta\xi\right)$. The stationary solutions of Eqs. (2.1) have the form $u_n = U_n\left(\tau\right) \exp\left(ib_1\xi\right)$ and $v_n = V_n\left(\tau\right) \exp\left(ib_2\xi\right)$, where $U_n\left(\tau\right)$ and $V_n\left(\tau\right)$ are real functions, and $b_{1,2}$ are real propagation constants verifying $b_2 = 2b_1 + \beta$. Continuous-discrete solitons arise from a balance between discrete diffraction, dispersion and quadratic nonlinearity. The families of odd, even, and twisted stationary continuous-discrete solitons have been obtained numerically by a standard relaxation method. For given coupling strengths $c_{u,v}$, dispersions $g_{1,2}$ and wave-vector mismatch β, the soliton families are parametrized by the nonlinear wave number shift b_1. The coupling coefficients $c_{u,v}$ were considered positive, and equal, so further we introduce single parameter C to describe coupling between neighboring guiding sites. Throughout this section we will always consider anomalous dispersions at both frequencies and we fixed $g_1 = -0.25$ and $g_2 = -0.5$. Note that in the continuous case, long-lived soliton-like propagation when the GVD is slightly normal at SH is known to occur [143, 144]; thus a similar behavior might occur in the continuous-discrete spatiotemporal case analyzed here.

Here we will restrict ourselves to three representative families of continuous-discrete unstaggered solitons, namely the odd soliton [see Fig. 2.1(a)], the even soliton [see Fig. 2.1(c)] and the twisted soliton [see Fig. 2.1(d)]. Note that for the twisted soliton, the fundamental frequency field is, in fact, an anti-symmetric one (the π jump of phase occurs only between the two central waveguides), whereas the second harmonic field is a symmetric one (having the form of an even discrete soliton). For all the solutions we deal with, the temporal profile, i.e. the shape of the pulses propagating in a specific waveguide, is a bell-shaped symmetric one [see Fig. 2.1 (b), below]. Besides these stationary solutions, there exist a whole "zoology" of localized solutions, including staggered solitons, dark or dark-bright solitons, but their study is beyond the scope of the present work. In Figs. 2.2(a) and (b) we show
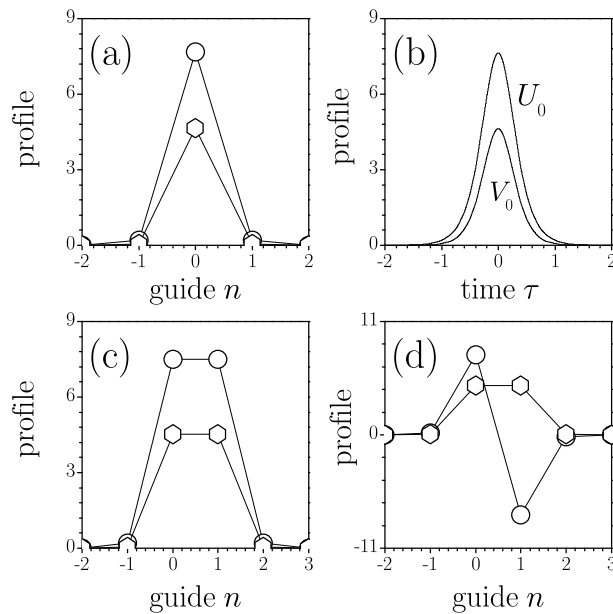
Figure 2.1: Amplitude profiles of the (a) odd, (c) even, and (d) twisted solitons. Lines with circles show FF field; lines with hexagons show SH field. In (b) the time slice in the central waveguide ($n = 0$) for odd soliton is shown. Even and twisted solitons feature the similar temporal profile. Here $C = 0.1$, $b_1 = 3$, and $\beta = 3$.

the dependencies of the peak amplitude A_u and the temporal full width at half maximum of the pulse in the central waveguide W_u as a function of the coupling coefficient C for a fixed wave number b_1 at phase matching ($\beta = 0$). Note that, with increase of coupling strength amplitude of odd and even solitons monotonically decreases and their width increases, whereas the amplitude and width of the twisted solitons are nonmonotonic function of C. This is illustrated also in Fig. 2.3 where profiles of odd solitons $|U_n(\tau)|$ at two different coupling constants are shown. Note that with increase of coupling constant soliton covers more guiding sites, while at $C \longrightarrow 0$ it is located primarily in the central guiding site.

Similar to the two-dimensional (continuous-continuous) solitons in uniform media, there exist cutoff b_{co} of the nonlinear wave number shift b_1 depending on the sign and absolute value of the mismatch parameter β. Moreover, as we have an additional degree of freedom, namely the discrete spatial coordinate, we have investigated the dependence of the cutoff wave number b_{co} on the coupling coefficient C for a given wave-vector mismatch. For a phase-matched geometry ($\beta = 0$), we have obtained almost linear
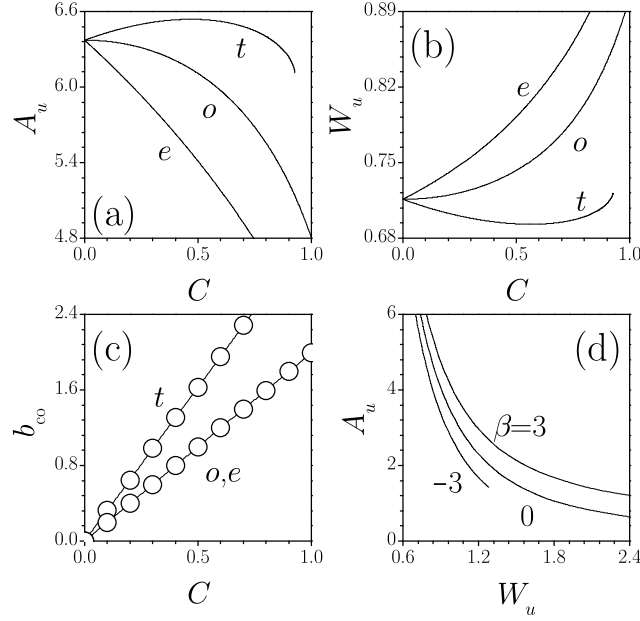
Figure 2.2: (a) Peak amplitude and (b) temporal width of FF wave in the central waveguide for odd, even and twisted solitons versus coupling coefficient at $b_1 = 3$ and $\beta = 0$. (c) Wave number cutoff versus coupling coefficient at $\beta = 0$. The symbols "o," "e," and "t" stand for the odd, even and twisted solitons respectively. (d) FF wave amplitude versus temporal width in the central waveguide for odd soliton at $C = 0.1$ and different phase mismatches. Only stable branch has been plotted for negative β.

dependencies of the cutoff wave number on the coupling coefficients for all three families of solutions we deal with [see Fig. 2.2(c)]. Note that cutoffs for odd and even solitons are equal. As a general rule, the stronger the coupling, the larger the cutoff wave number b_{co}. When $C = 0$ we got $b_{co} = 0$, thus recovering the known result for the continuous quadratic solitons: $b_{co} = \max\{-\beta/2, 0\}$.

We also have investigated the peak amplitude and the temporal width in the central waveguide for odd, even and twisted continuous-discrete solitons as functions of the wave-vector mismatch for fixed nonlinear wave number shift b_1 and linear coupling coefficient C. The solitons that form for larger phase mismatches have larger amplitudes and are narrower than those forming at smaller phase mismatches. This feature was observed for one- and two-dimensional continuous solitons in quadratic media for which at phase matching the product (peak amplitude)$\times$(width^2) is a constant quantity [145]. In Fig. 2.2(d) we plot the amplitude of the stationary odd soliton
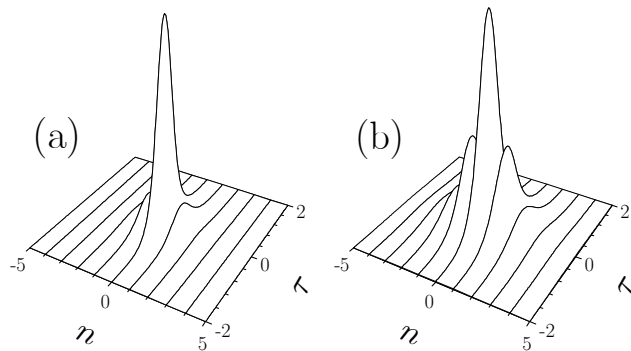
Figure 2.3: Profiles of odd solitons for (a) $C = 0.5$ and (b) $C = 1$ at $b_1 = 3$, $\beta = 0$. Only the modulus of the amplitude of the FF wave is shown. The SH shows similar features.

as function of its temporal width. We see that outside phase-matching the families of solitons exhibit a more complicated amplitude-width relationship, similar to the case of continuous quadratic solitons [145]. The scaling properties of Eqs. (2.1) can be written as:

$$u_n = \psi \tilde{u}_n, \ v_n = \psi \tilde{v}_n, \ b_1 = \psi \tilde{b}_1,$$
$$\beta = \psi \tilde{\beta}, \ \tau = \tilde{\tau}/\sqrt{\psi}, \ I = \psi^{3/2} \tilde{I}, \tag{2.4}$$

where ψ being the scaling parameter.

In Figs. 2.4(a)-(f) we have represented the dependencies energy flow I - wave number b_1 (left column) and Hamiltonian H - energy flow I (right column) that give us a deeper insight into the properties of continuous-discrete soliton families. One can see that odd solitons realize the minimum of Hamiltonian for a given energy flow, thus they are expected to be the most robust on propagation. The Peierls-Nabarro potential, that is the difference between Hamiltonian of the odd soliton and that of the even one [146], corresponding to the same energy flow, is negative everywhere. From a geometrical point of view, this would mean that odd solitons are stable in the entire domain of their existence [147]. Our numerical simulations, described in detail in the next subsection, show that, indeed, this is the case except for solitons at negative phase mismatches that are unstable only in a narrow region near cutoff [see Fig. 2.5(a)] [148, 145].
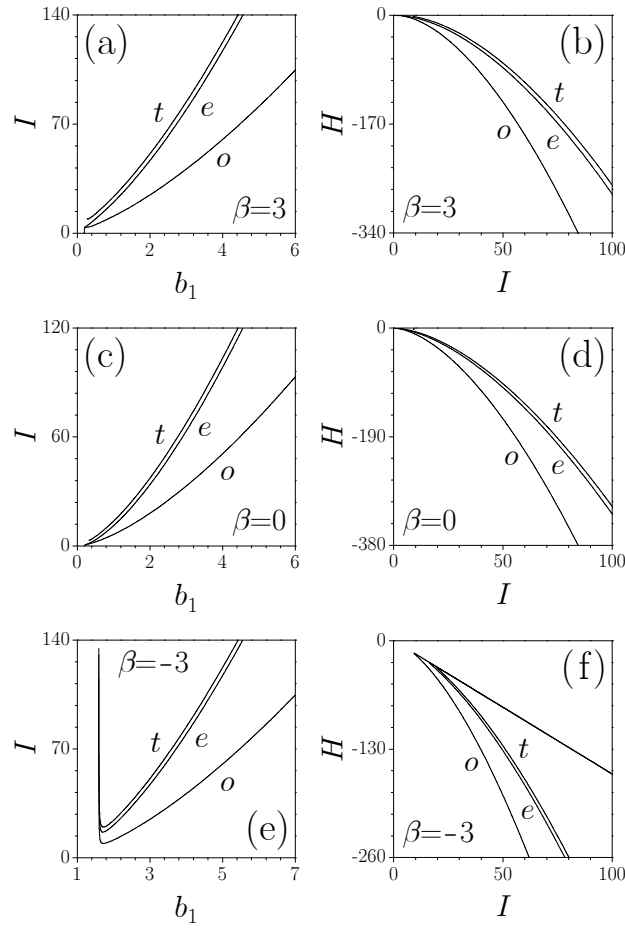
Figure 2.4: Energy flow versus wave number and Hamiltonian versus energy flow for odd, even, and twisted solitons at three representative values of phase mismatch and $C = 0.1$. The labels are the same as in Figures 2.2.

2.2.3   Stability analysis

A key issue concerning the soliton families we found is their stability on propagation. In order to elucidate if the localized continuous-discrete solitons are dynamically stable we have performed both a linear stability analysis and direct numerical simulations. We seek for perturbed solution of Eq. (2.1) in the form

$$u_n(\tau, \xi) = [U_n(\tau) + \mu f_n(\tau, \xi)] \exp(ib_1\xi),$$
$$v_n(\tau, \xi) = [V_n(\tau) + \mu h_n(\tau, \xi)] \exp[i(2b_1 + \beta)\xi], \qquad (2.5)$$

Here μ is a small parameter, $U_n(\tau)$ and $V_n(\tau)$ are the stationary solutions
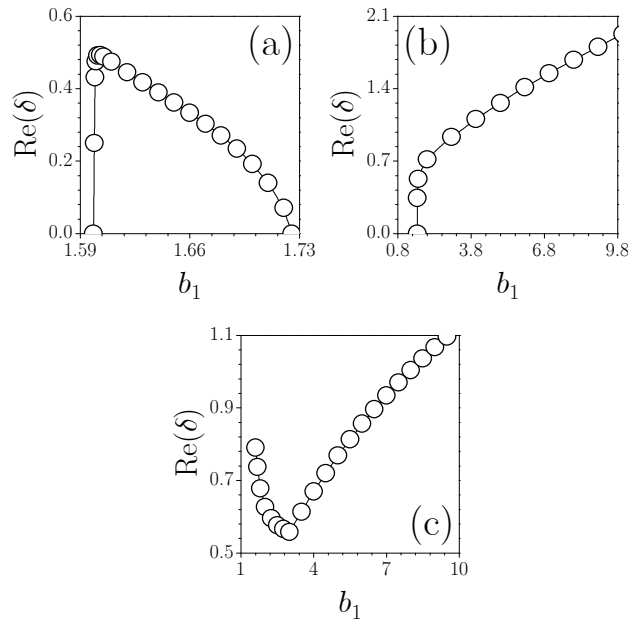
Figure 2.5: Growth rate versus wave number for (a) odd, (b) even, and (c) twisted solitons at $\beta = -3$ and $C = 0.1$.

and $f_n (\tau, \xi)$ and $h_n (\tau, \xi)$ are the perturbations. Then after linearizing the evolution equations (2.1) we are left with a system of linear coupled differential equations for the perturbations (see, e.g., Ref. [149]):

$$i \frac{\partial f_n}{\partial \xi} = -c_u \left(f_{n-1} + f_{n+1} \right) + \frac{g_1}{2} \frac{\partial^2 f_n}{\partial \tau^2} - \left(U_n^* h_n + V_n f_n^* \right) + b_1 f_n,$$

$$i \frac{\partial h_n}{\partial \xi} = -c_v \left(h_{n-1} + h_{n+1} \right) + \frac{g_2}{2} \frac{\partial^2 h_n}{\partial \tau^2} - 2 U_n f_n + \left(2 b_1 + \beta \right) h_n. \quad (2.6)$$

We have solved both this linear system and the nonlinear dynamical equations (2.1) with a combined Fast-Fourier Transform, to deal with the linear differential part in the temporal coordinate, and a fourth-order Runge-Kutta method, to deal with the cross-coupling terms. We have typically used 512 or 1024 points in the time domain and we have considered tens of array sites (e.g., 61), depending on the width of the solution whose stability is investigated. The step length along the propagation coordinate was of the order of 10^{-3}. The accuracy of the results was checked by doubling the number of points in the transverse coordinate and by halving the propagation step. As another check for the evolution equations (2.1) we have verified the conservation of the prime integrals (energy flow I and Hamiltonian H). In

order to let the radiation to escape from the computation window we have implemented transparent (absorbing) boundary conditions. We multiply a flat-top function after every step of longitudinal propagation distance, and this function has a very narrow tail which is zero.

We have determined the dominant eigenvalue δ of the linearized problem using the same approach as in Ref. [149]. The method gives us only the dominant eigenvalue, not the whole eigenvalue spectrum. This eigenvalue corresponds to the most rapidly (exponentially) developing instability. The noisy perturbation we consider at $\xi = 0$ develops, during evolution, to a localized eigenvector with a well defined symmetry, depending on the type of the solution considered. In the cases where an instability was detected, only real instability eigenvalues were found. The dominant eigenvalue was calculated in the form

$$
\mathrm{Re}(\delta) = \frac{1}{2\Delta\xi} \log\left\{ \left(\sum_n \int_{-\infty}^{\infty} \left[|f_n(\tau, \xi + \Delta\xi)|^2 + |h_n(\tau, \xi + \Delta\xi)|^2 \right] d\tau \right) \right.
$$
$$
\left. \times \left(\sum_n \int_{-\infty}^{\infty} \left[|f_n(\tau, \xi)|^2 + |h_n(\tau, \xi)|^2 \right] d\tau \right)^{-1} \right\}. \tag{2.7}
$$

This dominant eigenvalue tends to zero when one approaches the stability region. The results we got for the growth-rate calculations at negative phase mismatch ($\beta = -3$) are summarized in Fig. 2.5. They indicate instability for even and twisted solitons [122] and a stability region for odd solitons which starts at $b_1^{stab} \approx 1.725$. This result is in good agreement with the direct simulations of evolution Eq. (2.1). For positive wave-vector mismatches or at phase-matching the growth rate calculations indicate instability for even and twisted solitons and complete stability for odd solitons.

Our calculations show that odd continuous-discrete solitons obey the Vakhitov-Kolokolov stability criterion [150], i.e., they are stable provided $dI/db_1 > 0$, and unstable, otherwise. The Vakhitov-Kolokolov criterion was shown also to hold for discrete space-time solitons that exist in Kerr nonlinear media [139, 140]. Moreover, the unstable odd cubic continuous-discrete solitons can display collapse-type instabilities, a reminiscent feature of the two-dimensional stationary solutions of nonlinear Schrödinger equation, while the unstable quadratic discrete space-time odd solitons do not display this type of instability [141].

Let us stress that as compared to the one-dimensional discrete twisted solitons forming in quadratic media that can be stable, in specific parameter regions, in our case, the introduction of a time coordinate leads to the destabilization of these solutions. However, one of the central points of this work is that we found families of stable odd continuous-discrete multicolor
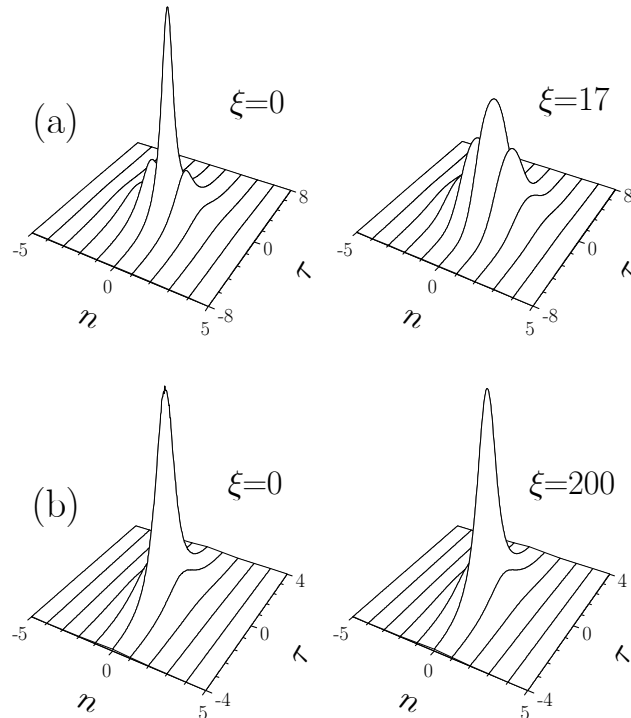
Figure 2.6: (a) Propagation of unstable odd soliton corresponding to $b_1 = 1.65$ in the presence of small perturbation found upon linear stability analysis. Perturbation amplitude $\mu = 0.01$. (b) Propagation of stable odd soliton at $b_1 = 1.735$ in the presence of white noise with variance $\sigma_{noise}^2 = 0.01$. Only the modulus of the amplitude of the SH wave is shown, at different propagation distances. Plots in left and right columns are shown with the same scale for easier comparison. Phase mismatch $\beta = -3$ and coupling constant $C = 0.1$.

solitons. As illustrated in Fig. 2.6(b), stable odd solitons can propagate for huge distances without altering their shape and eliminating the added random white noise during evolution. The case shown here corresponds to negative wave-vector mismatch $\beta = -3$ but similar stable evolution has been obtained for positive mismatches and phase-matching geometries except for odd solitons from the branch, where $dI/db_1 < 0$, which are unstable and will therefore decay after a finite propagation distance [see Fig. 2.6(a)].
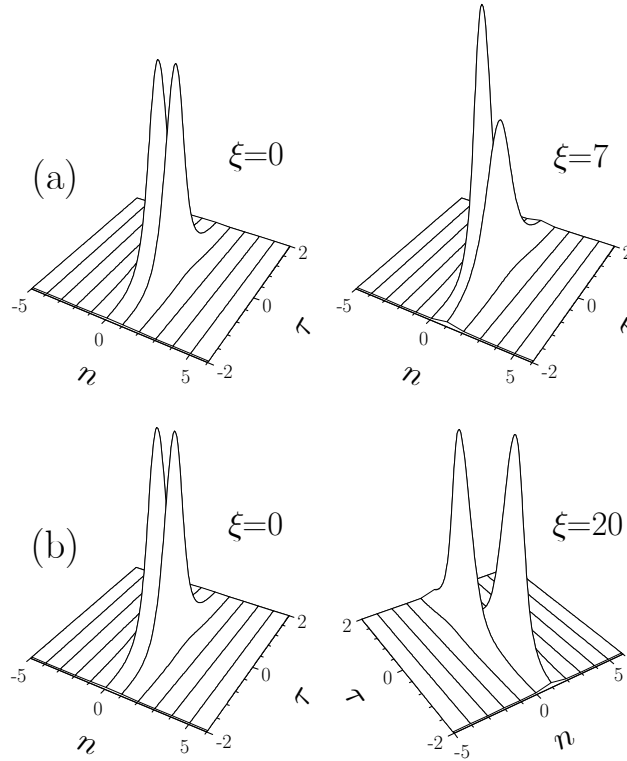
Figure 2.7: Propagation of unstable even (a) and twisted (b) solitons corresponding to $b_1 = 3$ in the presence of small perturbations found upon the linear stability analysis. Perturbation amplitude $\mu = 0.01$. Only the modulus of the amplitude of the SH wave is shown, at different propagation distances. Plots in left and right columns are shown with the same scale for easier comparison. Phase mismatch $\beta = -3$ and coupling constant $C = 0.1$.

In addition, we also thoroughly investigated the decay scenarios of the other two types of solitons: even and twisted. As stated before we have not observed any stable even or twisted continuous-discrete soliton. Fig. 2.7 shows possible instability scenarios for unstaggered even and unstaggered twisted solitons. We have found that a perturbed even soliton typically transforms into an odd one through increasing field oscillation in neighboring wave guides [Fig. 2.7(a)], and perturbed twisted soliton usually splits into two solitons which fly apart as when a repulsive force would act between them [Fig. 2.7(b)]. We have observed a π phase difference between the formed odd solitons and this could explain the repulsive force between them. Note that during the splitting process the resulting odd solitons are still locked in a specific waveguide, they are being allowed to repel in time. This unique feature comes with discreteness which does not allow the soliton energy to escape from the waveguide where it was initially located.

2.3 Multicolor vortex solitons in 2D photonic lattices

2.3.1 Introduction

The generation of nonlinear modes with a nontrivial phase, such as vortices is one important subject of study. In optics, vortices are associated with screw phase dislocations nested in light beams [151]. Here we are interested in vortices with a bright shape, i.e., dislocations nested in finite-size beams [152]. In homogeneous pure cubic and quadratic uniform media such ring-shaped vortex solitons suffer azimuthal instabilities which have been observed experimentally in different settings [153]. They can be made stable in media with competing nonlinearities [154], and in media with refractive index modulations that we address here.

Theoretical works showed that such complex localized structures, i.e., *lattice vortex solitons* exist when an optical lattice acts on a Kerr or photorefractive nonlinear crystal [91, 92, 155]. Recently, theoretical expectations were indeed confirmed experimentally by two independent groups [93, 94]. During the last years various families of solitons in arrays of weakly coupled waveguides made with quadratic nonlinear media have been also investigated [122, 123, 125, 126, 127, 156], and observed for the first time recently [128]. One-dimensional (1D) multicolor solitons in lattices with tunable strength have been also studied recently, and their potential applications for packing and steering single solitons have been investigated [157]. Two-dimensional geometries might support even robust soliton ensembles with phase dislocations, which is the aim of this work.

2.3.2 Model and stationary solutions

We study the system of coupled nonlinear equations that describe the interaction between the fundamental frequency (FF) and second-harmonic (SH) waves under conditions for type I second-harmonic generation in bulk materials in the absence of Poynting vector walk-off:

$$i\frac{\partial q_1}{\partial \xi} = \frac{d_1}{2}\left(\frac{\partial^2 q_1}{\partial \eta^2} + \frac{\partial^2 q_1}{\partial \zeta^2}\right) - q_1^* q_2 \exp\left(-i\beta\xi\right) - pR\left(\eta, \zeta\right) q_1$$

$$i\frac{\partial q_2}{\partial \xi} = \frac{d_2}{2}\left(\frac{\partial^2 q_2}{\partial \eta^2} + \frac{\partial^2 q_2}{\partial \zeta^2}\right) - q_1^2 \exp\left(i\beta\xi\right) - 2pR\left(\eta, \zeta\right) q_2, \quad (2.8)$$

where $q_1 = (2k_1/k_2)^{1/2} [2\pi\omega_0^2 \chi^{(2)} r_0^2/c^2] A_1$ and $q_2 = [2\pi\omega_0^2 \chi^{(2)} r_0^2/c^2] A_2$ represent the normalized complex amplitudes of the FF and SH fields, $k_1 = k(\omega_0)$, $k_2 = k(2\omega_0) \approx 2k_1$, r_0 is the transverse scale of the input beams, $\eta = x/r_0$, $\zeta = y/r_0$, $\xi = z/(k_1 r_0^2)$, $\beta = (2k_1 - k_2)k_1 r_0^2$ is the phase mismatch, $d_1 = -1$, $d_2 = -k_1/k_2 \approx -1/2$, and $p = 2\pi\omega_0^2 \delta\chi^{(1)} r_0^2/c^2$ is the lattice depth. The function $R(\eta,\zeta) = \cos(2\pi\eta/T)\cos(2\pi\zeta/T)$ describes the transverse refractive index profile, where T is the modulation period. The system (2.8) admits several conserved quantities, including the energy flow

$$U = \int \int_{-\infty}^{+\infty} (|q_1|^2 + |q_2|^2) d\eta d\zeta, \tag{2.9}$$

and the Hamiltonian

$$\begin{aligned} H = \int \int_{-\infty}^{+\infty} [&-\frac{d_1}{2}|\nabla q_1|^2 - \frac{d_2}{4}|\nabla q_2|^2 \\ &-\frac{1}{2}(q_1^*)^2 q_2 \exp(-i\beta\xi) - \frac{1}{2}q_1^2 q_2^* \exp(i\beta\xi) \\ &+\frac{\beta}{2}|q_2|^2 - pR(\eta,\zeta)|q_1|^2 - pR(\eta,\zeta)|q_2|^2] d\eta d\zeta, \end{aligned} \tag{2.10}$$

where $\nabla = \mathbf{e}_\eta(\partial/\partial\eta) + \mathbf{e}_\zeta(\partial/\partial\zeta)$, and $\mathbf{e}_\eta$, $\mathbf{e}_\zeta$ are unity vectors along η and ζ axes. We searched for the stationary solutions in the form

$$\begin{aligned} q_1 &= [u_1(\eta,\zeta) + iv_1(\eta,\zeta)]\exp(ib_1\xi) \\ q_2 &= [u_2(\eta,\zeta) + iv_2(\eta,\zeta)]\exp(ib_2\xi), \end{aligned} \tag{2.11}$$

where $u_{1,2}(\eta,\zeta)$ and $v_{1,2}(\eta,\zeta)$ are real functions, and $b_{1,2}$ are real propagation constants that verify $b_2 = \beta + 2b_1$. Substitution of the expressions (2.11) into Eq. (2.8) yields the following system of equations for the soliton profiles $u_{1,2}$ and $v_{1,2}$

$$\begin{aligned} \frac{d_1}{2}\left(\frac{\partial^2 u_1}{\partial\eta^2} + \frac{\partial^2 u_1}{\partial\zeta^2}\right) - u_1 u_2 - v_1 v_2 + b_1 u_1 - pR(\eta,\zeta)u_1 &= 0 \\ \frac{d_1}{2}\left(\frac{\partial^2 v_1}{\partial\eta^2} + \frac{\partial^2 v_1}{\partial\zeta^2}\right) - u_1 v_2 + v_1 u_2 + b_1 v_1 - pR(\eta,\zeta)v_1 &= 0 \\ \frac{d_2}{2}\left(\frac{\partial^2 u_2}{\partial\eta^2} + \frac{\partial^2 u_2}{\partial\zeta^2}\right) - u_1^2 + v_1^2 + b_2 u_2 - 2pR(\eta,\zeta)u_2 &= 0 \\ \frac{d_2}{2}\left(\frac{\partial^2 v_2}{\partial\eta^2} + \frac{\partial^2 v_2}{\partial\zeta^2}\right) - 2u_1 v_1 + b_2 v_2 - 2pR(\eta,\zeta)v_2 &= 0. \end{aligned} \tag{2.12}$$

We solved the system of coupled equations (2.12) numerically by using a standard relaxation method. The lattice vortex soliton families are one-parameter families defined by the propagation constant b_1 for any given period of the modulation T, lattice depth p and phase mismatch β. Since one can use scaling transformations $q_{1,2}(\eta, \zeta, \xi, \beta, p) \rightarrow \chi^2 q_{1,2}(\chi\eta, \chi\zeta, \chi^2\xi, \chi^2\beta, \chi^2 p)$ to obtain various families of solitons from a given family, we have selected the transverse scale r_0 such that the modulation period is given by $T = \pi/2$ and then we have varied b_1, β, and p.
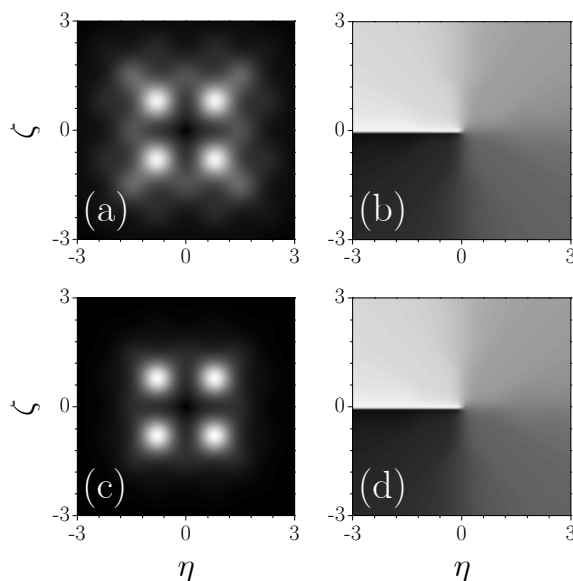
Figure 2.8: (a) Profile and (b) phase of vortex solitons supported by the harmonic lattice at $b_1 = 1.07$. (c) Profile and (d) phase of vortex soliton at $b_1 = 2$. Only the FF wave is shown. Lattice depth $p = 4$, phase mismatch $\beta = 0$.

The simplest vortex soliton with unit topological charge in two-dimensional periodic lattice is shown in Fig. 2.8. It comprises four main humps arranged in a square configuration with a stair-like phase structure that is topologically equivalent to the phase of a conventional vortex in uniform medium [see Fig. 2.8(b,d)]. The positions of the soliton intensity maxima almost coincide with the positions of the local maxima of the lattice. Note that the singularity of these vortex solitons is centered between four lattice sites, that is they belong to the class of the, so called, *off-site* vortex soliton. In the model we investigated here there exist also a family of *on-site* vortex

solitons (not shown here). In that case the phase singularity is centered on
a lattice site [91, 93, 94]. We will restrict ourselves here to the case of the
off-site vortex solitons. It is interesting to note that these stationary struc-
tures somehow resemble the four-soliton molecules carrying orbital angular
momentum that were investigated in a variety of nonlinear media in both
two-dimensional and three-dimensional geometries [158, 159, 160]. The typ-
ical stair-like phase distribution in the case of the above mentioned soliton
molecules is clearly seen in panels (b) and (d) of Fig. 2.8 for the lattice vor-
tex solitons. We want to mention that the 1D quadratic waveguides were
also shown to support various families of multipeaked solitons, which display
combinations of in-phase and out-of-phase odd solitons, the latter ones with
π phase jumps between neighbor solitons [157].
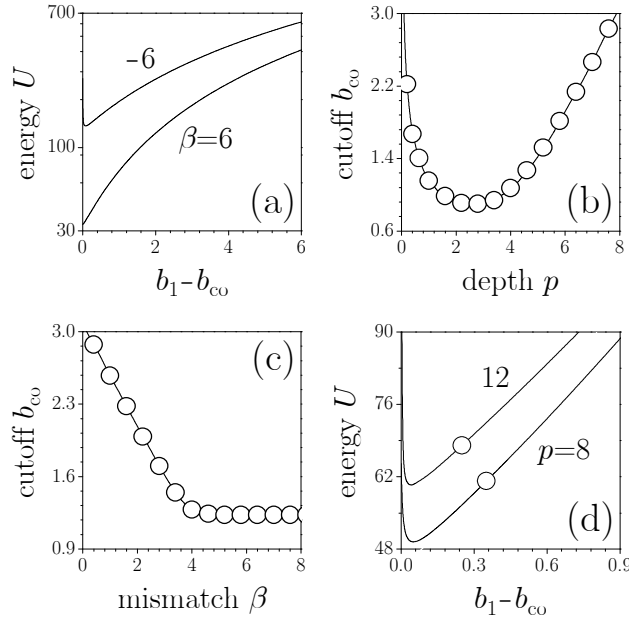
Figure 2.9: (a) Vortex soliton energy flow versus propagation constant for
different values of phase mismatch at $p = 8$. (b) Propagation constant cutoff
versus lattice depth at $\beta = 0$. (c) Cutoff versus phase mismatch at $p = 8$.
(d) Stability and instability domains for different lattice depths at $\beta = 0$.
Circles show critical value of propagation for stabilization.

It should be noted that at low powers (small b_1) the lattice vortex soli-
tons are quite wide and spread out over many lattice sites [Fig. 2.8(a)], while
at high powers the energy is mainly localized within the corresponding four
peaks [Fig. 2.8(c)]. We did not find four-hump structures with higher topo-
logical charges (2 or more), and all other higher-order stationary structures

we have found (for example, lattice vortex solitons with eight humps) were found to be unstable on propagation. Thus, in this work we will restrict ourselves to the study of the properties of simplest four-hump lattice vortex solitons.

In order to characterize the families of lattice vortex solitons we have calculated the energy flows associated with these stationary solutions as well as their existence domains for given lattice depth p and phase mismatch β. As a general rule, the energy flow of the four-hump lattice vortex solitons is a non-monotonic function of the propagation constant [even if this cannot be seen directly from Fig. 2.9(a) without zooming]. Note that in Fig. 2.9(a,d) on the abscise we have plotted the difference $(b_1 - b_{co})$ between the propagation constant b_1 and cutoff value b_{co}. The cutoff value depends on both the phase mismatch β and lattice depth p. For example at $p = 8$ cutoff is given by $b_{co} = 6.065$ for $\beta = -6$, while $b_{co} = 1.23$ for $\beta = 6$. The cutoff b_{co} is a nonmonotonic function of the lattice depth p [Fig. 2.9(b)]. It tends to infinity at $p \to 0$ and $p \to +\infty$. One can see from Fig. 2.9(c) that in the presence of the lattice the dependence $b_{co}(\beta)$ differs from that for quadratic solitons in continuous media: $b_{co}(\beta) = \max\{-\beta/2, 0\}$. Thus at $\beta \to -\infty$ cutoff is approximately given by $(\beta - \beta_0)/2$, while at $\beta \to +\infty$ one has $b_{co} = b_0$, where β_0 is the mismatch shift due to the lattice. Both b_0 and β_0 growth with p. This property holds also for the one-dimensional lattice solitons in quadratic nonlinear media [157].

The periodic refractive index modulation affects also the energy sharing between FF and SH waves. For example, at a given phase mismatch β, the fraction of the total energy flow carried by the SH wave increases with increase of the lattice depth. Moreover, near the cutoff, the SH wave spreads over more lattice sites than the FF beam. As in the case of a uniform media, in the lattice with fixed depth p the part of energy flow carried by the SH wave decreases with increase of phase mismatch β.

2.3.3 Dynamics and excitation

To investigate the stability of the lattice vortex solitons, we have performed extensive numerical simulations of the evolution dictated by Eq. (2.8) with the input conditions $q_1(\xi = 0) = [u_1(\eta, \zeta) + iv_1(\eta, \zeta)][1 + \rho_1(\eta, \zeta)]$ and $q_2(\xi = 0) = [u_2(\eta, \zeta) + iv_2(\eta, \zeta)][1 + \rho_2(\eta, \zeta)]$, where $u_{1,2}$ and $v_{1,2}$ are the exact solutions of Eq. (2.12) and $\rho_{1,2}$ are random functions with Gaussian
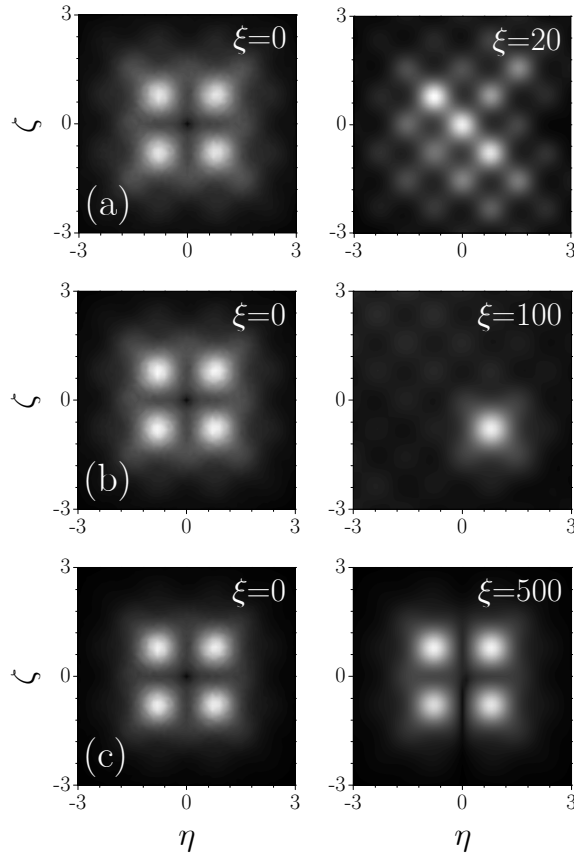
Figure 2.10: Propagation of vortex solitons with $b_1 = 3.1$ (a), 3.4 (b), and 5 (c) in the presence of input noise with variance $\sigma^2_{noise} = 0.01$. FF wave profile is shown at different propagation distances. Lattice depth $p = 8$, phase mismatch $\beta = 0$.

distribution and variance $\sigma^2_{noise} = 0.01$. We have propagated the perturbed four-hump lattice vortex solitons over thousands of units for various values of the physical parameters involved (β, p, U).

Our simulations show that there exists a narrow instability band near the propagation constant cutoff b_{co} for vortex solitons, but above a certain critical value of propagation constant they appear to become free of instability. We have found that the width of instability domain of lattice vortex solitons decreases with increase of the depth of the lattice p [Fig. 2.9(d)]. For example, as depicted in Fig. 2.9(d), the width of instability domain on propagation constant for $p = 12$ is approximately given by 0.24, while for $p = 8$ it is 0.35.

A few representative decay scenarios for the unstable four-hump lattice vortex solitons with unit topological charge are shown in Fig. 2.10. In the row (a) of Fig. 2.10 we show the typical decay of the unstable vortex soliton in the vicinity of the cutoff on propagation constant b_{co}. The initial energy of the localized structure is spreading out during evolution across the whole lattice and the vortex soliton disappears. Notice that this type of instability develops exponentially. In the rest part of the instability domain located closer to critical value of the propagation constant, we encountered oscillatory-type instability. Upon development of this instability vortex soliton transforms into a fundamental (ground state) lattice soliton that is the most robust and energetically stable state of the system [see row (b) of Fig. 2.10], through increasing oscillations of four intensity maxima of the vortex.
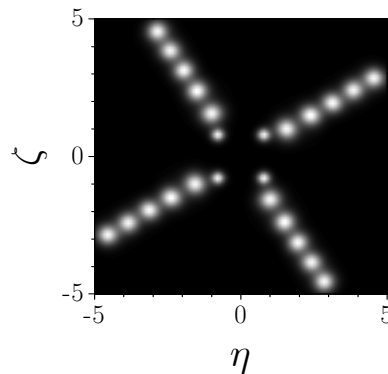
Figure 2.11: Snapshot images showing decay of the stable vortex solitons caused by removal of the lattice. Only SH wave profile is shown. Images are taken after each 2.5 propagation units. Lattice depth $p = 8$, phase mismatch $\beta = 0$.

One of the important results of this study is that the lattice vortex soliton becomes completely stable when its propagation constant exceeds a critical value b_{cr}, i.e., almost in the entire existence domain [see Fig. 2.9(d)]. In row (c) of Fig. 2.10 we have plotted, for the sake of illustration, the initial and the final (after 500 propagation units) intensity distributions of a stable lattice vortex soliton. Comparing to the soliton molecules investigated in bulk nonlinear media, which were shown to be *metastable* physical objects under suitable conditions, we conclude that, as expected on physical grounds, the effect of the two-dimensional lattice is to arrest the rotation of the soliton molecule and thus to assure the complete stabilization of the soliton complex. Since lattice causes strong azimuthal modulation of the vortex soliton, lattice

removal results in complete soliton decay into four filaments, as shown in Fig. 2.11. Escape angles of filaments decrease with increase of input energy flow of vortex soliton.

To understand lattice vortex solitons generation from a radially symmetric input beam carrying a screw phase dislocation nested in the center and to show that different sets of output solitons can be obtained with different combinations of topological charges and shapes of the input beams we performed a comprehensive set of simulations of Eq. (2.8) with the input conditions corresponding to Gaussian beams with a phase dislocation nested in the center:

$$q_1(\xi = 0, r, \varphi) = Ar^{|m_1|} \exp(im_1\varphi) \exp(-r^2/w_1^2)$$
$$q_2(\xi = 0, r, \varphi) = Br^{|m_2|} \exp(im_2\varphi) \exp(-r^2/w_2^2), \qquad (2.13)$$

where $r = (\eta^2 + \zeta^2)^{1/2}$ is the radius, φ is the azimuthal angle, A and B are amplitudes of FF and SH waves , w_1 and w_2 are beam widths. Below we set the width $w_1 = w_2 = 1$ and suppose that topological charge of FF wave is given by $m_1 = 1$.
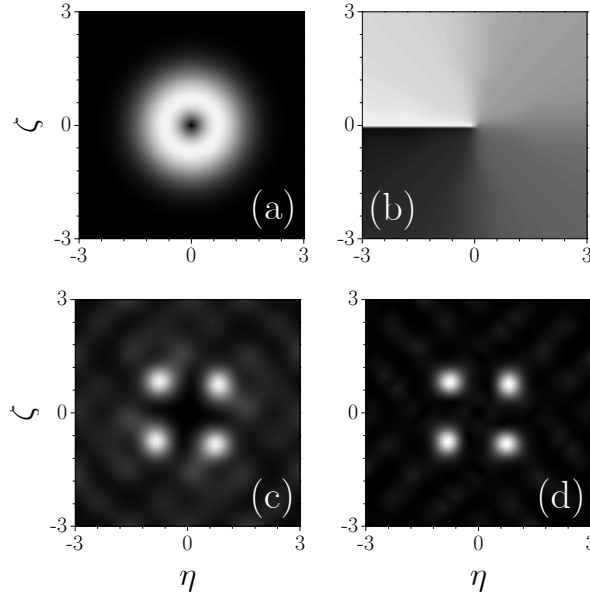
Figure 2.12: Generation of the vortex solitons with only FF input. (a) Field and (b) phase distributions of the input FF beam with topological charge $m_1 = 1$. (c) FF beam and (d) SH beam at $\xi = 15$. Lattice depth $p = 8$, phase mismatch $\beta = 0$.
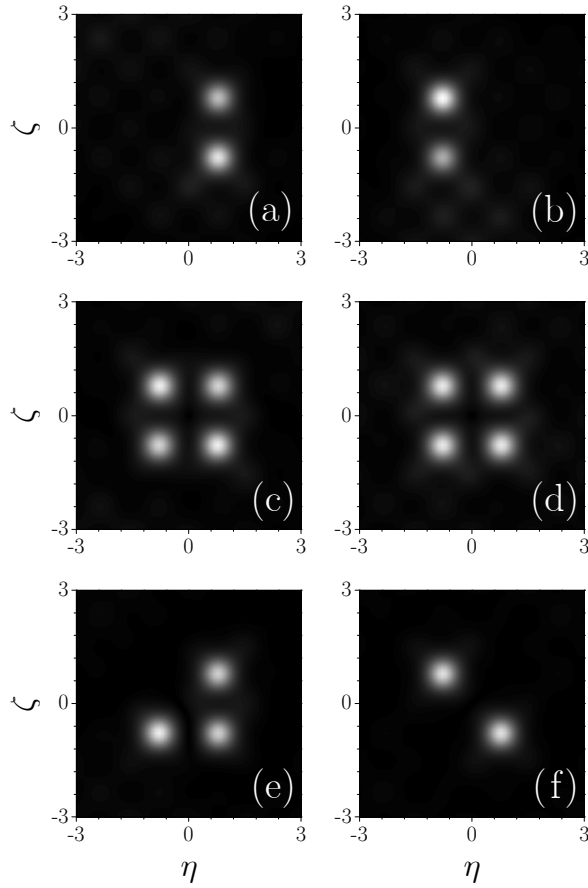
Figure 2.13: Soliton algebra. The output soliton distribution depends on the topological charges m_1 of FF wave and m_2 of SH wave, respectively. In all cases, $m_1 = 1$. In (a)-(d), the amplitude of FF wave $A = 20$ and the amplitude of SH wave $B = 2$. In (e) and (f) $A = 20$ and $B = 0.5$. Plots (a)-(f) correspond the topological charges $m_2 = 1, 3, 4, 6, 7, 8$ respectively and show the output SH field distribution at $\xi = 100$. Lattice depth $p = 8$, phase mismatch $\beta = 0$.

First, we consider nonseeded vortex soliton generation at $B = 0$. At low input powers both input FF wave and generated SH wave exhibit complete diffraction, and input beam energy is redistributed between many lattice sites. With the increase of input energy flow [i.e. by increasing A in Eqs. (2.13)] the generation of lattice vortex soliton with unit topological charge becomes possible as shown in Fig. 2.12. Lattice soliton generation is accompanied with energy radiation [Fig. 2.12(c) and (d)] but the ratio between radiative losses and the output soliton energy flow decreases with increase of input energy flow.

In the case of seeded SH generation ($B \neq 0$ and $B \ll A$), the output field distribution can be controlled by the input topological charge of SH wave. For $m_1 = 1$ vortex soliton generation is possible only for the vorticity-matched case when $m_2 = 2$, while all other values of m_2 correspond to formation of trivial-phase soliton distributions, whose structure is dictated by lattice symmetry and energy exchange between FF and SH waves at the initial stage of propagation. Some representative output distributions are shown in Fig. 2.13. These plots show that the concept of "soliton algebra" previously explored in homogeneous media [161], does also apply in the presence of lattices, offering new opportunities for controlling the soliton dynamics.

2.4   Summary

We have studied stable, spatiotemporal continuous-discrete solitons in quadratic nonlinear waveguide arrays. Families of unstaggered odd, even and twisted stationary solutions have been found and thoroughly characterized. The linear stability analysis is in agreement with the direct simulations indicating that the odd continuous-discrete solitons obey the Vakhitov-Kolokolov stability criterion. The salient point put forward is that most of the spatiotemporal unstaggered odd solitons are stable against perturbations. This result is important in view of the generation of discrete solitons with pulsed light in the context of the exploration of their potential application to switching schemes.

In particular, we have discovered that periodic lattices imprinted in quadratic nonlinear media can support four-hump vortex solitons with unit topological charge that are stable provided that their propagation constant

is above a certain critical value. Below this critical value we have identified two types of instabilities: (i) an exponential-type of instability leading to the final decay and spread out of the solitons across the lattice and (ii) an oscillatory-type instability leading to the transformation of the lattice vortex soliton into a fundamental soliton without internal vorticity. We investigated the generation of the multicolor lattice vortex soliton from Gaussian beams with nested phase dislocations. The possibility to generate different output lattice soliton patterns, with and without vorticity, by varying the topological charges and amplitudes of the input beams in seeded excitation configurations, has been discussed. The generation of a 2D periodic potential in quadratic nonlinear media is a challenging issue, even though fabrication of 1D lattices has been already achieved using techniques which might be extended to 2D geometries. Also, the results presented here might be relevant to suitable atomic-molecular Bose-Einstein condensates held in optical lattices.

Chapter 3

Reconfigurable Optically-induced Networks

3.1   Introduction

As shown in the preceding chapter, a periodic array of optical waveguides creates a novel kind of devices in which new types of spatial solitons (discrete or lattice) can be generated and studied experimentally. Discrete optical solitons in waveguide arrays have attracted large attention because of their potential for all-optical switching and power- and angle-steering (for a recent review see Ref. [119]). In particular, the possibility of construction of two-dimensional soliton networks of nonlinear waveguide arrays was established [162, 163]. In landmark recent experiment [87, 88, 89, 131, 164, 165], it was shown that periodic nonlinear lattices with flexibly controlled refractive index modulation depth and period can be induced all-optically, in particular, in photorefractive media. Such lattices constituted by continuous nonlinear media with an optically imprinted modulation of refractive index offer a number of new opportunities for all-optical manipulation of light as well [166, 167], since they can operate in both weak- and strong-coupling regimes, depending on the depth of refractive index modulation.

The technique of optical lattice induction opens a wealth of opportunities for creation of waveguiding configurations with various nondiffracting light beams. An important example is set by Bessel beams, which under ideal conditions do not diffract upon propagation. Single-mode Bessel beams allow creation of optically-induced lattices with radial symmetry, where solitons

can be set into controllable rotary motion [95, 168]. Combination of several incoherent Bessel beams can be used to build couplers and switching junctions that can trap and steer solitons, while junction properties [169] can be tuned by intensity, intersection angles, and widths of central cores of Bessel beams [170]. Notice that combinations of coherent or incoherent Bessel beams can be created experimentally [171, 172], by using computer generated holograms [173] or reconfigurable spatial light modulators.

In this chapter, we put forward the concept of reconfigurable structures created with arrays of mutually incoherent parallel Bessel beams in Kerr-type nonlinear media. Each of the Bessel beams forming the structure induces a well-pronounced guiding channel that overlaps with its neighboring through slowly decaying tails. In Section 3.2, the theoretical model governing such optically-induced networks is introduced. In section 3.3, we address the properties of reconfigurable directional couplers optically induced by Bessel beams. In section 3.4, reconfigurable soliton networks optically-induced by arrays of nondiffracting Bessel beams are investigated. In section 3.5, we consider the reconfigurable junctions optically-induced by nondiffracting Bessel beams.

3.2   Model

We consider the propagation of light along the ξ axis of a focusing Kerr-type nonlinear media with an optically-induced modulation of the refractive index in the transverse direction. The evolution of the complex light field amplitude q is described by the reduced equation

$$i\frac{\partial q}{\partial \xi} = -\frac{1}{2}(\frac{\partial^2 q}{\partial \eta^2} + \frac{\partial^2 q}{\partial \zeta^2}) - q|q|^2 - pR(\eta, \zeta, \xi)q, \qquad (3.1)$$

where the transverse η, ζ and the longitudinal ξ coordinates are scaled to the characteristic beam width and diffraction length, respectively. We suppose here that the refractive index modulation is induced optically by the multiple incoherent zero-order Bessel beams, so that the refractive index profile features the total intensity of the interference pattern, as it occurs in photorefractive crystals. The guiding parameter p is proportional to the refractive index modulation depth, which is assumed to be comparable to the nonlinear contribution of the refractive index. The function $R(\eta, \zeta, \xi)$

describing the refractive index modulation profile is given by

$$R(\eta, \zeta, \xi) = \sum_{k=1}^{N} J_0^2\{(2b_{\texttt{lin}})^{1/2}[(\eta - \eta_k + \alpha_k\xi)^2 + (\zeta - \zeta_k)^2]^{1/2}\}, \qquad (3.2)$$

where N is the total number of beams in the array, the scaling parameter $b_{\texttt{lin}}$ defines the radii of rings of Bessel beams and here is taken small enough to ensure that the width of the central core of Bessel beams (20 μm) largely exceeds the wavelength; finally, η_k and ζ_k are the coordinates of Bessel beam center, and α_k defines the head-on intersection angle. Note that Eq.(3.1) admits several conserved quantities including the power or energy flow

$$U = \int_{-\infty}^{\infty} \int_{-\infty}^{\infty} |q|^2 d\eta d\zeta. \qquad (3.3)$$

The stationary solutions of Eq.(3.1) that propagate along the guiding channels of the network have the form $q(\xi, \eta, \zeta) = \omega(\eta, \zeta)\texttt{exp}(ib\xi)$, where $\omega(\eta, \zeta)$ is a real function and b is the real propagation constant. General families of soliton solutions are defined by the propagation constant, and by guiding and scaling parameters p and $b_{\texttt{lin}}$. Since scaling transformation $q(\eta, \zeta, \xi, p) \to \chi q(\chi\eta, \chi\zeta, \chi^2\xi, \chi^2 p)$ can be applied to obtain various soliton families from a given one (note that this also implies variation of the lattice), below we fix $b_{\texttt{lin}}$ and vary b and p. Families of stationary solutions were obtained by solving Eq.(3.1) with a relaxation algorithm.

3.3 Reconfigurable directional couplers

First, we address the properties of reconfigurable directional couplers induced with collinear incoherent Bessel beams (namely, intersection angle $\alpha_k = 0$). Because of the overlap of the soliton tails guided by neighboring Bessel channels on propagation. The rate of the energy exchange is given by the overlap integral, which increases with a decrease of separation between waveguides or with an increase of refractive-index modulation depth.

Figure 3.1 shows different soliton switching scenarios in two-core [Figs. 3.1 (a)-(c)] and three-core [Figs. 3.1 (d)-(f)] couplers for different input powers. At small powers one achieves almost total energy transfer from the input guiding channel into neighboring channels at coupling length $\xi = L_c$ [Figs. 3.1 (a) and (d)]. Note that in a three-core coupler the energy is equally
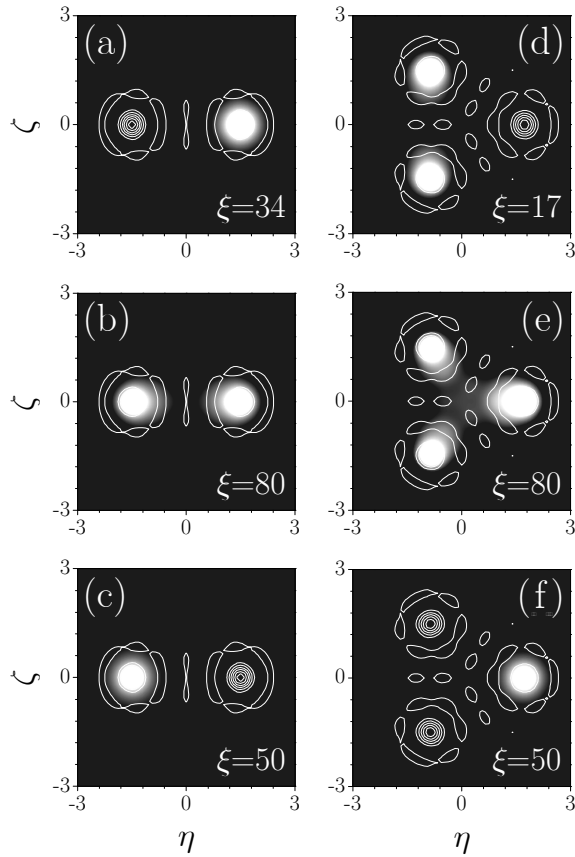
Figure 3.1: Switching in (a)-(c) two- and (d)-(f) three-core optically induced couplers. Output intensity distributions are shown at $\xi = L_c$. White contour curves are aids to the eye and show the positions of optically induced channels. In the two-core coupler the soliton was launched into the left-hand channel; in the three-core coupler it was launched into the right-hand channel. Input power (a) $U = 1.56$, (b) 1.67, (c) 3.1, (d) 1.56, (e) 2.15, and (f) 2.68. Parameters: modulation depth $p = 5$, separation between Bessel beams $2\eta_0 = 3$, $b_{\tt lin} = 10$.

redistributed between two output channels. Similar phenomena occur with more-complicated Bessel beam arrays arranged in ring configurations when the energy flow of a soliton launched into a single channel is redistributed among all other channels at the output. Because of the periodic character of the energy exchange the input field distribution is completely restored at $\xi = 2L_c$. At the critical power level, the energy is equally distributed among all channels of the coupler [Figs. 3.1 (b) and (e)]. In this case, coupling length L_c diverges. Finally, at high powers there is no energy transfer into neighboring channels [Figs. 3.1 (c) and (f)]. Thus the optically induced coupler behaves as the sought-after nonlinear directional coupler.
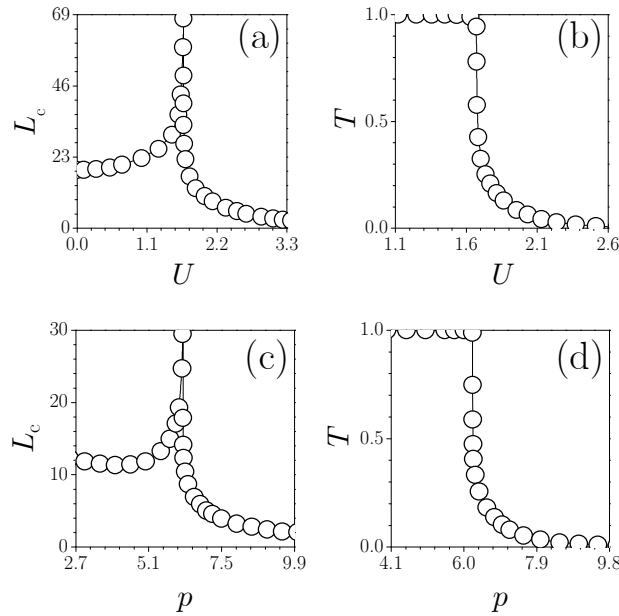
Figure 3.2: (a) Coupling length and (b) normalized transmission efficiency versus input power at $p = 5$, and separation between Bessel beams $2\eta_0 = 3$. (c) Coupling length and (d) normalized transmission efficiency versus modulation depth at $U = 2$ and separation between Bessel beams $2\eta_0 = 2$. In both cases $b_{\texttt{lin}} = 10$.

The variation of the coupling length and the normalized transmission efficiency versus the input power for a two-core coupler are shown in Figs. 3.2 (a) and (b), respectively. The transmission efficiency is defined as the ratio of energy concentrated in the output channel to that concentrated in the input channel. The coupling length increases and the transmission efficiency decreases as the input power approaches the critical value corresponding to

equal energy distribution in all channels. To stress the reconfigurability afforded by optically-induced couplers, in Figs. 3.2 (c) and (d) we plot the coupling length and the transmission depth p at fixed input power. The modulation depth can be directly controlled by intensities of Bessel beams forming the coupler. Because at fixed power the soliton supported by a single channel becomes narrower with increasing p, the transmission efficiency decreases above the critical modulation depth, and all switching conditions from total to negligible energy transfer can be achieved.
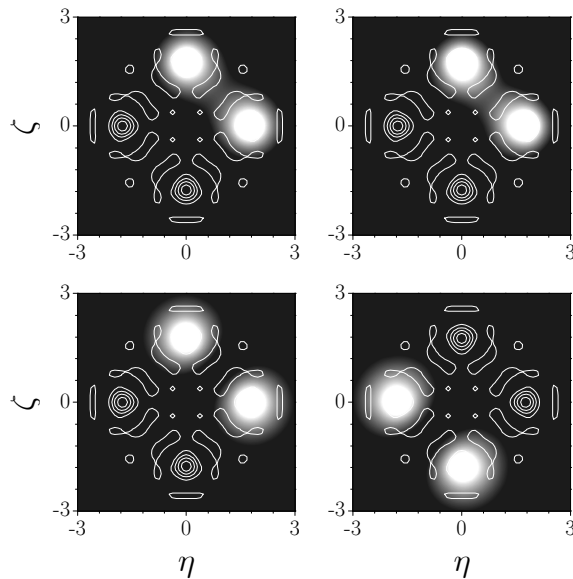
Figure 3.3: Switching scenarios in the matrix of four Bessel waveguides when two solitons are launched into neighboring optically-induced guides. Top: input (left) and output (right) intensity distributions for in-phase solitons. Bottom: input (left) and output (right) intensity distributions for out-of-phase solitons. Input power $U = 2.14$, modulation depth $p = 5$, separation between Bessel beams $\eta_0 = 2.5$, and $b_{\mathtt{lin}} = 10$.

We also study soliton switching in multi-core directional couplers creased by arrays of incoherent Bessel beams. Two representative examples of the existing possibilities with four Bessel-beam couplers are shown in Fig. 3.3 and Fig. 3.4.

Here we focus on the results obtained by simultaneous excitation of several coupler channels. We launch into neighboring or opposite channels two identical solitons whose profiles were found from Eq. (3.1) by means of relaxation method, under the assumption that only one Bessel beam is present. In the presence of other guiding channels (with the second beam launched

into one of them) the propagation process is accompanied by periodic transfer of the energy between different channels that are coupled via their tails. The energy exchange is very sensitive to the relative phase of input beams. We show the output intensity distributions at the distance corresponding to the maximal energy transfer into two channels that were not initially occupied. Thus, in Fig. 3.3, where solitons are launched into neighboring channels, one finds that the energy transfer is negligible for in-phase solitons and almost 100% efficient for out-of-phase solitons. The outcome changes drastically when input solitons are launched into the opposite coupler channels. Therefore, the important result is that by varying the refractive index modulation depth (which is proportional to the intensity of nondiffracting Bessel beams inducing the coupler), the separation between Bessel channels, the power and phases of input solitons, one obtains a variety of switching scenarios.
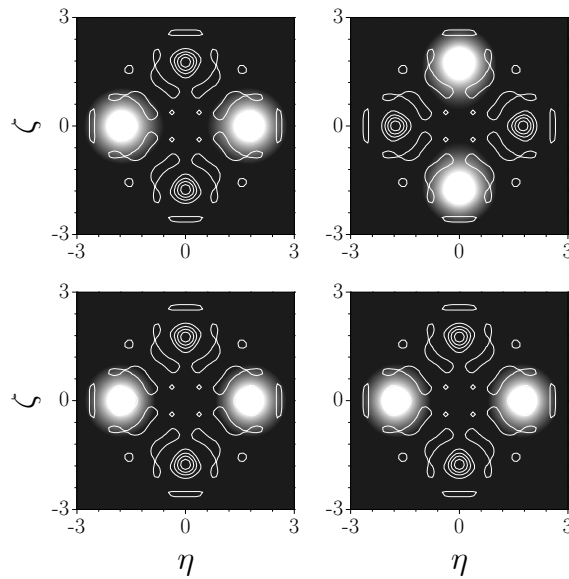
Figure 3.4: Switching scenarios in the multicore coupler optically-induced by four Bessel beams when two solitons are launched into opposite waveguides. Top: input (left) and output (right) intensity distributions for in-phase solitons. Bottom: input (left) and output (right) intensity distributions for out-of-phase solitons. Input power $U = 2.14$, modulation depth $p = 5$, separation between Bessel beams $\eta_0 = 2.5$, and $b_{\texttt{lin}} = 10$.

3.4   Reconfigurable soliton networks

One can construct more complex structures by collinear Bessel Beams, the simplest *line* network created with an array of Bessel beams equally spaced along $\eta-$axis is shown in Fig.3.5(a). Because of the mutual incoherence of Bessel beams in the network, the interference pattern between pronounced guiding channels is suppressed. Such network can support stationary solitons whose profiles are elongated along the η direction. This is especially evident for low-power solitons that extend over several network channels [Fig. 3.5(b)]. With increase of the propagation constant (or power) the soliton width decreases [Fig. 3.5(c)], so that in the limit $b \to \infty$ soliton occupies only one channel and its power approaches the critical value of the unstable soliton supported by uniform cubic media. Nevertheless, for the considered set of parameters the soliton power was found to be a monotonically growing function of propagation constant that implies stability of stationary soliton solutions in the entire domain of their existence according to the Vakhitov-Kolokolov criterion. Below we consider broad low-power solitons that can be set in motion across the network by imposing the initial linear phase tilt (or angle) $\exp(i\theta\eta)$ onto the input field distribution. Such tilted beams are no more stationary solitons, but they can travel across the uniform network along the η direction almost without the radiation losses [Fig. 3.5(d)], that otherwise unavoidably appear upon crossing of the guiding channels of the structure and that then lead to a fast trapping of high-power narrow solitons.

One of the interesting results found in this work is shown in Fig. 3.5(d): Removal of one of the Bessel beams from the array can cause deflection of soliton in the direction opposite to the input tilt. This process is accompanied by a strong beam reshaping in the deflection point, but the resulting beam shape and the modulus of the propagation angle are typically very close to the input ones. The soliton deflection at the network defect is a simplest example of operation accessible with optically-induced networks whose structure (open and closed paths) can be easily changed by blocking or switching of the individual Bessel beams from the array. The potential of such structures for creation of all-optical photonic circuits is readily apparent.

Arrays of Bessel beams can be used to induce more complex networks that feature one or several bends at different angles that can even exceed
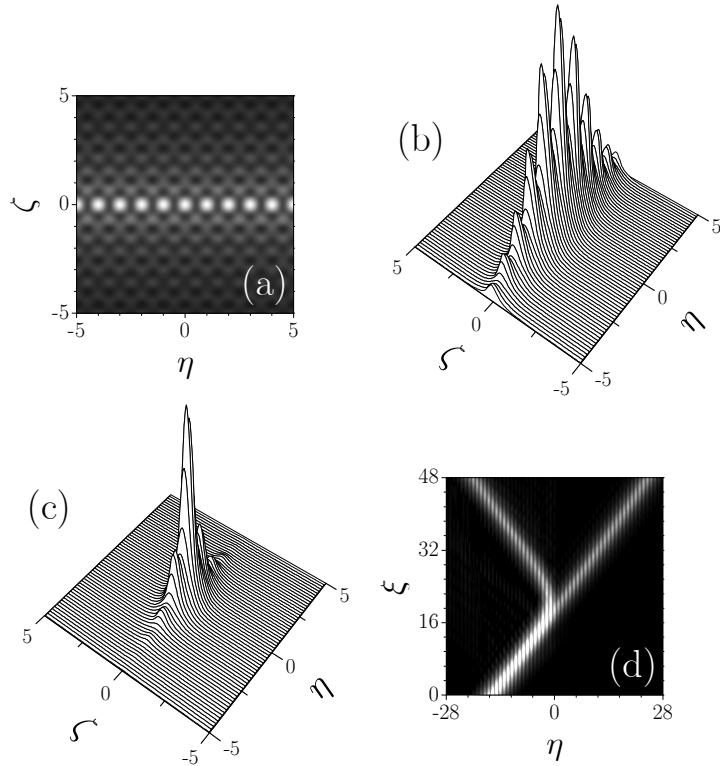
Figure 3.5: (a) Linear network created with array of Bessel beams. Profiles of solitons with power $U = 0.8$ (b) and $U = 1.34$ (c) supported by network shown in (a). (d) Drift of soliton with power $U = 0.8$ and incident angle $\theta = 1$ in uniform network and its reflection on the network defect. Intensity distributions showing drift and deflection are superimposed and taken at $\zeta = 0$. In all cases modulation depth $p = 15$ and separation between Bessel waveguides $\eta_0 = 1$.

$90°$. Two representative examples of broad soliton propagation in such bent networks are shown in Fig. 3.6(a) and (b). Upon passing through the network, the soliton beams experience only slight transformation of their shape despite of the fact that they are forced to change propagation plane. The radiative losses in both cases shown in Fig. 3.6 are small (less than 4%). The networks shown in Fig. 3.6(a) and (b) are similar to the technologically fabricated networks studied in Refs [162, 163]; however, the tunability afforded by the technique of optical-induction offers the additional advantage of the reconfigurability. Another interesting phenomenon occurs in the circular network, as the one depicted in Fig. 3.6(c). In this case soliton
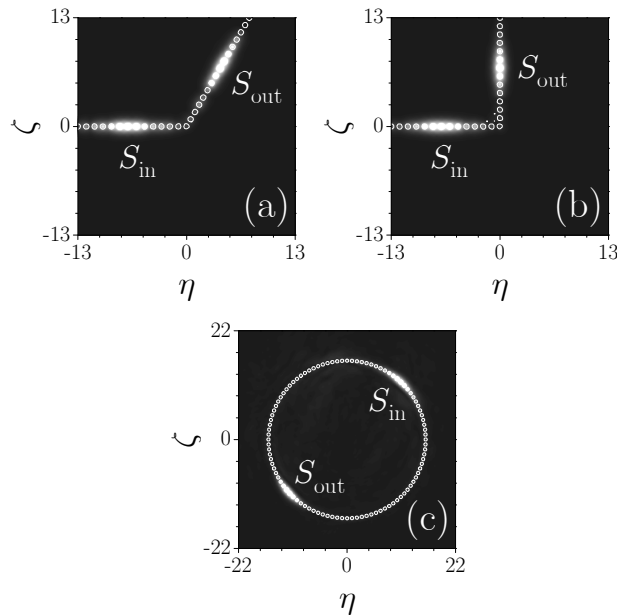
Figure 3.6: Soliton propagation across 60°-bend (a), 90°-bend (b), and circular (c) networks created with arrays of Bessel beams. White contour lines are to help the eye and show positions of the induced guiding channels. Labels S_{in}, S_{out} stand for input and output soliton positions. Input power $U = 0.8$, incident angle $\theta = 1$, modulation depth $p = 15$, and separation between Bessel waveguides $\eta_0 = 1$.

can perform rotary motion across the ring, with its power remaining almost constant because of small radiation losses. Switching off elements of the circular networks causes reversal of the soliton rotation direction. The similar results were obtained in a variety of cases, in terms of input light conditions and lattice-creating Bessel beams. These examples illustrate that the networks induced by the Bessel beam behave like *soliton wires* and thus they can be effectively used to manage soliton paths.

3.5   X-Junctions

In this section, we address properties of X-junctions created with two intersecting Bessel beams ($N = 2$), and intersection angle $\alpha_1 = -\alpha_2 = \alpha$. The initial separation between guiding channels is high enough that, at the initial stage of propagation, a soliton launched into the right-hand channel of the junction is almost unaffected by the presence of the left-hand channel.

We calculate the transmission efficiency, defined as the ratio of output power concentrated in the central core of the left channel at $\xi = 2\eta_0/\alpha$ to the input power concentrated in the central core of the right channel at $\xi = 0$.
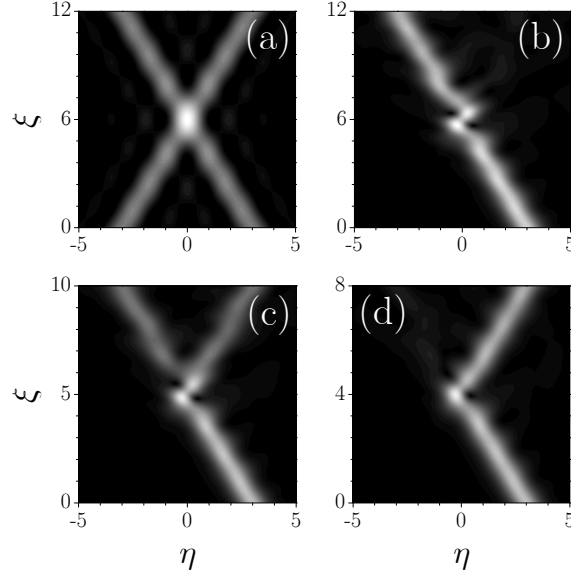
Figure 3.7: (a) X-junction made by intersecting incoherent Bessel beams at $\alpha = 0.5$. Different soliton propagation scenarios at (b) $\alpha = 0.5$, (c) $\alpha = 0.6$, and (d) $\alpha = 0.75$ are shown. Intensity distribution are shown at $\zeta = 0$. In all cases $p = 5$, $U = 2$, separation between Bessel beams $2\eta_0 = 6$, and $b_{\mathtt{lin}} = 2$.

Figure 3.7(a) shows that the intersection of two incoherent Bessel beams produces an area of locally increased refractive index that is elongated along the ξ axis. The smaller the intersection angle, the longer the area of locally increased refractive index. When the soliton from the right-hand channel enters this area it is bounced back, as one can see from Figs 3.7(b)-(d). Depending on the intersection angle (i.e., the length of intersection area), the soliton remains in the input channel [Fig. 3.7(b)], splits into two beams [Fig. 3.7(c)], or experiences total switching into the left-hand channel [Fig. 3.7(d)]. The potential applications of this effect for angle-controlled soliton switching are clearly visible.

The normalized transmission efficiency versus intersection angle is shown in Fig. 3.8(a). Almost 100% switching contrast can be achieved in such an X-junction. With further growth of α the transmission efficiency monotonically decreases. Small angles are not shown in Fig. 3.8(a) because in this case
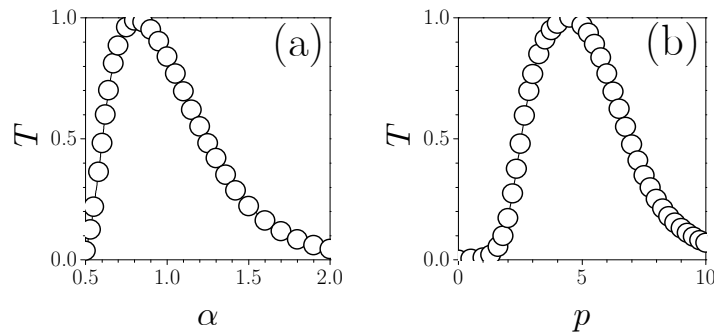
Figure 3.8: (a) Nonlinear transmission efficiency versus intersection angle at $p = 5$ and $U = 2$. (b) Normalized transmission efficiency versus modulation depth at $\alpha = 0.75$ and $U = 2$. Parameters: separation between Bessel beams $2\eta_0 = 6$ and $b_{\texttt{lin}} = 2$.

small modifications of the input angle result in drastic changes in switching dynamics and fast oscillations of the curve $T(\alpha)$ at $\alpha \to 0$. We found that switching with high contrast can be achieved by tuning the depth of refractive index modulation p [Fig. 3.8(b)]. There exists an optimal value of p that yields almost total soliton switching into the left-hand channel at fixed input power and intersection angle. This is another confirmation of the potential of reconfigurable guiding structures induced with arrays of Bessel beams for all-optical soliton control.

3.6   Summary

In conclusion, we have studied reconfigurable couplers, soliton networks, and X-junctions induced by multiple incoherent nondiffracting Bessel beams in Kerr-type nonlinear media. We showed that dynamics of soliton beams propagating in such optically-induced structures can be used for all-optical manipulation of light, with the important additional advantage of the *reconfigurability* afforded the optical-induction concept. The scheme holds for light signals propagating in focusing media and for Bose-Einstein condensates trapped in optical lattices induced by Bessel beams.

Chapter 4

Solitons in Nonlocal Optical Lattices

4.1 Overview

Properties of solitons supported by media with local nonlinear response are well established. However, under appropriate conditions, the nonlinear response of materials can be highly nonlocal, a phenomenon that drastically affects the propagation of intense laser radiation [174, 175]. The nonlocality of nonlinear response comes into play when the transverse extent of the laser beam becomes comparable with the characteristic response length of the medium. The nonlocal nonlinear response allows suppression of the modulation instability of the plane waves in focusing media [176, 177, 178, 179]; it prevents catastrophic collapse of multidimensional beams [180, 181, 182, 183], and stabilizes complex soliton structures, including vortex solitons [184, 185]. Principally new effects attributed to nonlocality have been studied in photorefractive crystals [57, 186], thermo-optical materials [187], liquid crystals [51, 198], plasmas [188], and Bose-Einstein condensates with long-range interparticle interactions [189, 190, 191].

In this chapter, we investigate soliton dynamics in nonlocal nonlinear media with an optically-induced lattice. In section 4.2, we address the soliton mobility in the symmetric Kerr-type nonlocal nonlinear media. In Section 4.3, we address the impact of the asymmetric nonlocal diffusion nonlinearity of gap solitons supported by photorefractive crystals with an imprinted optical lattice.

4.2   Soliton mobility

4.2.1   Introduction

One of the principal properties featured by the corresponding discrete or lattice solitons is their restricted mobility in the transverse plane, the effect that might be employed for various switching and routing operations [86, 166]. Recent progress in creation of reconfigurable optical lattices in photorefractive crystals [87, 88, 131, 93, 94, 164] and nematic liquid crystals [51, 198] opened a direct way to explore the properties of solitons by varying the lattice depth and period. However, photorefractive media and liquid crystals may feature a strong nonlocal nonlinear response. Therefore, a principal question arises about the effect of the interplay of periodic refractive index modulation and nonlocality of nonlinear response on fundamental soliton properties, including their mobility. An intuitively similar, but physically drastically different scenario is the tunable self-bending of solitons in lattices made in media with diffusive nonlinearity [192].

Here, we address the properties of solitons in Kerr-type *nonlocal* nonlinear media with an imprinted transverse periodic modulation of the refractive index. Our central discovery is that a *tunable nonlocality* can greatly enhance the soliton mobility, opening the possibility of almost radiationless soliton propagation across the lattice. We employ a generic model for the nonlocal nonlinearity, which provides insight for all physical settings governed by nonlocality kernels with an exponential-decaying range, including photorefractive and liquid crystal optical media, as well as in models of Bose-Einstein condensates with long-range interparticle interactions [189, 190, 191].

4.2.2   Model and stationary solutions

For concreteness, here we consider the propagation of the light beam along the ξ axis in a nonlocal nonlinear Kerr-type medium with an imprinted modulation of linear refractive index described by the system of phenomenological equations for dimensionless complex light field amplitude q and nonlinear correction to the refractive index n [175, 176, 177, 178, 179]:

$$i\frac{\partial q}{\partial \xi} = -\frac{1}{2}\frac{\partial^2 q}{\partial \eta^2} - qn - pR(\eta)q,$$

$$n - d\frac{\partial^2 n}{\partial \eta^2} = |q|^2, \tag{4.1}$$

where η and ξ stand for the transverse and longitudinal coordinates scaled to the beam width and diffraction length, respectively; the parameter d stands for the degree of nonlocality of the nonlinear response; the parameter p is proportional to the refractive index modulation depth; and the function $R(\eta) = \cos(2\pi\eta/T)$ describes the transverse refractive index profile, where T is the modulation period. We assume that the depth of the refractive index modulation is small compared to the unperturbed index. In the limit $d \to 0$, the system (4.1) reduces to the nonlinear Schrödinger equation. The opposite case $d \to \infty$ corresponds to the strongly nonlocal regime. Among the conserved quantities of system (4.1) are the energy flow U

$$U = \int_{-\infty}^{\infty} |q|^2 d\eta, \tag{4.2}$$

and the Hamiltonian H

$$H = \int_{-\infty}^{\infty} [\frac{1}{2}|\frac{\partial q}{\partial \eta}|^2 - pR(\eta)|q|^2$$

$$-\frac{1}{2}|q|^2 \int_{-\infty}^{\infty} G(\eta - \lambda)|q(\lambda)|^2 d\lambda]d\eta, \tag{4.3}$$

where $G(\eta) = (1/2d^{1/2})\exp(-|\eta|/d^{1/2})$ is the response function of the nonlocal medium. We search for stationary solutions of Eq.(4.1) in the form $q(\eta, \xi) = w(\eta)\exp(ib\xi)$, where $w(\eta)$ is a real function and b is a real propagation constant. Substitution into (4.1) yields

$$\frac{d^2 w}{d\eta^2} + 2wn + 2pRw - 2bw = 0,$$

$$d\frac{d^2 n}{d\eta^2} - n + w^2 = 0, \tag{4.4}$$

where n stands for the stationary refractive index profile. We solved these equations numerically with a relaxation method. We set $T = \pi/2$ and vary b, p and d. To elucidate the linear stability of the solitons, we searched for perturbed solutions in the form $q(\eta, \xi) = [w(\eta) + u(\eta, \xi) + iv(\eta, \xi)]\exp(ib\xi)$, where the real $u(\eta, \xi)$ and imaginary $v(\eta, \xi)$ parts of the perturbation can

grow with a complex rate δ upon propagation. Linearization of Eq. (4.1) around a stationary solution yields the eigenvalue problem

$$\delta u = -\frac{1}{2}\frac{d^2v}{d\eta^2} + bv - nv - pRv,$$

$$\delta v = \frac{1}{2}\frac{d^2u}{d\eta^2} - bu + nu + w\Delta n + pRu, \tag{4.5}$$

where $\Delta n = 2\int_{-\infty}^{\infty} G(\eta-\lambda)w(\lambda)u(\lambda)d\lambda$. The system (4.5) can also be solved numerically.
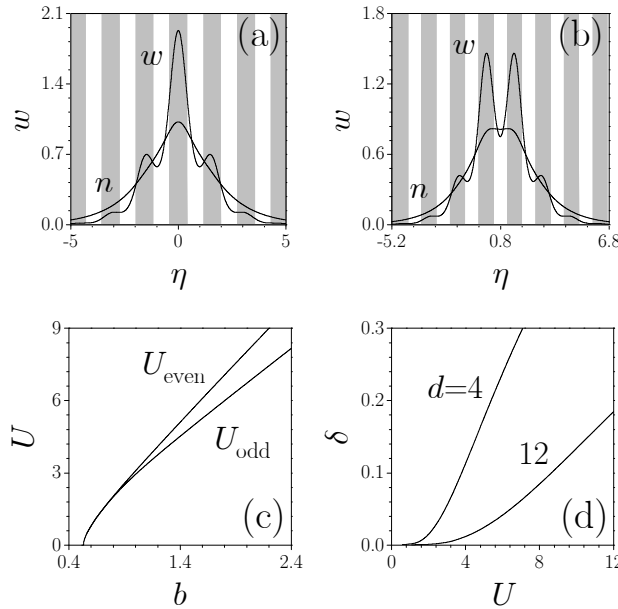
Figure 4.1: Profile of (a) odd and (b) even solitons with energy flow $U = 4$ and corresponding nonlinear refractive index distributions. (c) Energy flow versus propagation constant for odd and even solitons. In (a)-(c) the degree of nonlocality $d = 2$. (d) Perturbation growth rate versus energy flow of even solitons at a different degree of nonlocality. Lattice depth $p = 3$. Gray regions in (a) and (b) correspond to $R(\eta) \geq 0$, while in white regions $R(\eta) < 0$.

First, we address properties of lowest-order odd and even solitons. The absolute intensity maximum for odd solitons coincides with one of the local maxima of $R(\eta)$ [Fig. 4.1(a)], whereas even solitons are centered between neighboring lattice sites [Fig. 4.1(b)], and can be viewed as a nonlinear superposition of in-phase odd solitons. With an increase of lattice depth
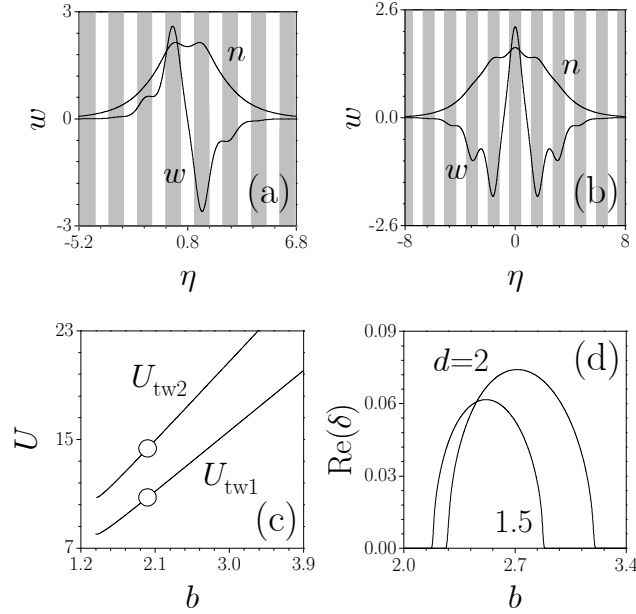
Figure 4.2: Profile of (a) first and (b) second twisted solitons and nonlinear refractive index distributions corresponding to points marked by circles in dispersion diagram (c). Lattice depth $p = 3$; nonlocality degree $d = 2$. (d) Real part of perturbation growth rate for first twisted soliton at $p = 2.5$ and various d values.

the soliton energy concentrates in the guiding lattice sites (the regions of local refractive index maxima) so that lattice solitons approach their discrete counterparts [86]. The energy flow U for both odd and even solitons is a monotonically growing function of the propagation constant b, and it vanishes in the cutoff b_{co} point, which is identical for odd and for even solitons [Fig. 4.1(c)]. The cutoff b_{co} for odd and even solitons is a monotonically growing function of lattice depth p, and we found that it does not depend on the nonlocality degree d. This is the consequence of the fact that both odd and even solitons reside in the semi-infinite gap of Floquet-Bloch spectrum of linear lattice that is independent of the nonlocality degree d so that b_{co} always coincides with the lower edge of this gap (see Ref. [193] for a detailed discussion of the band-gap lattice structure and bifurcations of gap solitons in local cubic media). At fixed energy flow and lattice parameters the soliton gets broader and its peak amplitude decreases with an increase of d . Linear stability analysis revealed that odd solitons are stable, and even solitons are unstable in the entire domain of their existence, similar to

the case of local medium [193]. However, the perturbation growth rate for an even soliton is drastically reduced with an increase of nonlocality [Fig. 4.1(d)], so that even solitons with moderate energy flows U can propagate undistorted in a highly nonlocal medium, even in the presence of random perturbations of the initial conditions, over distances exceeding any experimentally feasible crystal length by several orders of magnitude. Therefore, a first important result uncovered is that nonlocality largely reduces the strength of symmetry-breaking instabilities.

We also found families of twisted solitons that can be considered combinations of several odd solitons with engineered phases [132, 194] (see Fig. 4.2 for illustrative examples). The energy flow of twisted solitons is a non-monotonic function of propagation constant, and there exists a lower cutoff for the existence of such solitons [Fig. 4.2(c)]. The slope dU/db of the curve $U(b)$ becomes negative in a narrow region near the cutoff, not even visible in Fig. 4.2(c). Contrary to the case of odd and even solitons the cutoff b_{co} for twisted solitons increases with an increase of the nonlocality degree d. Stability analysis revealed that twisted solitons feature both exponential and oscillatory instabilities near the lower cutoff for their existence [see Fig. 4.2(d)]. However, we found that they become completely stable above a certain energy flow threshold. The width of the instability domain for twisted solitons decreases with an increase of lattice depth and increases with the growth of the nonlocality degree.

4.2.3   Soliton mobility analysis

As one can see from Figs. 4.1(a) and (b), and 4.2(a) and (b), for all solitons found the nonlinear refractive index distribution in nonlocal media with $d \sim 1$ always features a smooth symmetric bell-like shape without pronounced local maximums on top of it, thereby smoothing over the total refractive index profile $n + pR$. This is in clear contrast to the local cubic medium, where focusing nonlinearity tends to further increment the transverse refractive index modulation that, in turn, results in a restricted mobility of high-energy excitations. Therefore, the nonlocality of the non-linear response could greatly enhance transverse soliton mobility, which is the central result in this section.

Figure 4.3 confirms this central result. The plot shows the Peierls-Nabarro (PN) barrier, defined as a difference $\delta H = H_{\text{even}} - H_{\text{odd}}$ between
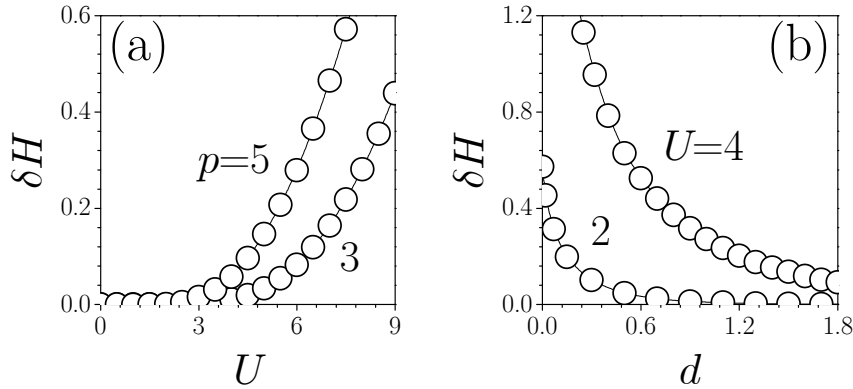
Figure 4.3: Height of the PN barrier versus (a) soliton energy flow at $d = 4$ and (b) degree of nonlocality at $p = 3$.

Hamiltonians for even and odd solitons carrying the same energy flow U [195, 196]. Since upon motion across the lattice the solitons pass through odd and even states, thus accompanied by the corresponding changes in Hamiltonian (or potential energy, when solitons are viewed as particles), the higher the barriers the larger the incident angle (or kinetic energy) required to overcome them. As expected, the height of the PN barrier grows with the increase of soliton energy flow U and lattice depth p [Fig. 4.3(a)]. However, the nonlocality reduces drastically the value of PN barrier [Fig. 4.3(b)]. The physical implication is that corresponding solitons can move across the lattice almost without radiation losses, because even small angles are sufficient to overcome the reduced PN barrier. Therefore an increasing degree of nonlocality affords very significant enhancement of the mobility of high-energy lattice solitons, a feature with both fundamental and potential practical relevance. Since odd solitons are ground-state solutions and realize the most energetically favorable state of the system, the difference δH can also serve as a measure of the instability of even solitons that is drastically reduced with an increase of the nonlocality degree. Notice that on physical grounds, the enhanced mobility of nonlocal lattice solitons cannot be attributed to any variation of soliton stability (as it occurs in some discrete systems with intersite interactions [197], but solely to refractive index smoothing induced by the nonlocality.

The expectations based on the reduction of the PN barrier are fully confirmed by numerical integration of Eq. (4.1). Fig. 4.4 illustrates the point. To stress the physical robustness of our findings, here we present
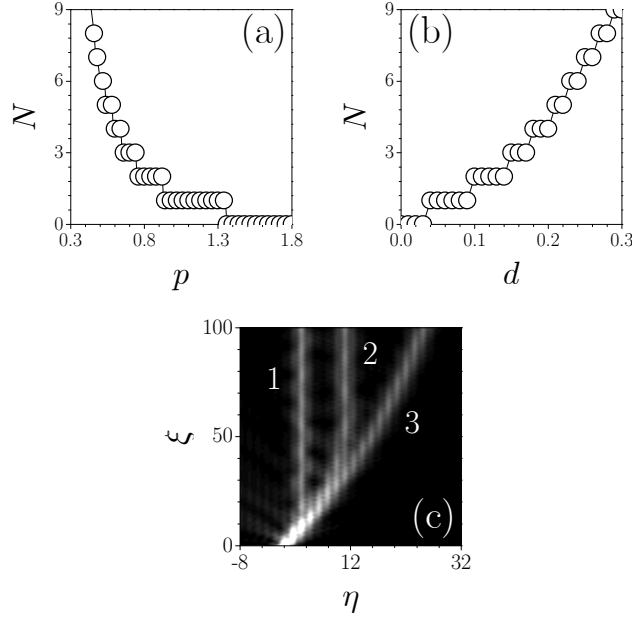
Figure 4.4: (a) Output channel number versus lattice depth at $d = 0.08$. (b) Output channel number versus nonlocality degree at $p = 1$. (c) Soliton propagation trajectories at $d = 0.1$ (1), 0.26 (2), and 0.4 (3). Lattice depth $p = 1$. In all cases the input soliton form factor $\chi = 1.2$ and incident angle $\alpha = 0.5$.

results obtained with inputs in the form $q(\eta, \xi = 0) = \chi\texttt{sech}(\chi\eta)\texttt{exp}(i\alpha\eta)$, where α stands for the incident angle. In general, soliton motion across the lattice is accompanied by radiative losses that eventually lead to soliton capture in one of the lattice channels [Fig. 4.4(c)]. The radiation losses are drastically reduced by the nonlocality. For example, a soliton with $\chi = 1.2$ trapped in the 10th channel of the lattice imprinted in a fully local medium loses about 40% of its input energy flow, while in a nonlocal medium with $d = 0.3$ the energy losses are less than 10%. Further decreases of the radiation are achieved by increasing the degree of nonlocality. Let the soliton be trapped in the N-th channel if $NT - T/2 < \eta_{\texttt{max}} < NT + T/2$ at $\xi \to \infty$, where $\eta_{\texttt{max}}$ is the transverse coordinate of the soliton center. The output channel number decreases with an increase of lattice depth p [Fig. 4.4(a)], but we found that it does grow with increase of nonlocality [Fig. 4.4(b)]. Importantly, small variations of the nonlocality impact strongly the value of the output channel number, a result that stresses the new degree of freedom afforded by the nonlocality.

It is worth stressing that the physical mechanism behind the enhanced soliton mobility in nonlocal media put forward here is principally different from the tunable bending that occurs in media with diffusion asymmetric nonlinearity [192], where a highly anisotropic nonlinear response results in asymmetric self-induced refractive index profiles and causes soliton bending, while lattices are used to tune the bending rate. In contrast, the principal physical feature behind the phenomena uncovered here is the tunability of a symmetric nonlocality, itself. Such an aim can be achieved in a variety of ways. In particular, it has been experimentally demonstrated that the nonlocality of nematic liquid crystals vary with the voltage applied to the crystal [198, 199]. An increase in the voltage causes a reorientation of the molecules of a liquid crystal, which, in turn, results in a modification of the character of a nonlinear response from highly nonlocal to predominantly local. Since lattices can be imprinted in liquid crystals [51, 198], they are very promising candidates for the demonstration of enhanced mobility of nonlocal lattice solitons. Thus, the variation of the output channel upon a slight modification of the nonlocality degree depicted in Fig. 4.4 can be used to implement soliton-based switching and routing schemes controlled by the applied voltage. Another example of tunable nonlocality is encountered with thermal nonlinearity, e.g., in dye-doped liquid crystals [200, 201].

4.3 Gap solitons in nonlocal media

4.3.1 Introduction

Self-action of light in periodic nonlinear structures generates rich optical phenomena [119]. In particular, such nonlinear structures, or optical lattices, support various types of solitons that appear as defect nonlinear modes residing in gaps of the Floquet-Bloch lattice spectrum. Finite gaps give rise to solitons forming because of nonlinear coupling between waves having equal longitudinal wave vector components and opposite wave vector components in the transverse direction when both of them experience Bragg scattering [202]. Gap solitons were studied in different geometries and materials, including photonic crystals and layered microstructures [203, 204], fiber Bragg gratings [205], Bose-Einstein condensates [206, 207, 208], waveguide arrays [193, 209], and optically induced lattices [88, 90].

Previous studies focused on gap soliton formation in local nonlinear media. However, nonlocality of nonlinear response may drastically modify conditions necessary for gap soliton existence, especially when the mechanism behind gap soliton formation relies on Bragg rather than on total internal reflection from the periodic structure. It is shown that nonlocality strongly affects solitons even for symmetric nonlinear response [178]. Asymmetric nonlocality exhibited by photorefractive crystals [210, 211, 212, 213] may have an even stronger impact on the properties of solitons emerging from finite gaps, a feature that is the focus in this section. In particular, we reveal that gap solitons in photorefractive crystals with nonlocal diffuse nonlinearity have largely asymmetric oscillating profiles and that they cease to exist when the nonlocality degree exceeds a threshold. We also study the impact of nonlocality on the mobility of gap solitons, studied previously only in focusing nonlocal media [192, 214].

4.3.2   Model and stationary solutions

We consider propagation of light along the ξ axis of a biased photorefractive crystal that exhibits defocusing drift and asymmetric diffusion components of the nonlinear response in the presence of an imprinted optical lattice. The dynamics of propagation is described by the nonlinear Schrödinger equation for dimensionless complex light field amplitude q:

$$i\frac{\partial q}{\partial \xi} = -\frac{1}{2}\frac{\partial^2 q}{\partial \eta^2} + q|q|^2 + \mu q\frac{\partial}{\partial \eta}|q|^2 - pR(\eta)q. \qquad (4.6)$$

Here η and ξ stand for the transverse and longitudinal coordinates scaled to the beam width and diffraction length, respectively; the parameter p characterizes the lattice depth; the function $R(\eta) = \cos(2\pi\eta/T)$ describes the transverse lattice profile, where T is the modulation period; and the parameter μ stands for the strength of the nonlocal diffusion nonlinearity. Equation (4.6) can be derived from the Kukhtarev-Vinetskii material equaitons [210, 211, 212, 213], and it describes propagation of light at low light intensities $I \ll I_{\text{bg}}$, where I_{bg} is the intensity of background illumination. At higher intensities the saturation of photorefractive nonlinear response becomes significant, but in this regime self-bending effects arising from asymmetric response dominate over lattice effects, a situation that corresponds to the opposite limit than the one addressed here. We verified numerically

that for the power levels where nonlocal and lattice effects compete on similar footing, the full saturable model and Eq. (4.6) give qualitatively similar results. The strength of the diffusion component of the nonlinear response in Eq. (4.6) increases as beam width decreases. When $\mu \to 0$ (for broad beams) one recovers the local medium. The nonlocality is significant for tightly focused light bemas; however, in most physically realistic situation $\mu < 1$. Equaiton (4.6) is derived by taking into account the lowest-order space-charge field effects [212], an approach that is justified for most photorefractive crystals with paraxial light beams. The largest correction to Eq. (4.6) arising on account of the higher-order space-charge field effects results in a correction to the parameter μ, while corrections proportional to $\partial^2|q|^2/\partial\eta^2$ and $(\partial|q|^2/\partial\eta)^2$ are negligible for paraxial beams (e.g., for a beam width of 10 μm these terms are of the order of 10^{-3}). Equation (4.6) conserves the total energy flow

$$U = \int_{-\infty}^{\infty} |q|^2 d\eta. \tag{4.7}$$

To study the conditions necessary for the existence of gap solitons we analyze the Floquet-Bloch lattice spectrum by solving linearized Eq. (4.6) with $q(\eta, \xi) = w(\eta)\exp(ib\xi + ik\eta)$, where b is the propagation constant, k is a Bloch wave number, and $w(\eta) = w(\eta + T)$. A typical spectrum $b(p)$ is depicted in Fig. 4.5(a) for $T = \pi/2$. All possible propagation constant values are arranged into bands, where Eq. (4.6) admits Bloch wave solutions. These bands are separated by gaps where periodic waves do not exist. The Floquet-Bloch spectrum possesses a single semi-infinite gap and an infinite number of finite gaps. Solitons emerge as defect modes whose propagation constants are located inside the gaps of the Floquet-Bloch spectrum. Lowest-order (odd) solitons existing in a semi-infinite gap in focusing media rely on the mechanism of total internal reflection and feature bell-shaped profiles [202]. Solitons from finite gaps rely on the mechanism of Bragg reflection and feature transverse shape oscillations [193].

To elucidate the effect of nonlocality on properties of gap solitons we searched for stationary solutions of Eq. (4.6) numerically in the form $q(\eta, \xi) = w(\eta)\exp(ib\xi)$, where $w(\eta)$ is a real function. To analyze stability we looked for perturbed solutions in the form $q(\eta, \xi) = [w(\eta)+u(\eta, \xi)+iv(\eta, \xi)]\exp(ib\xi)$, where the real $u(\eta, \xi)$ and the imaginary $v(\eta, \xi)$ perturbation parts can grow
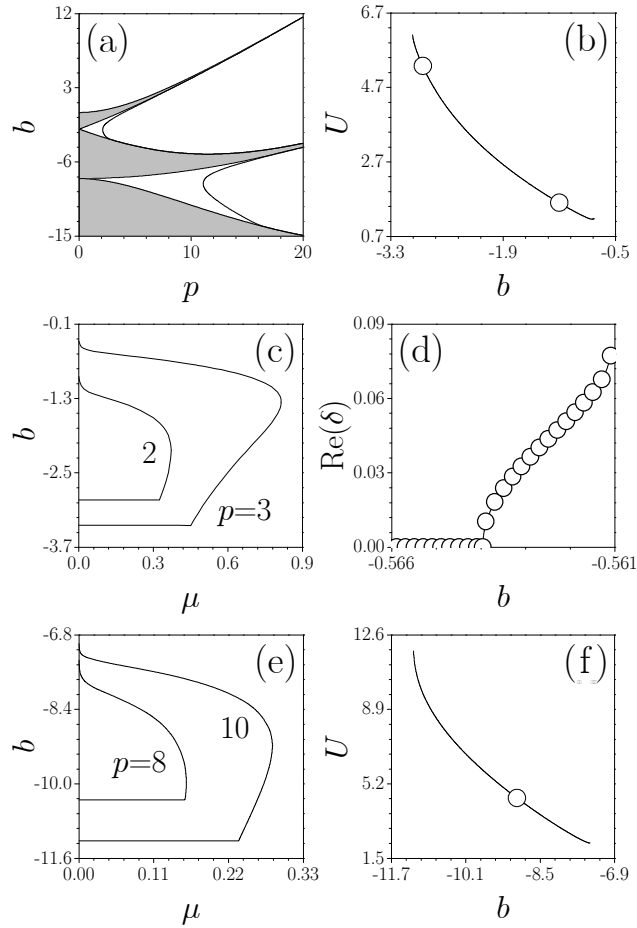
Figure 4.5: (a) Bandgap structure of periodic lattice and domains of existence of gap solitons in the presence of nonlocal nonlinearity with $\mu = 0.4$. Shaded areas, bands; unshaded areas, gaps. (b) Energy flow versus propagation constant for soliton from the first finite gap at $p = 3$ and $\mu = 0.5$. Points marked by circles correspond to profiles shown in Figs. 4.6(a) and 4.6(b). (c) Domains of existence of solitons from the first finite gap on (μ, b) plane. (d) Real part of perturbation growth rate versus propagation constant for soliton from the first finite gap at $p = 3$ and $\mu = 0.1$. (e) Domains of existence of solitons from the second finite gap on (μ, b) plane. (f) Energy flow versus propagation constant for soliton originating from the second finite gap at $p = 10$ and $\mu = 0.05$. The point marked by the circle corresponds to profile shown in Fig. 4.6(c).

with a complex rate δ upon propagation. Linearization of Eq. (4.6) around $w(\eta)$ yields the eigenvalue problem

$$\delta u = -\frac{1}{2}\frac{d^2 v}{d\eta^2} + bv - pRv + 2\mu w\frac{dw}{d\eta}v + w^2 v,$$

$$\delta v = \frac{1}{2}\frac{d^2 u}{d\eta^2} - bu + pRu - 4\mu w\frac{dw}{d\eta}u - 3w^2 u - 2\mu w^2\frac{du}{d\eta}, \quad (4.8)$$

which we solved numerically. At $\mu \neq 0$ gap solitons feature strongly asymmetric shapes because of the action of diffusion nonlocality [Fig. 4.6]. For a fixed b the position of the integral gap soliton center shifts in a positive direction of the η axis with an increase of μ. Energy flow is a nonmonotonic function of the propagation constant [Figs. 4.5(b) and 4.5(f)]. It decreases with b in most parts of the existence domain, except for the very narrow region near the upper cutoff on b where $dU/db > 0$. There exists also a lower cutoff for soliton existence. In clear contrast to a local case ($\mu = 0$), solitons do not occupy the whole gap at $\mu > 0$; i.e. cutoffs typically do not coincide with gap edges [see Fig. 4.5(a) where the domain of gap soliton existence at $\mu > 0$ is mapped onto the bandgap spectrum]. Physically, lower (high-power) cutoff appears because of the interplay between the nonlocality and lattice strength. The impact of nonlocality causing soliton profile deformation rapidly increases with peak amplitude, so that at certain μ the lattice cannot prevent high-energy solitons from bending. Thus lower cutoff starts increasing with μ when it exceeds a threshold [Fig. 4.5(c) and 4.5(e)]. Contrary to expectations that nonlocality affects strongly only solitons with high peak intensity, we found that upper (low-power) cutoff decreases with μ. This indicates that nonlinearity breaks energy exchange balance between waves with opposite transverse wave vectors, resulting in the formation of gap soltions when amplitudes of these waves become too small. At fixed p the soliton existence domain shrinks with an increase of μ, so that solitons cease to exist when μ exceeds a critical value [Fig. 4.5(c) and (e)]. The critical value increases with the lattice depth. For fixed μ gap solitons may exist only above a minimal lattice depth, which is much higher for second-gap solitons than for first-gap solitons [Fig. 4.5(a)]. The strongest localization of gap solitons is achieved deep inside existence domains, while near cutoffs solitons become spatially extended and strongly asymmetric.

A comprehensive linear stability analysis indicates that first-band solitons are stable in most parts of their existence domain. At $\mu \ll 1$ we found
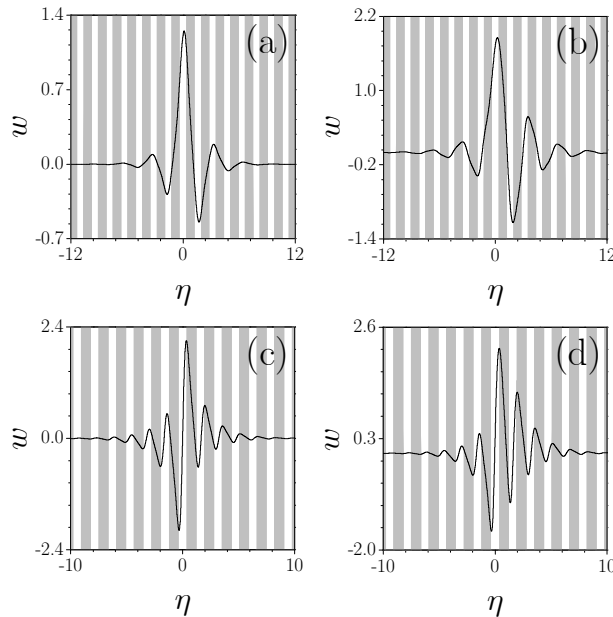
Figure 4.6: Profiles of solitons from the first finite gap, with (a) $b = -1.2$ and (b) $b = -2.9$ at $p = 3$ and $\mu = 0.5$. Profiles of solitons from the second finite gap, when (c) $\mu = 0.05$ and (d) $\mu = 0.28$ at $b = -9$ and $p = 10$. Shaded areas, $R(\eta) \leq 0$; unshaded areas, $R(\eta) > 0$.

regions of weak oscillatory instability near the lower and upper cutoffs, while at moderate values of μ we encountered only a narrow domain of exponential instability near the upper cutoff, where $du/db > 0$ [Fig. 4.5(d)]. We found that asymmetric nonlocality destabilizes second-band solitons. Direct simulations of Eq. (4.6) in the presence of broadband input noise confirmed the above results in all cases. Namely, first-band solitons remain stable and propagate undistorted in the presence of input noise [Fig. 4.7(a)].

4.3.3   Mobility and excitation

More important, we found that the mobility of gap solitons with low and even moderate amplitudes covering several lattice periods is substantially enhanced at $\mu > 0$. Strong enough asymmetric diffusion responses may cause a significant drift of gap solitons. An illustrative example is shown in Fig. 4.7(b), where we launched a gap soliton obtained for $\mu = 0$ into a media with $\mu > 0$ without any input tilt (approximations to such solitons can be generated experimentally, e.g., with spatial light modulators). Notice the low level of radiation losses that accompany the excitation and propagation of such solitons. We found that the curvature of the propagation trajectory
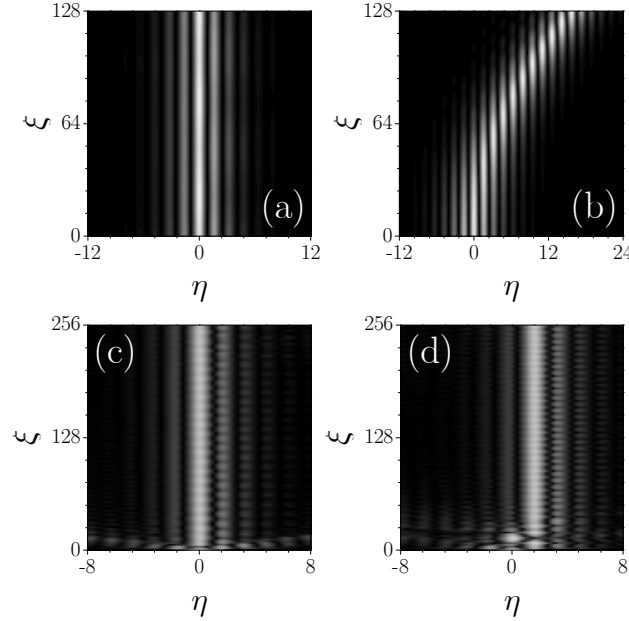
Figure 4.7: (a) Stable propagation of solitons from the first finite gap corresponding to $b = -0.57$, $p = 3$, and $\mu = 0.1$ in the presence of white input noise with varience $\sigma^2_{\texttt{noise}} = 0.01$. (b) Drift of soliton from the first finite gap corresponding to $b = -0.6$, $p = 3$, and $\mu = 0$, launched into a nonlocal medium with $\mu = 0.07$. Excitation of gap solitons by a Gaussian beam with (c) $A = 1.6$ and (d) 1.8 at $p = 2$ and $\mu = 0.2$.

increases with an increase of nonlocality degree [see Fig. 4.8(a)], while the trajectory itself is close to a parabolic one at the initial stage of propagation and almost linear for large propagation distances. Changing the lattice depth for fixed μ also enables control of the gap soliton mobility [Fig. 4.8(b)]. While strong enough lattices support immobile solitons, in shallow lattices solitons drift with a curvature that increases as lattice strength decreases.

Another practically important issue is the excitation of well-localized gap solitons covering only a few lattice periods. We found that they can be excited with a single Gaussian beam $A\texttt{exp}(-\eta^2/\eta_0^2)$ with properly selected width and amplitude. Figures 4.7(c) and (d) illustrate the typical excitation dynamics. The peak of the excited well-localized gap soliton may be located away from the input lattice channel. Under the action of asymmetric response the soliton center may jump into a neighboring lattice channel, with the number of jumps depending on the amplitude of the input beam. The implications for soliton control and routing are thus readily apparent.
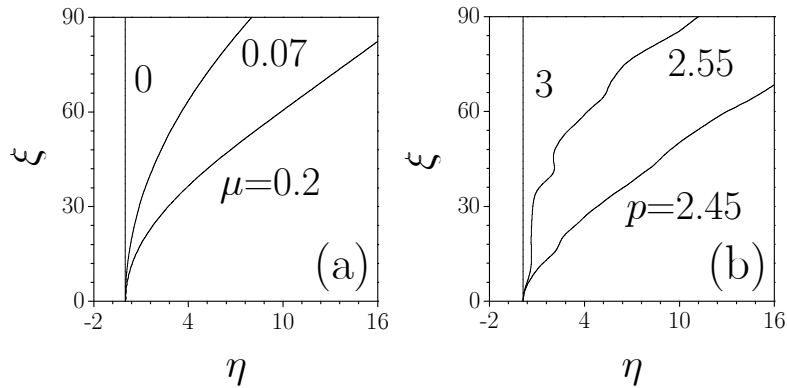
Figure 4.8: Trajectories of propagation for soliton from the first finite gap launched into a nonlocal medium. In (a) we set $b = -0.6$, $p = 3$, and vary the nonlocality degree. In (b) we set $b = -1$, $\mu = 0.2$, and vary the lattice depth.

4.4 Summary

In conclusion, in this chapter we have addressed the properties of solitons propagating in optical lattices imprinted in Kerr-type nonlinear, nonlocal media. We revealed that the nonlocality introduces principal new effects into the soliton transverse mobility. In particular, we discovered that the Peierls-Nabarro potential barrier for solitons moving across the lattice is drastically reduced in the presence of the nonlocality, a result of fundamental importance because mobile lattice solitons appear to be very rare in nature. Our predictions can be directly tested with light beams propagating in photorefractive and in liquid crystals, but we addressed a canonical, generic nonlocal model that provides insight for all analogous physical settings governed by symmetric nonlocality kernels featuring exponentially-decaying ranges.

In addition, we addressed the impact of the asymmetric nonlocal diffusion nonlinearity of gap solitons supported by photorefractive crystals with an imprinted optical lattice. We revealed how the asymmetric nonlocal response alters the domains of existence and the stability of solitons originating from different gaps. We found that in such media gap solitons cease to exist above a threshold of the nonlocality degree. We also discussed how the interplay between nonlocality and lattice strength impacts the gap soliton mobility.

Chapter 5

Soliton Complexes in Nonlocal Nonlinear Media

5.1 Overview

As discussed in the previous chapter, a nonlocality of the nonlinear response can play an important role in the properties of solitons. The interaction between solitons is also strongly affected by the nonlocality. In this chapter, we will address the impact of nonlocality on the formation of multihump bound states in homogeneous nonlocal nonlinear media. In Sec. 5.2, We address the stability of multipole-mode solitons in one-dimensional (1D) scalar nonlocal Kerr-type nonlinear media. In Sec. 5.3, We present the experimental observation of scalar multipole solitons in two-dimensional (2D) highly nonlocal nonlinear media. In Sec. 5.4, we study the vector soliton complexes in one-dimensional (1D) nonlocal nonlinear media.

5.2 Stability of multipole-mode solitons in 1D case

5.2.1 Introduction

The interactions that arise between optical solitons generate a variety of phenomena. Unlike the interactions of scalar solitons, which tend to repel or attract each other depending on their relative phase difference only [27], the interaction between solitons, which incorporates several field components, may be more complex. Thus the formation of vector multipole-mode solitons is possible in local saturable [104, 105] and quadratic [106, 107, 108] media.

The properties of solitons are also strongly affected by a nonlocality of the nonlinear response. In particular, nonlocality affects soliton interactions [215, 216] and allows soliton bound states to be formed [108, 216, 217, 218]. Dipole-mode bright solitons [219] and the attraction of dark solitons [220] were observed. However, the important issue on stability of bound states of bright solitons in nonlocal media has not been addressed. In particular, an open question is: How many solitons can be packed into a stable bound state? In this section we report the outcome of such a stability analysis.

5.2.2 Model and ground-state solitons

We consider the propagation of a slit laser beam along the ξ axis in media with a nonlocal focusing Kerr-type nonlinearity described by the system of phenomenological equations for dimensionless complex light field amplitude q and nonlinear correction to the refractive index n:

$$i\frac{\partial q}{\partial \xi} = -\frac{1}{2}\frac{\partial^2 q}{\partial \eta^2} - qn,$$

$$n - d\frac{\partial^2 n}{\partial \eta^2} = |q|^2, \qquad (5.1)$$

where η and ξ stand for the transverse and the longitudinal coordinates scaled to the beam width and the diffraction length, respectively; and parameter d stands for the degree of nonlocality of the nonlinear response. When $d \to 0$ Eqs. (5.1) are reduced to a single nonlinear Schrödinger equation; $d \to \infty$ corresponds to a strongly nonlocal regime. Equations (5.1) describe the nonlinear response of liquid crystals in steady state [198, 215]. We neglect transient effects, assuming continuous wave illumination (see [221] for a recent discussion of the reorientational relaxation time in typical crystals). Eq. (5.1) conserves the energy flow $U = \int_{-\infty}^{\infty}|q|^2 d\eta$ and Hamiltonian

$$H = \int_{-\infty}^{\infty}[\frac{1}{2}|\frac{\partial q}{\partial \eta}|^2 - \frac{1}{2}|q|^2\int_{-\infty}^{\infty}G(\eta - \lambda)|q(\lambda)|^2 d\lambda]d\eta, \qquad (5.2)$$

where $G(\eta) = (1/2d^{1/2})\exp(-|\eta|/d^{1/2})$ is the response function of the nonlocal medium. We search for stationary soliton solutions of Eqs. (5.1) numerically in the form $q(\eta, \xi) = w(\eta)\exp(ib\xi)$, where $w(\eta)$ is the real function and b is a propagation constant. To elucidate the linear sta-

bility of soliton families we searched for perturbed solutions in the form $q(\eta, \xi) = [w(\eta) + u(\eta, \xi) + iv(\eta, \xi)]\texttt{exp}(ib\xi)$, where the real $u(\eta, \xi)$ and the imaginary $v(\eta, \xi)$ parts of perturbation can grow with a complex rate δ on propagation. Linearization of Eqs. (5.1) around the stationary solution $w(\eta)$ yields the eigenvalue problem

$$\delta u = -\frac{1}{2}\frac{d^2 v}{d\eta^2} + bv - nv,$$

$$\delta v = \frac{1}{2}\frac{d^2 u}{d\eta^2} - bu + nu + w\Delta n, \qquad (5.3)$$

where $\Delta n = 2\int_{-\infty}^{\infty} G(\eta - \lambda)w(\lambda)u(\lambda)d\lambda$ is the refractive-index perturbation. We have solved the system of Eqs. (5.3) numerically.
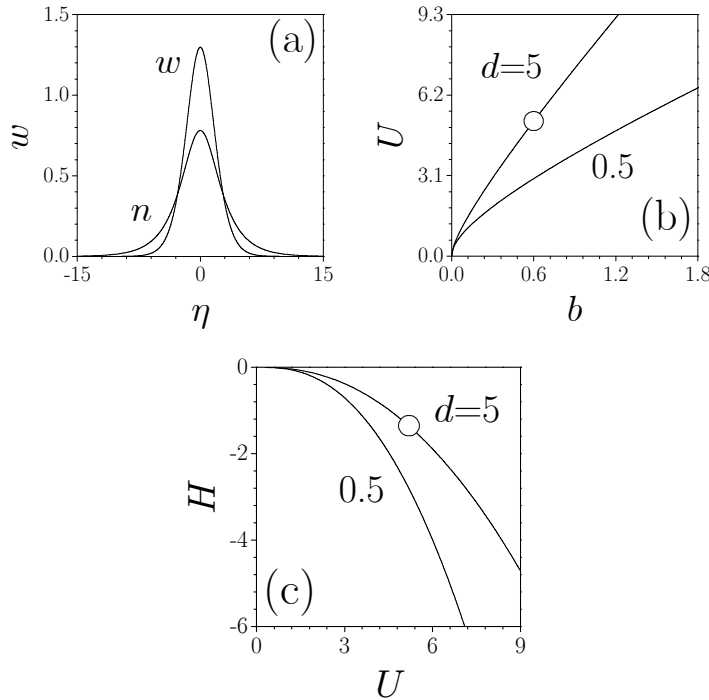
Figure 5.1: (a) Profile of a ground-state soliton that corresponds to the points marked by circles in (b) the dispersion diagram and (c) the Hamiltonian-energy diagram.

First we recall the properties of ground-state solitons (Fig. 5.1). The width of a ground-state soliton increases while its peak amplitude decreases with increasing degree of nonlocality d at fixed U. Energy flow U is a monotonically growing function of b [Fig. 5.1(b)]. As $b \to 0$ the soliton

broadens drastically while its energy flow vanishes. Ground-state solitons are stable in the entire domain of their existence and achieve the absolute minimum of Hamiltonian H for a fixed energy flow U [Fig. 5.1(c)].

5.2.3   Stability analysis

The central result is that several types of multipole-mode solitons can also be made completely stable in nonlocal media. Intuitively, multipole-mode solitons can be viewed as nonlinear combinations (bound states) of fundamental solitons with alternating phases. Such bound states cannot exist in a local Kerr-type medium, in which a π phase difference between solitons causes a local decrease of refractive index in the overlap region and results in repulsion. By contrast, in nonlocal media the refractive-index change in the overlap region depends on the whole intensity distribution in the transverse direction, and under appropriate conditions the nonlocality can lead to an increase in refractive index and to attraction between solitons. The proper choice of separation between solitons results in bound-state formation. Properties of the simplest bound states of two solitons are summarized in Fig. 5.2. One can see that the refractive-index distribution features a small dip near point $\eta = 0$, where the light field vanishes [Fig. 5.2(a)]. This dip is more pronounced at a small degree of nonlocality, whereas at $d \gg 1$ the refractive-index distribution becomes almost bell shaped. The energy flow of such solitons increases monotonically with increasing b [Fig. 5.2(b)]. At small energy flows, dipole-mode solitons are transformed into two well-separated out-of-phase solitons, whose amplitudes decrease as b decreases [Fig. 5.2(d)]. The important result is that dipole-mode solitons are stable in the entire domain of their existence, even for small degrees of nonlocality $d \sim 0.1$ and at low energy levels, when solitons forming a bound state are well separated [Fig. 5.2(d)].

Note that bound soliton states were also studied in quadratic media, which can be regarded as nonlocal under appropriate conditions and can lead to similar equations for profiles of stationary solitons [108]. However, the principle difference between the two systems becomes apparent in a stability analysis, which results in different eigenvalue problems and, hence, in completely different stability properties of bound soliton states.

To answer the important question about the maximal number of solitons that can be incorporated into a stable bound state we performed stability
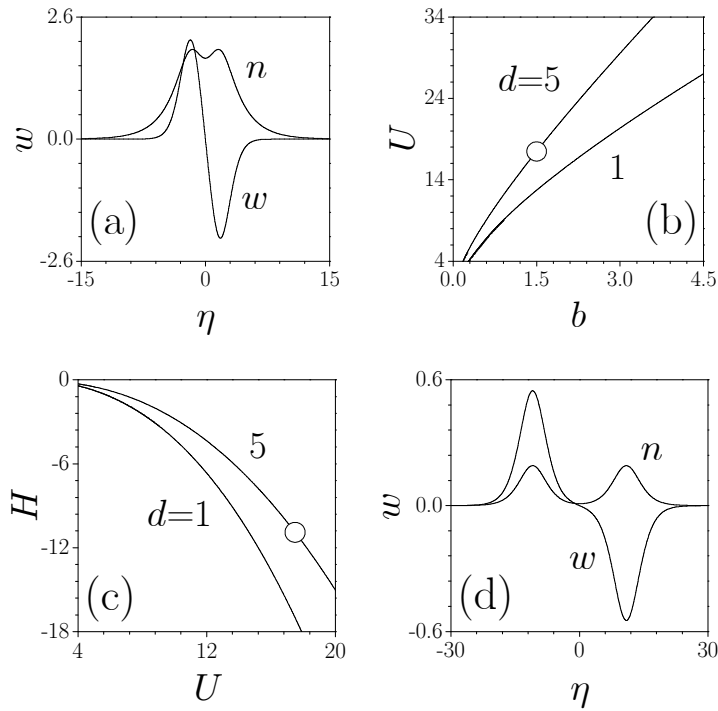
Figure 5.2: (a) Profile of a dipole-mode soliton that corresponds to the points marked by circles in (b) the dispersion diagram and (c) the Hamiltonian-energy diagram. (d) Profile of a low-energy dipole-mode soliton that corresponds to $b = 0.13$ at $d = 5$.

analysis of a number of higher-order soliton solutions. The results of the stability analysis are summarized in Fig. 5.3. The energy flow of such solitons also grows monotonically with increasing b. In all cases in the regime of strong nonlocality ($d \gg 1$) the refractive-index distribution for multipole-mode solitons features bell-shaped profile with a small modulation on its top in accordance with the number of peaks in the soliton [Figs. 5.3(a) and 5.3(c)]. Stability analysis revealed that low-energy triple- and quadrupole-mode solitons are oscillatory unstable [Figs. 5.3(b) and 5.3(d)], but their complete stabilization is possible when the soliton energy flow exceeds a certain threshold. The width of the instability domain as well as the maximum growth rate decreases with increasing degree of nonlocality for both triple- and quadrupole-mode solitons [see, for example, Fig. 5.3(b)]. It should be pointed out that at fixed d the width of the instability domain for a triple-mode soliton is narrower than that for a quadrupole-mode soliton [Fig. 5.3(d)]. One of the most important finding is that bound states
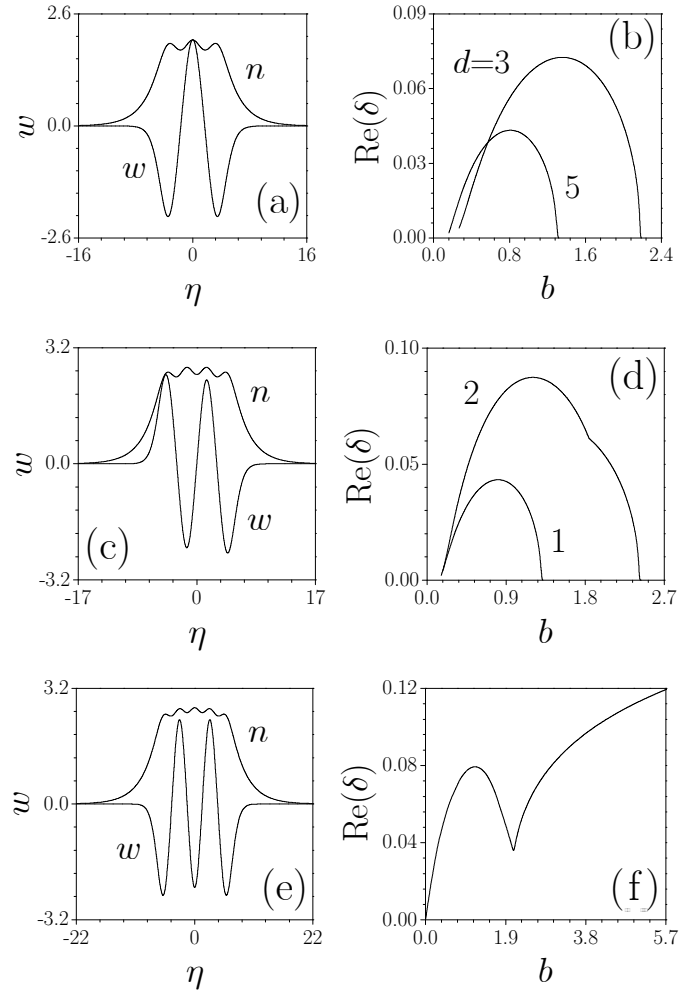
Figure 5.3: (a) Profile of a triple-mode soliton at $b = 1.5$ and $d = 5$. (b) Real part of the perturbation growth rate for the triple-mode soliton versus a propagation constant. (c) Profile of a quadrupole-mode soliton at $b = 2$ and $d = 5$. (d) Real part of the perturbation rate for 1, triple-, and 2, quadrupole-mode solitons versus propagation constant at $d = 5$. (e) Profile of a fifth-order soliton at $b = 2$ and $d = 8$. (f) Real part of the perturbation growth rate for the fifth-order soliton at $d = 8$.

incorporating five or more solitons were all oscillatory unstable with the framework of model equation (5.1) [see Fig. 5.3(e) and 5.3(f) for a typical profile and dependence $\mathtt{Re}\delta(b)$ of an unstable fifth-order soliton). We found this by performing linear stability analysis for bound states of as many as 12 solitons and d values from the interval (0, 100). In all cases the growth rate for unstable bound states was found to increase as $b \to \infty$, similarly to Fig. 5.3(f).
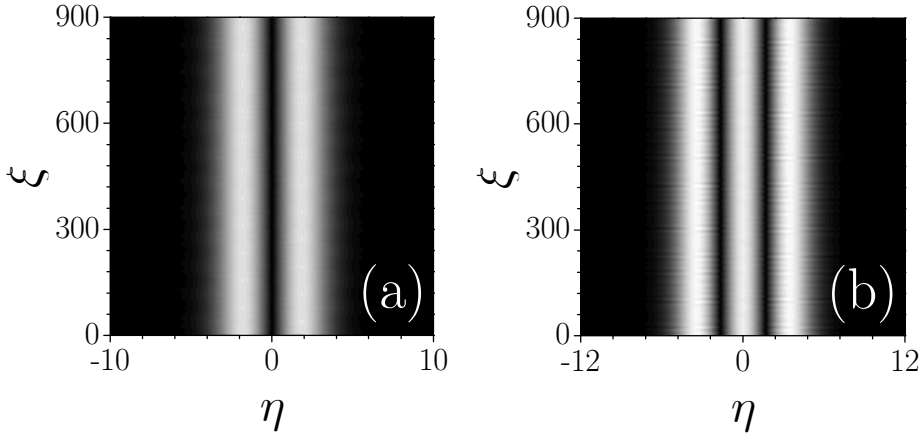
Figure 5.4: Stable propagation of (a) dipole-mode and (b) triple-mode solitons that correspond to $b = 1.5$ and $d = 5$ in the presence of white input noise with variance $\sigma^2_{\mathtt{noise}} = 0.01$.

To confirm the results of linear stability analysis, we performed numerical simulations of Eqs. (5.1) with input conditions $q(\eta, \xi = 0) = w(\eta)[1 + \rho(\eta)]$, where $w(\eta)$ is the profile of the stationary wave and $\rho(\eta)$ is a random function with a Gaussian distribution and variance $\sigma^2_{\mathtt{noise}}$. Stable dipole- and triple-mode solitons survive over huge distances in the presence of quite considerable broadband input noise (Fig. 5.4), whereas higher-order solitons self-destroy on propagation.

We also found that the stability of bound soliton states is defined to a great extent by the character of the nonlocal nonlinear response. Thus, in contrast to materials with an exponential response function $G(\eta) = (1/2d^{1/2})\mathtt{exp}(-|\eta|/d^{1/2})$ produced by Eqs. (5.1) (as in liquid crystals), materials with a Gaussian response function $G(\eta) = (\pi d)^{-1/2}\mathtt{exp}(-\eta^2/d)$ admit of no upper threshold for the number of solitons that can be incorporated into stable bound states. Such a difference makes the search for materials with different characteristics of nonlocal response especially important.

5.3   Multipole solitons in 2D case

5.3.1   Introduction

The preceding section focused on one-dimensional soltions in nonlocal non-
linear media, however, in two-dimensional nonlinear media, except dipole-
[222, 223], multihump solitons [104], solitons can be organized as necklaces
[158, 159, 160], and even more complex beams carrying angular momen-
tum, like rotating propellers [115]. Typically, bright solitons possessing
complicated forms in conservative systems necessitate the presence of mul-
tiple fields; i.e., they are vector (composite) solitons [222, 158, 159, 160]
(in contrast to nonconservative systems, where stable soliton complexes are
possible [237, 225]). In fact, in local nondissipative nonlinear media the
only examples of multihump scalar solitons are necklace solitons [158], rings
of out-of-phase bright spots holding each other together and arresting the
instabilities. The diffraction broadening of such a beam is indeed elim-
inated by the nonlinearity; yet these scalar self-trapped necklace beams
still inevitably (slowly) expand, because there is a net outward force ex-
erted on each spot by all other spots composing the ring [158]. Adding
angular momentum to the necklace introduces rotation that slows down
the expansion but never stops it completely [158]. Thus the general con-
clusion is that scalar solitons in homogeneous, local, nonlinear media with
no gain (or loss) cannot form complex states. The picture changes dras-
tically when the nonlinear material response is nonlocal. Nonlocality has
profound effects on the complexity of solitons as shown in the preceding sec-
tion, since it makes it possible to overcome repulsion between out-of-phase
bright [186, 215, 217, 218, 226, 109, 227, 228] or in-phase dark solitons [216]
that can form bound states observed in 1D settings [219, 220]. In two trans-
verse dimensions, however, the only complex structures thus far observed
with scalar solitons have been bright vortex rings [40]. Even thought the
simplest bound states of 2D solitons in nonlocal media were predicted in the
1980s [218], they still were not observed experimentally.

Here we present the experimental observation of various types of multi-
pole scalar solitons in a thermal nonlocal nonlinear medium. We find that
multipole solitons in such a medium are oscillatory unstable, yet their in-
stability decay rates can be very small under appropriate conditions, giving
rise to experimentally accessible metastable complex soliton states.

5.3.2 Model and theoretical predictions

The system is described by the evolution equation for the slowly varying light field amplitude A coupled to the steady-state heat transfer equation describing the temperature distribution in the lead glass sample [40]. The light beam is slightly absorbed and acts as a heat source. Heat diffuses, creating a non-uniform temperature distribution, which gives rise to a refractive index change proportional to the temperature change. The resulting system of equations in dimensionless form reads as [40]

$$i\frac{\partial q}{\partial \xi} = -\frac{1}{2}(\frac{\partial^2 q}{\partial \eta^2} + \frac{\partial^2 q}{\partial \zeta^2}) - qn,$$
$$\frac{\partial^2 n}{\partial \eta^2} + \frac{\partial^2 n}{\partial \zeta^2} = -|q|^2. \tag{5.4}$$

Here $q = (k_0^2 w_0^4 \alpha \beta / \kappa n_0)^{1/2} A$ is the dimensionless light field amplitude; $n = k_0^2 w_0^2 \delta n / n_0$ is proportional to nonlinear change δn in the refractive index n_0; k_0 being the optical wavenumber; α, β, and κ are the optical absorption coefficient, the thermal dependence of the refractive index ($\beta = dn/dT$), and the thermal conductivity coefficient, respectively; the transverse coordinates η, ζ are scaled to the beam width w_0, while the longitudinal coordinate ξ is scaled to diffraction length $k_0 w_0^2$. In our lead glass sample, $n_0 = 1.8$, the thermal coefficient is $\beta = 14 \times 10^{-6} \mathrm{K}^{-1}$, the absorption coefficient is $\alpha \approx 0.01 \mathrm{cm}^{-1}$, and the thermal conductivity is $\kappa = 0.7 \mathrm{W/(mK)}$. Such glass parameters are sufficient to support solitons with widths of $\sim 50~\mu\mathrm{m}$, which give rise to an index change $\delta n \sim 5 \times 10^{-5}$ for a total optical power 1 W. Notice that system (5.4) conserves the energy flow

$$U = \int \int_{-\infty}^{\infty} |q|^2 d\eta d\zeta. \tag{5.5}$$

We search for soliton solutions of Eqs. (5.4) of the form $q(\eta, \zeta, \xi) = w(\eta, \zeta)\mathrm{exp}(ib\xi)$, where $w(\eta, \zeta)$ is a real function and b is the propagation constant. The soliton intensity vanishes at the boundaries of the integration window, while the refractive index $n \to n_b$, where the limiting value n_b is related to the temperature of the sample boundaries, which are kept at fixed and equal temperature. Mathematically, adding the constant background n_b in the refractive index is equivalent to a shift of propagation constant b by the same amount; henceforth we set $n_b = 0$. In this case, the soliton

properties are determined solely by b and the width of integration window. We then set the window size $\eta, \zeta \in [-20, 20]$, closely resembling the actual transverse size of our sample. Using the numerical methods described in Refs. [109, 40], we find a variety of well-localized multipole solitons and test their stability by propagating them numerically in the presence of complex (amplitude and phase) noise. Figure 5.5 shows illustrative examples of multi-pole solitons, including dipole [Fig. 5.5(b)], tri-pole [Fig. 5.5(d)], as well as necklace solitons [Fig. 5.5(f)] comprising several bright spots with phase changing by π between adjacent spots. In a highly nonlocal nonlinear medium, the refractive index is determined by the intensity distribution over the entire transverse plane, and under proper conditions the nonlocality can lead to an increase of refractive index in the overlap region between out-of-phase solitons even when intensity there is zero, thus giving rise to formation of multipole solitons. Note that the width of the refractive index distribution (the light-induced potential) greatly exceeds the width of an individual light spot. This is a direct indication of the very large range of nonlocality in thermal media. We find that for all types of solitons the energy flow monotonically increases with b, which is accompanied by a decrease in the integral soliton width. Similarly, the separation δW between the intensity maxima of the multipole solitons is also found to decrease with b.

5.3.3   Experimental observation

In this section we describe the outcome of the experimental observations conducted by our collaborating group led by Prof. M. Segev from Israel Institute of Technology (http://physics.technion.ac.il/ msegev/).

The experiments are carried out in lead glass samples with a square 2 mm $\times$ 2 mm cross section, which are 84 mm long in the propagation direction. All four transverse boundaries of the sample are thermally connected to a heat sink and maintained at room temperature. In these experiments we use an 1.8 W laser beam at a 488 nm wavelength. We launch the dipole soliton by introducing a π phase jump across the Gaussian laser beam by inserting a piece of flat glass (of a proper thickness) through one half of the beam cross-section and imaging it (demagnified) onto the input face of the sample at normal incidence. We launch the tripole soliton in a similar fashion, with two parallel pieces of glass, each introducing a π phase-delay, passing
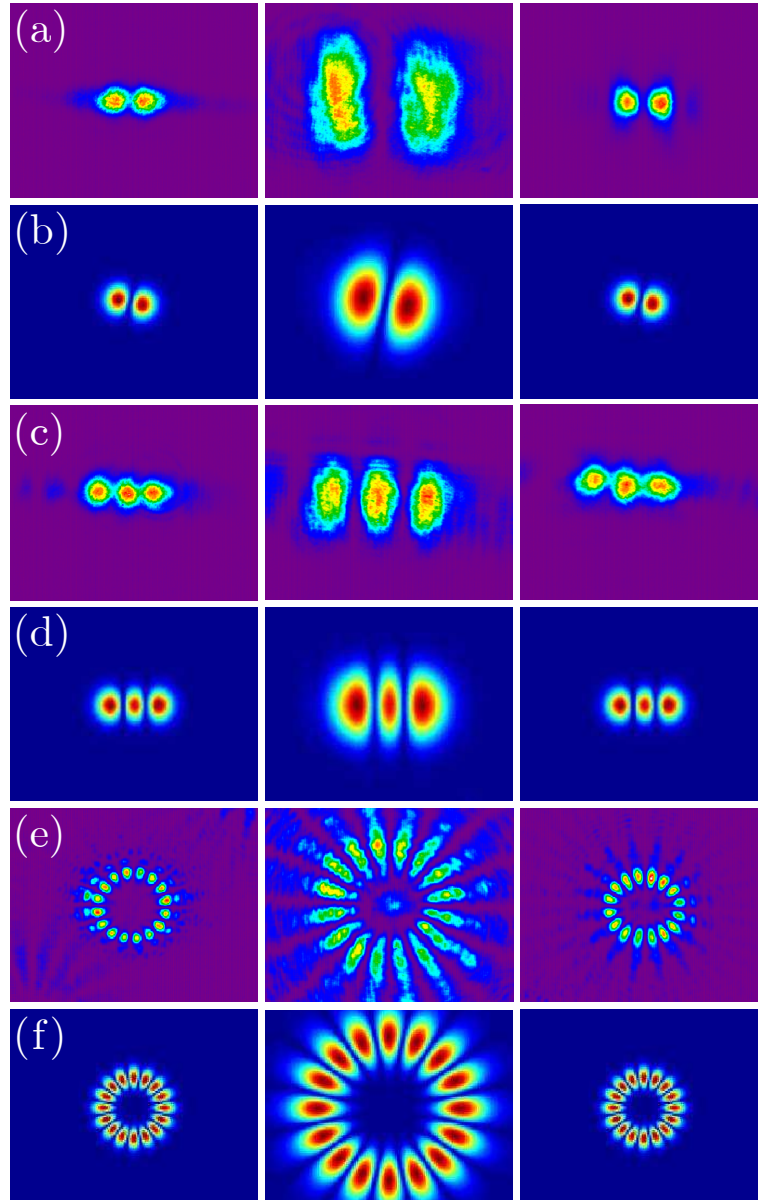
Figure 5.5: Comparison of experimental and theoretical results for dipole-mode solitons (a), (b), triple-mode solitons (c), (d), and necklace solitons (e), (f). Left-hand columns show input beams, the central columns show linear diffraction output after 84 mm of propagation, and the right-hand columns show self-trapped beams in nonlinear regime after the same distance.

through either one third or two thirds of the beam cross section. In order to create the 16-lobe necklace soliton, we reflect the laser beam off a properly designed phase mask and subsequently image the beam onto the input face of the sample. We monitor the intensity distribution at the input and output faces by imaging the input and output beams onto a CCD camera. Typical experimental results, with comparisons with the theoretical simulations, are summarized in Fig. 5.5. The left-hand column of each row shows the input beam in each case. At low power (10 mW), the beams linearly diffract for 84mm, after which they broaden significantly (middle columns). At high power (1.8 W), each beam forms a soliton, which maintains its intensity profile while propagating for 84mm (right-hand columns).
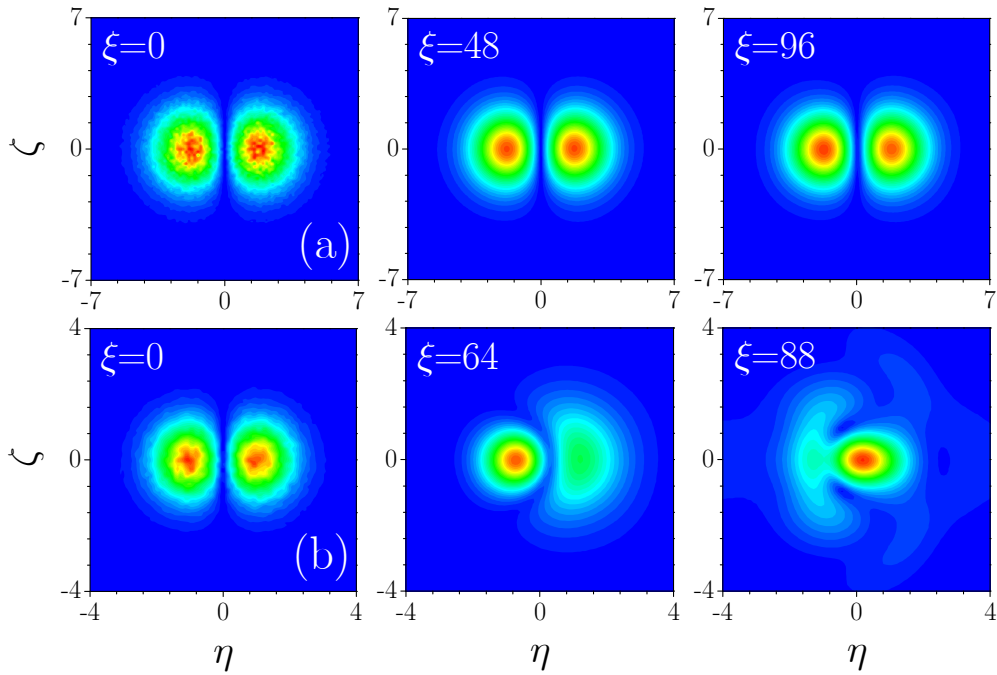
Figure 5.6: Propagation dynamics of slightly perturbed dipole-mode solitons with (a) $b = 3$ and (b) $b = 12$.

Extensive simulations of the propagation dynamics of perturbed solitons reveal that, in fact, all multipole solitons in thermal media are oscillatory unstable. Small perturbations in the input field distribution cause progressively increasing oscillations in the intensities of bright spots comprising the soliton, leading eventually to the destruction of the multipole soliton structure. For example, Fig. 5.6 shows the long-range dynamics of a perturbed (5% complex amplitude noise) dipole soliton and its transformation into a ground-state soliton for two values of b. The strength of the instability dramatically decreases with decreasing energy flow U, so that already at moderate energy levels the solitons survive over large distances (hundreds of diffraction lengths), greatly exceeding the present experimentally feasible sample lengths. We emphasize that we find the necklace solitons also to be metastable in our nonlocal thermal media. To our knowledge, these necklaces are the only known case where nonlocality acts to **destabilize** a self-trapped structure (that in this case is not stationary, but is otherwise robust in local nonlinear media [158]), in contrast to the natural tendency of nonlocality to stabilize self-trapped states [175, 180, 181].
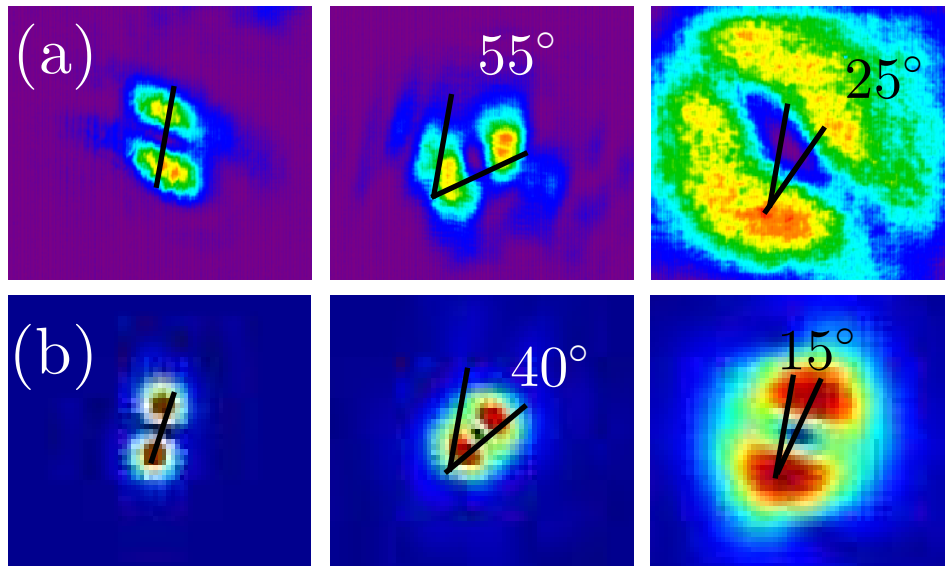
Figure 5.7: Comparison of experimental (a) and theoretical (b) results for rotating dipole mode solitons. Left-hand column shows input beams, central column shows self-trapped beams in nonlinear regime after 84 mm of propagtion, and right-hand column shows linear diffraction output after the same distance.

Last, we demonstrate a rotating dipole-type soliton, which constitutes the first experimental observation of any scalar complex soliton carrying angular momentum. In local media, scalar dipole solitons carrying angular momentum are always unstable. For this reason, all experiments with rotating complex solitons in local nonlinear media were performed with composite solitons that comprise of at least two fields. Recent theoretical work has shown that scalar dipole solitons can exhibit stable rotation in nonlocal media [229]. In our experiments, we create a rotating dipole beam by reflecting a Gaussian beam off a vortex phase mask, which is intersected by a black wire in the middle of the mask. In this way, we create a two-lobe beam with π phase jump between the lobes, and an additional tangential phase introduced by the vortex mask. We then demagnify the beam onto the input face of the sample, and monitor the beam at the input and the output faces of the sample. Figure 5.7 shows typical experimental results (upper row), compared to numerical simulations (lower row) of a rotating dipole soliton. The input beam (left-hand column), linearly diffracts at low power, broadening considerably after 84 mm of propagation (right-hand column), whereas at high power (1.8 W) the beam forms a soliton while rotating for 55 degrees, and maintaining its original shape (central column).

5.4   Vector soliton complexes

5.4.1   Introduction

The mutual interaction between nonlinear excitations is under active consideration in different areas of physics, including condensed matter, solid state, dynamical biomolecules, and nonlinear optics. This includes a rich variety of effects connected with the vectorial nature of the nonlinear excitations. For example, vectorial coupling was observed in multicomponent Bose-Einstein condensates [230, 231] and in topological defects arising due to the interspecies interaction [232, 233]. In nonlinear optics, vectorial coupling between several light waves resulting in the formation of vector solitons has been extensively studied for coherent [234, 235, 236, 237] and incoherent [104, 105, 238, 239, 240, 241, 242] interactions in materials with local nonlinearity. One important result introduced in Ref [104] is the existence of multihumped solitons afforded by the vectorial interactions. Recently, vector solitons in media with transverse periodic modulation of refractive

index were addressed as well [130, 243, 244, 245]. It was shown that vectorial coupling in local Kerr-type media could lead to the existence of complex multihumped structures that have no counterpart in the scalar case. However, in a local saturable medium such structures were found to be stable only when the total intensity distribution *does not feature more than three* humps [105].

On the other hand, it is shown that nonlinearity may be highly nonlocal, a property that drastically alters the propagation and interaction of nonlinear waves [174]. In this section, we introduce vector soliton structures in nonlocal media, and reveal that such a combination affords remarkable new phenomena. In particular, we discovered that because of the nature of soliton interactions in nonlocal media, vector solitons can form stable bound states that feature *several field oscillations* in *each* component, in sharp contrast to the behavior encountered in local media. We reveal that nonlocal nonlinear response plays a strong stabilizing action for vector solitons of higher orders. Complex patterns with a large number of humps in one field component, that are unstable when propagating alone, can be made stable in nonlocal media due to the mutual coupling with stable solitons propagating in other field components.

5.4.2   Model

We consider the propagation of two mutually incoherent laser beams along the ξ axis of a nonlocal focusing Kerr-type medium described by the system of equations for dimensionless complex light field amplitudes $q_{1,2}$ and nonlinear correction to refractive index n given by

$$i\frac{\partial q_1}{\partial \xi} = -\frac{1}{2}\frac{\partial^2 q_1}{\partial \eta^2} - q_1 n,$$
$$i\frac{\partial q_2}{\partial \xi} = -\frac{1}{2}\frac{\partial^2 q_2}{\partial \eta^2} - q_2 n,$$
$$n - d\frac{\partial^2 n}{\partial \eta^2} = |q_1|^2 + |q_2|^2. \tag{5.6}$$

Here η and ξ stand for the transverse and longitudinal coordinates scaled to the input beam width and diffraction length, respectively; the parameter d describes the degree of nonlocality of the nonlinear response. In the limit $d \to 0$ the system (5.6) reduces to a system of coupled nonlinear Schrödinger

equations for the fields $q_{1,2}$ whose vector soliton solutions are well established [104, 105, 238, 239, 240, 241, 242]. The opposite limit $d \to \infty$ corresponds to a strongly nonlocal regime. Under appropriate conditions the mathematical model (5.6) adequately describes the nonlinear response of some thermo-optical materials, liquid crystals or partially ionized plasmas [187, 51, 188, 40]. Among the conserved quantities of system (5.6) are the energy flows $U_{1,2}$ and the Hamiltonian H:

$$U = U_1 + U_2 = \int_{-\infty}^{\infty} (|q_1|^2 + |q_2|^2) d\eta,$$

$$H = \int_{-\infty}^{\infty} [\frac{1}{2}|\partial q_1/\partial \eta|^2 + \frac{1}{2}|\partial q_2/\partial \eta|^2$$

$$-\frac{1}{2}(|q_1|^2 + |q_2|^2) \int_{-\infty}^{\infty} G(\eta - \lambda)(|q_1|^2 + |q_2|^2) d\lambda] d\eta, \qquad (5.7)$$

where $G(\eta) = (1/2d^{1/2})\exp(-|\eta|/d^{1/2})$ is the response function of the non-local medium. We searched for the stationary solutions of Eq. (5.6) numerically in the form $q_{1,2}(\eta, \xi) = w_{1,2}(\eta)\exp(ib_{1,2}\xi)$, where $w_{1,2}(\eta)$ are real functions and $b_{1,2}$ are real propagation constants. The resulting system of equations obtained after substitution of light field in such form into Eq. (5.6) was solved with a standard relaxation method. To elucidate the linear stability of the solutions, we searched for perturbed solutions in the form $q_{1,2}(\eta, \xi) = [w_{1,2}(\eta) + u_{1,2}(\eta, \xi) + iv_{1,2}(\eta, \xi)]\exp(ib_{1,2}\xi)$, where real $u_{1,2}(\eta, \xi)$ and imaginary $v_{1,2}(\eta, \xi)$ parts of the perturbation can grow with a complex rate δ upon propagation. Linearization of Eq. (5.6) around a stationary solution $w_{1,2}$ yields the eigenvalue problem

$$\delta u_1 = -\frac{1}{2}\frac{d^2 v_1}{d\eta^2} + b_1 v_1 - nv_1,$$

$$\delta v_1 = \frac{1}{2}\frac{d^2 u_1}{d\eta^2} - b_1 u_1 + nu_1 + w_1 \Delta n,$$

$$\delta u_2 = -\frac{1}{2}\frac{d^2 v_2}{d\eta^2} + b_2 v_2 - nv_2,$$

$$\delta v_2 = \frac{1}{2}\frac{d^2 u_2}{d\eta^2} - b_2 u_2 + nu_2 + w_2 \Delta n, \qquad (5.8)$$

where $\Delta n = 2 \int_{-\infty}^{\infty} G(\eta - \lambda)[w_1(\lambda)u_1(\lambda) + w_2(\lambda)u_2(\lambda)]d\lambda$ is the perturbation of refractive index. We solved Eqs. (5.8) numerically to find the profiles of perturbations and the associated growth rates.

5.4.3   Stability analysis

The simplest vector solitons can be found with $b_1 = b_2$ in the form $w_1(\eta) = w(\eta)\cos\varphi$ and $w_2(\eta) = w(\eta)\sin\varphi$, where $w(\eta)$ describes the profile of scalar soliton, and φ is an arbitrary projection angle. The most interesting situation is encountered, however, when $b_2 \neq b_1$ and the first and second soliton components possess different types of symmetry. Below, without loss of generality, we search for solutions with $b_2 \leq b_1$. The properties of vector soliton composed from the first nodeless and second dipole-mode components are summarized in Fig. 5.8. At fixed propagation constant b_1 and nonlocality degree d there exist lower $b_2^{\mathtt{low}}$ and upper $b_2^{\mathtt{upp}}$ cutoffs on b_2 for vector soliton existence. As $b_2 \to b_2^{\mathtt{low}}$ the second dipole-mode component gradually vanishes [Fig. 5.8(a)], while in the opposite limit $b_2 \to b_2^{\mathtt{upp}}$ the nodeless component ceases to exist [Fig. 5.8(b)]. Such transformation of the internal structure of the vector soliton is accompanied by the development of a two-humped refractive index distribution near $b_2^{\mathtt{upp}}$. Notice that with increase of nonlocality degree, the width of the refractive index distribution increases substantially and far exceeds the width of the actual intensity distribution $w_1^2 + w_2^2$. The deep on top of the refractive index distribution becomes more pronounced in local limit ($d \to 0$) and almost vanishes in strongly nonlocal medium ($d \to \infty$). At small degrees of nonlocality and at $b_2 \to b_2^{\mathtt{upp}}$ the vector soliton transforms into two very well separated solitons with bell-shaped second components having opposite signs, while at $b_2 \to b_2^{\mathtt{low}}$ a small second component broadens substantially in comparison with the localized first component. In strongly nonlocal media both components remain well localized in the cutoffs. The total energy flow U is found to be a monotonically increasing function of b_2 [Fig. 5.8(c)]. The energy sharing $S_{1,2} = U_{1,2}/U$ as a function of b_2 is depicted in Fig. 5.8(d). We found that the width of the existence domain on b_2 for vector solitons shrinks substantially with the increase of nonlocality degree d [Fig. 5.8(e)] and expands with the increase of b_1 [Fig. 5.8(f)]. A comprehensive linear stability analysis revealed that vector solitons composed of nodeless and dipole-mode components are stable in the entire domain of their existence.

We also found vector solitons composed of first nodeless and second triple-mode components, whose properties are summarized in Fig. 5.9. The generic properties of such solitons are reminiscent to those of solitons discussed in Fig. 5.8, but the existence domain for such solitons is substan-
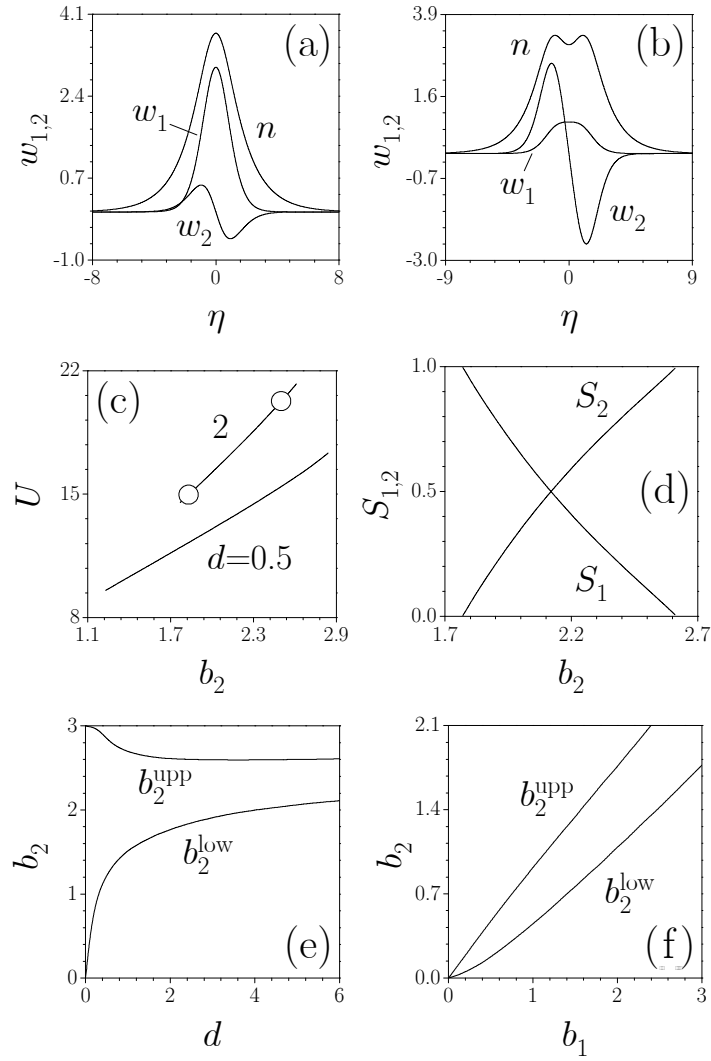
Figure 5.8: Soliton profiles corresponding to $b_1 = 3$, $d = 2$, and (a) $b_2 = 1.8$, (b) $b_2 = 2.5$. (c) Energy flow vs propagation constant b_2 at $b_1 = 3$. Points marked by circles correspond to solitons shown in (a) and (b). (d) Energy sharing between w_1 and w_2 soliton components vs b_2 at $b_1 = 3$, $d = 2$. Domains of existence of vector solitons at (d, b_2) plane for $b_1 = 3$ (e) and at (b_1, b_2) plane for $d = 2$ (f).
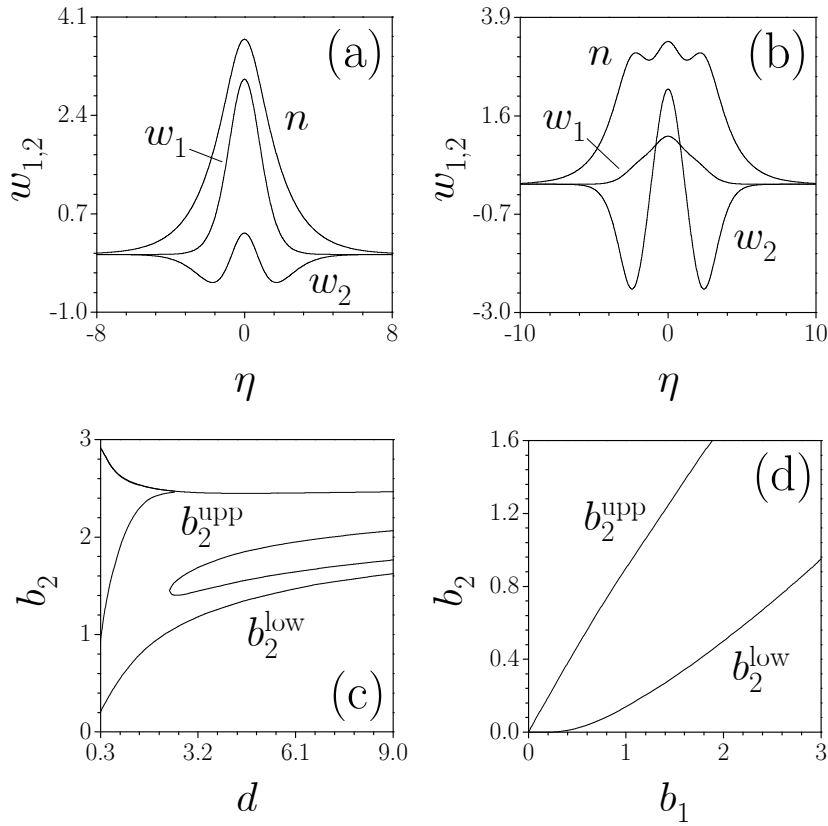
Figure 5.9: Soliton profiles corresponding to $b_1 = 3$, $d = 2$, and (a) $b_2 = 1$, (b) $b_2 = 2.3$. Domains of existence of vector solitons at (d, b_2) plane for $b_1 = 3$ (c) and at (b_1, b_2) plane for $d = 2$ (d).

tially wider [compare Figs. 5.9(c) and 5.8(e)]. The linear stability analysis revealed that solitons composed from nodeless and triple-mode components are unstable for small values of d. With decrease of d the instability domain emerges near upper cutoff b_2^{upp} and occupies the entire domain of soliton existence as $d \to 0.2$ [Fig. 5.9(c)]. In contrast, at moderate nonlocality degrees $d \sim 2.3$ such solitons are stable near lower and upper cutoffs and feature only a narrow instability band inside their existence domain. At small values of d the instability is of exponential type while for $d > 2.3$ we encountered only oscillatory instabilities. It should be pointed out that, in contrast to the case of local saturable medium [105, 238, 239, 240, 241, 242], multihumped vector solitons in nonlocal media may be stable when total intensity and refractive index distributions develop three or even more humps.

One of the central results is that vector solitons were found to form stable bound states that feature *several field oscillations* in *both* components and that, to the best of our knowledge, were not encountered previously in any model of local Kerr-type media. Such bound states exist because of the specific character of soliton interactions in nonlocal medium, whose sign is determined not only by the phase difference, but also by the separation between solitons [216, 217, 218]. Thus, in nonlocal media both w_1 and w_2 can change their sign in contrast to the case of local media where one of the components remains nodeless [104, 105, 238, 239, 240, 241, 242]. Several representative examples are shown in Fig. 5.10, including solitons incorporating dipole-mode first and triple- [Fig. 5.10(a)] or quadrupole-mode [Fig. 5.10(b)) second components, as well as more complex structures [Figs. 5.10(c)-5.10(f)]. The total number of humps in the refractive index distribution is determined by the relative weights of the components. While borders of the existence domain for bound states [e.g., Figs. 5.10(a), and 5.10(b)] look qualitatively similar to those shown in Figs. 5.8 and 5.9, the complexity of the structure of stability (instability) domains increases progressively with the increase of the number of humps in each component, so that typically several stability windows appear in the (d, b_2) plane.

To confirm the outcome of the linear stability analysis, we performed numerical simulations of Eq. (5.6) with the input conditions $q_{1,2}(\eta, \xi = 0) = w_{1,2}(\eta)[1 + \rho_{1,2}(\eta)]$, where $w_{1,2}(\eta)$ stands for the profiles of stationary solitons, and $\rho_{1,2}(\eta)$ are random functions with Gaussian distribution and variance $\sigma_{\texttt{noise}}^2$. Numerical simulations confirmed the results of the linear stability analysis in all cases. Stable solitons shown in Figs. 5.8-5.10 propagate over huge distances, exceeding experimentally feasible nonlinear material lengths by several orders of magnitude, even in the presence of considerable broadband input noise (Fig. 5.11).

Another important result that we encountered is that complex patterns with a large number of humps, that are unstable when propagating alone, can be made stable in suitable parameter regions due to the mutual coupling with stable single-humped or multi-humped components. Illustrative examples are shown in Figs. 5.10(c)-5.10(f), where stabilization of five- and six-hump components (that are unstable when propagating alone in a medium with exponential response function G [109]) is achieved because of the coupling with first stable fundamental and stable quadrupole-mode
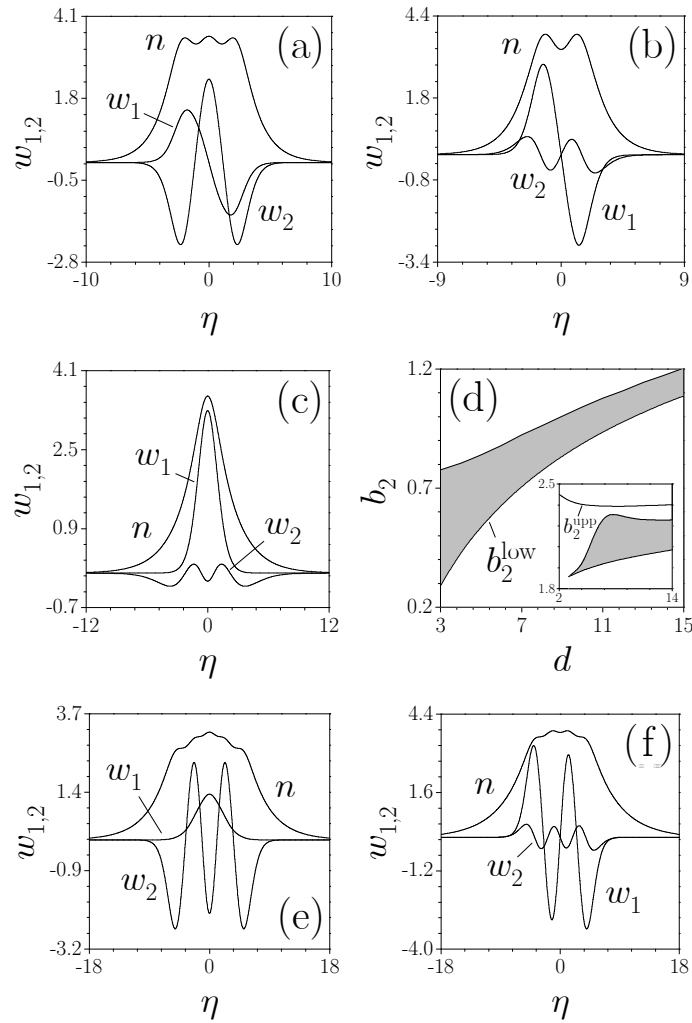
Figure 5.10: Profiles of various higher-order vector solitons at (a) $b_2 = 2.55$, $d = 2$, (b) $b_2 = 1.5$, $d = 2$, (c) $b_2 = 0.45$, $d = 4$, (e) $b_2 = 2.15$, $d = 10$, and (f) $b_2 = 2.37$, $d = 16$. Panel (d) shows stability (shaded) and instability domains on (d, b_2) plane for solitons incorporating nodeless w_1 and five-hump w_2 components [see panels (c) and (e) for soliton profiles]. In all cases $b_1 = 3$.
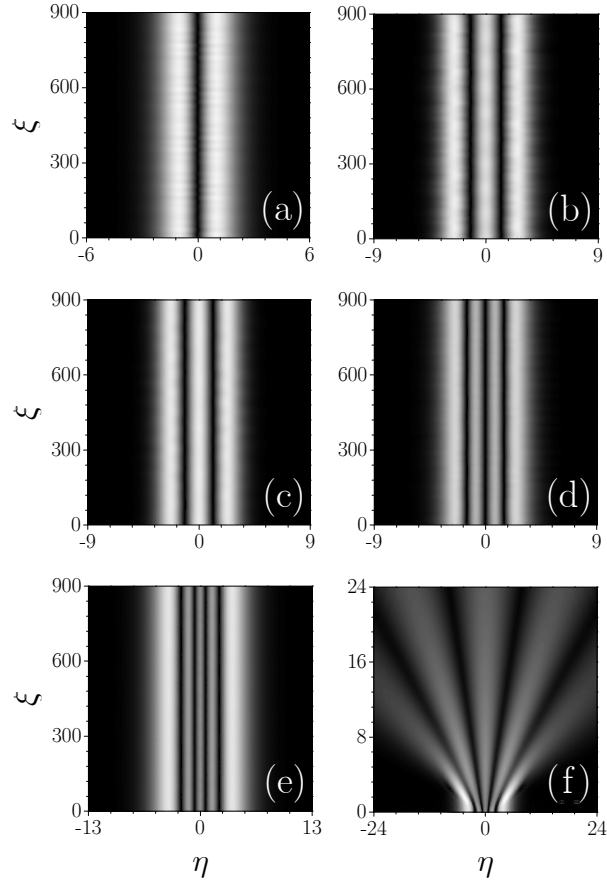
Figure 5.11: Propagation dynamics of vector solitons in nonlocal medium. (a) Soliton involving nodeless w_1 and dipole-mode w_2 components at $b_1 = 3$, $b_2 = 2$, $d = 2$. (b) Soliton involving nodeless w_1 and triple-mode w_2 components at $b_1 = 3$, $b_2 = 2.4$, $d = 3$. (c) Soliton involving dipole-mode w_1 and triple-mode w_2 components at $b_1 = 3$, $b_2 = 2.55$, $d = 2$. (d) Soliton involving dipole-mode w_1 and quadrupole-mode w_2 components at $b_1 = 3$, $b_2 = 1.5$, $d = 2$. (e) Soliton involving nodeless w_1 and five-hump w_2 components at $b_1 = 3$, $b_2 = 0.45$, $d = 4$. (f) Decay of soliton depicted in (e) in the absence of w_1 component. In (a)-(e) white noise with variance $\sigma^2_{\mathtt{noise}} = 0.01$ is added into input profiles. Only w_2 components are shown.

components, respectively. To stress that *stabilization of such complex multihumped structures* takes place in a *wide parameter regions* we show in Fig.5.10(d) the stability (instability) domains for solitons depicted in Figs 5.10(c) and 5.10(e). Besides the expected stability domain which adjoins the lower cutoff b_2^{low}, where the vector soliton bifurcates from the stable fundamental scalar soliton, another stability domain that appears at $d = 3$ [shaded area in the inset of Fig. 5.10(d)] was found. In this latter domain, stabilization of the five-hump component is achieved at the expense of coupling with a weak fundamental component. For a soliton profile belonging to this stability domain, see Fig. 5.10(e). Dropping the first component causes fast splitting and decay of the second component [Fig. 5.11(f)] that is stable in the presence of coupling [Fig. 5.11(e)]. Similar results were obtained for more complex solitons, e.g., Fig. 5.10(f). Therefore, vectorial coupling of *unstable* solitons in one field component with *stable* solitons in other field component allows a substantial increase of the number of solitons that can be packed into the composite, *stable* vector soliton complex.

5.5   Summary

In conclusion, in this chapter we addressed the stability of multiple-mode solitons in focusing, nonlocal Kerr-type nonlinear media. We revealed that, in media with exponential nonlocal response, bound states are stable if they contain less than five solitons, however, the materials with a Gaussian nonlocal response admit of no upper threshold for the number of solitons that can be incorporated into stable bound states.

Second, in collaboration with Prof. M. Segev's group from Israel Institute of Technology (http://physics.technion.ac.il/ msegev/), we have demonstrated experimentally two-dimensional metastable multi-pole solitons in highly nonlocal nonlinear media. The long range of nonlocality enables the formation of a variety of scalar solitons possessing complex structures, varying from dipole solitons, to tri-poles, to necklaces. Moreover, such high nonlocality is even able to support single-field (scalar) complex soliton structures carrying angular momentum, as exemplified by our experimental observation of a rotating scalar dipole soliton.

Finally, we explained that vectorial coupling in Kerr-type nonlocal media features important soliton phenomena. In particular, we revealed that

in such media vector solitons could form stable bound states that exhibit several field oscillations in each component, thus affording an extended number of peaks that can be packed into stable soliton trains. Our predictions open a route to the experimental observation of such multihumped soliton complexes. We based our analysis on a general model that combines nonlocal nonlinearity and vectorial coupling, potentially relevant to a variety of multicomponent nonlinear excitations in strongly nonlocal materials with symmetric nonlocal kernels. Formation of stable vector soliton complexes with rich internal structure might be possible in several of such systems.

Chapter 6

Conclusions

Optical solitons are light beams that do not broaden because of the balance between diffraction/dispersion and nonlinearity. They propagate and interact with one another while displaying properties that are normally associated with real particles. The properties of optical solitons in optical fibers and crystals have been investigated comprehensively during the last few years. However, solitons in optical lattices, which might be used for all-optical signal processing and routing, have recently emerged a new area of research. The main objective in this dissertation has been the investigation of *new techniques for soliton control* in nonlinear media with/without an imprinted optical lattice.

Chapter 2, for the first time, has studied discrete two-dimensional spatiotemporal solitons in quadratic nonlinear waveguide arrays. In addition to the temporal dispersion of the pulse, we have assumed the contribution of the discrete diffraction, that arises because of the weak coupling between neighboring waveguides. Novel families of unstaggered odd, even and twisted stationary solutions have been found and thoroughly characterized. The salient point put forward is that most of the spatiotemporal unstaggered odd solitons are stable against perturbations. However, still much more problems in this system remain open, such as the whole "zoology" of localized solutions, including staggered solitons, dark or dark-bright solitons, etc. It is known that in homogeneous quadratic uniform media ring-shaped vortex solitons suffer azimuthal instabilities. In the second part of Chapter 2, we have shown that optically-induced periodic lattices in quadratic media can support stable vortex solitons with unit topological charge, which comprise four main humps arranged in a square configuration. In addition,

we have investigated the generation of such multicolor lattice soliton from Gaussian beams with nested phase dislocation.

The technique of optical lattice induction opens a wealth of opportunities for creation of waveguiding configurations with various nondiffracting light beams. Chapter 3, for the first time, has put forward the concept of reconfigurable structures created with arrays of mutually incoherent parallel Bessel beams in Kerr-type nonlinear media. The salient point uncovered is that broad solitons can propagate in networks with bends at different angles that can even exceed 90° with low radiative losses (less than 4%). The networks shown are similar to the technologically fabricated networks, such as, photonic crystal bends. However, the tunability afforded by the technique offers the additional advantage of the *reconfigurability*.

In addition to optically-induced lattices, nonlocal response of nonlinear media can play an important role in the properties of solitons. Chapter 4 has considered how the interplay between nonlocality and optically-induced lattices in Kerr-type nonlinear media affects soliton dynamics. In particular, one salient point is that a *tunable nonlocality* can greatly enhance the soliton mobility, a result of fundamental importance because mobile lattice solitons appear to be very rare in nature. In addition, for the first time, we have addressed the impact of the asymmetric nonlocal diffusion nonlinearity on gap solitons supported by photorefractive crystals with an imprinted optical lattice. In particular, we have revealed how the asymmetric nonlocal response alters the domains of existence and stability of solitons originating from different gaps.

Chapter 5 has been devoted to the impact of nonlocality on the stability of solitom complexes in uniform nonlocal Kerr-type nonlinear media. First, we have studied the stability of multiple-mode solitons in one-dimensional focusing, nonlocal Kerr-type nonlinear media. The salient point uncovered is that in media with an exponential nonlocal response, bound states are stable if they contain less than five solitons, however, the materials with a Gaussian nonlocal response admit of no upper threshold for the number of solitons that can be incorporated into stable bound states. Second, in collaboration with Prof. M. Segev's group from Israel Institute of Technology (http://physics.technion.ac.il/ msegev/), we have demonstrated experimentally two-dimensional metastable multi-pole solitons in a lead glass, a highly nonlocal nonlinear medium. In particular, for the first time we have demon-

strated experimental observation of a rotating scalar dipole soliton carrying angular momentum. Finally, for the first time, we have addressed the interplay between nonlocal nonlinearity and vectorial coupling, and introduced one-dimensional vector soliton structures in such system. In particular, we have shown that because of the nature of soliton interactions in nonlocal media, vector solitons can form stable bound states that feature *several field oscillations* in *each* component.

The rapid progress in the area of spatial solitons has led to many interesting fundamental ideas and possible applications. Now I shall list some of possible prospects for research related to spatial solitons. There are different directions which the research may take. One direction is to investigate properties of solitons in existing and accessible media; another one is to look for new materials, which is specially useful for potential soliton applications. As shown in this dissertation, materials with nonlocal response, such as lead glass or liquid crystals, have shown fascinating unique properties and applications. Thus, one interesting idea is to study novel type of solitons in such kind of media, such as surface solitons at the interface between a dielectric medium (air) and a thermal nonlinear media [43] or other combinations in nonlocal nonlinear media [246]. Another novel kind of solitons, namely, incoherent solitons are self-trapped wave-packets upon which the phase distribution is random (for a detailed review see ref. [25, 27]), which can be extended to nonlocal media, and one can study even more complex situation, such as surface solitons with random phases [247].

Another main direction is towards solitons in new materials: for example, to extend soliton concepts to materials with random lattices, nonlinear metamaterials, nano lattices, and nano-particle suspensions [248].

In addition, the concepts addressed in this dissertation, may also end up having an impact in other areas of nonlinear sciences, such as in the physics of atom-molecular Bose-Einstein Condensates, nonlinear atom optics, etc. It is my sincere hope that the discoveries made in this thesis open new perspectives to the researchers advancing the science frontier.

Bibliography

[1] Report of 14th Meeting of the British Association for Advancement of Science, York, September 1844, pp311-390.

[2] N. J. Zabusky and M. D. Kruskal, Phys. Rev. Lett. **15**, 240 (1965).

[3] M. J. Ablowitz and P. A. Clarkson, *Solitons, nonlinear Evolution Equations, and Inverse Scattering*, (Cambridge University Press, New York, 1991).

[4] J. T. Taylor, Ed., *Optical Solitons-Theory and Experiment*, (Cambridge University Press, New York, 1992).

[5] F. K. Abdullaev, S. Darmanyan, and P. Khabibulaev, *Optical Solitons*, (Springer, Berlin, 1993).

[6] P. G. Drazin, *Solitons: An Introduction*, (Cambridge University Press, New York, 1993).

[7] G. L. Lamb, Jr., *Elements of Soliton Theory*, (Dover, New York, 1994).

[8] C. H. Gu, *Soliton Theory and its Applications*, (Springer, New York, 1995).

[9] N. N. Akhmediev and A. A. Ankiewicz, *Solitons: Nonlinear pulses and Beams*, (Chapman and Hall, London, 1997).

[10] T. Miwa, *Mathematics of Solitons*, (Cambridge University Press, New York, 1999).

[11] Y. R. Shen, *Principles of Nonlinear Optics*, (Wiley, New York, 1984).

[12] P. N. Butcher and D. N. Cotter, *The Elements of Nonlinear Optics*, (Cambridge University Press, Cambridge, UK, 1990).

[13] R. W. Boyd, *Nonlinear Optics*, (Academic Press, San Diego, CA, 1992).

[14] G. P. Agrawal, *Nonlinear Fiber Optics*, (Academic, San Diego, CA, 2001).

[15] A. Hasegawa and T. Tappert, Appl. Phys. Lett. **23**, 142 (1973).

[16] L. F. Mollenauer, R. H. Stolen, and J. P. Gordon, Phys. Rev. Lett. **45**, 1095 (1980).

[17] A. Hasegawa and Y. Kodama, *Solitons in Optics Communications*, (Oxford University Press, New York, 1995).

[18] G. P. Agrawal, *Applications of Nonlinear Fiber Optics*, (Academic, San Diego, CA, 2001).

[19] B. A. Malomed, D. Mihalache, F. Wise, and L. Torner, J. Opt. B, **7**, R53 (2005)

[20] R. Y. Chiao, E. Garmire, and C. H. Townes, Phys. Rev. Lett. **13**, 479 (1964).

[21] A. Barthelemy, S. Maneuf, and G. Froehly, Opt. Commun. **55**, 201 (1985).

[22] M. Shih, P. Leach, M. Segev, M. H. Garrett, G. Salamo, and G. C. Valley, Opt. Lett. **21**, 324 (1996).

[23] G. I. Stegeman, D. J. Hagan, and L. Torner, Opt. Quantum. Electron. **28**, 1691 (1996).

[24] M. Segev, Opt. Quantum. Electron. **30**, 503 (1998).

[25] S. Trillo and W. Torruellas, *Spatial Solitons*, (Springer, New York, 2001).

[26] A. V. Buryak, P. Di Trapani, D. V. Skryabin, and S. Trillo, Phys. Rep. **370**, 63 (2002).

[27] Yu. S. Kivshar and G. P. Agrawal, *Optical solitons: From Fibers to Photonic Crystals*, (Academic, San Diego, 2003).

[28] F. Reynaud and A. Barthelemy, Europhy. Lett. **12**, 401 (1990).

[29] P. L. Kelley, Phys. Rev. Lett. **15**, 1005 (1965).

[30] M. Hercher, J. Opt. Soc. Am. **54**, 563 (1964).

[31] J. S. Aitchison, A. M. Weiner, Y. Silberberg, M. K. Oliver, J. L. Jackel, D. E. Leaird, E. M. Vogel, and P. W. Smith, Opt. Lett. **15**, 471 (1990).

[32] E. L. Dawes, and J. H. Marburger, Phys. Rev. **179**, 179 (1969).

[33] J. Z. Wilcox, and T. J. Wilcox, Phys. Rev. Lett. **34**, 1160 (1975).

[34] P. K. Kaw, K. Nishikawa, Y. Yoshida, and A. Hasegawa, Phys. Rev. Lett. **35**, 88 (1975).

[35] K. I. Pushkarov, D. I. Pushkarov, and I. V. Tomov, Opt. Quantum. Electron. **11**, 471 (1979).

[36] J. E. Bjorkholm, and A. Ashkin, Phys. Rev. Lett. **32**, 129 (1974).

[37] F. W. Dabby, and J. R. Whinnery, Appl. Phys. Lett. **13**, 284 (1968).

[38] M. D. Iturbe Castillo, J. J. Sanchez-Mondragon, and S. Stepanov, Opt. Lett. **21**, 1622 (1996).

[39] S. J. Bentley, R. W. Boyd, W. E. Butler, and A. C. Melissinos, Opt. Lett. **25**, 1192 (2000).

[40] C. Rotschild, O. Cohen, O. Manela, M. Segev, and T. Carmen, Phys. Rev. Lett. **95**, 213904 (2005).

[41] C. Rotschild, M. Segev, Z. Xu, Y. V. Kartashov, L. Torner, and O. Cohen, Opt. Lett. **31**, 3312 (2006).

[42] C. Rotschild, B. Alfassi, O. Cohen, and M. Segev, Nature. Phys. **2**, 769 (2006).

[43] B. Alfassi, C. Rotschild, O. Manela, M. Segev, and D. N. Christodoulides, Phys. Rev. Lett. **98**, 213901 (2007).

[44] I. C. Khoo, and N. T. Wu, *Optics and Nonlinear Optics of Liquid Crystals*, (World Scientific, Singapore, 1993).

[45] E. Braun, L. P. Faucheux, and A. Libchaber, Phys. Rev. A. **48**, 611 (1993).

[46] D. W. Mclaughlin, D. J. Muraki, M. J. Shelley, and X. Wang, Physica D **88**, 55 (1995).

[47] D. W. Mclaughlin, D. J. Muraki, and M. J. Shelley, Physica D **97**, 471 (1996).

[48] G. Assanto, A. Fratalocchi, and M. Peccianti, Opt. Express. **15**, 5248 (2007).

[49] M. A. Karpierz, M. Sierakowski, M. Swillo, and T. Wolinski, Mol. Cryst. Liq. Cryst. **320**, 157 (1998).

[50] M. Peccianti, G. Assanto, A. De Luca, C. Umeton, and I. C. Khoo, Appl. Phys. Lett. **77**, 7 (2000).

[51] M. Peccianti, K. A. Brzdakiewicz, and G. Assanto, Opt. Lett. **28**, 2231 (2003); C. Conti, M. Peccianti, and G. Assanto, Phys. Rev. Lett. **91**, 073901 (2003); **92**, 113902 (2004); A. Fratalocchi, G. Assanto, K. A. Brzdakiewicz, and A. Karpierz, Opt. Lett. **29**, 1530 (2004).

[52] M. Peccianti, C. Conti, G. Assanto, A De Luca, C. Umeton, Nature (London) **432**, 733 (2004).

[53] M. Peccianti, A. Dyadyusha, M. Kaczmarek, and G. Assanto, Nature Physics (London) **2**, 737 (2006).

[54] P. Yeh, *Introduction to Photorefractive Nonlinear Optics*, (Wiley, New York, 1993).

[55] L. Solymar, D. J. Webb, and A. Grunnet-Jepsen, *The Physics and Applications of Photorefractive Materials*, (Ocford, New York, 1996).

[56] M. Segev, B. Crosignani, A. Yariv, and B. Fischer, Phys. Rev. Lett. **68**, 923 (1992).

[57] G. C. Duree, J. L. Shultz, G. J. Salamo, M. Segev, A. Yariv, B. Crosignani, P. Di Porto, E. J. Sharp, and R. R. Neurgaonkar, Phys. Rev. Lett. **71**, 533 (1993).

[58] M. Segev, G. C. Valley, B. Crosignani, P. Diporto, and A. Yariv, Phys. Rev. Lett. **73**, 3211 (1994).

[59] D. N. Christodoulides, and M. I. Carvalho, J. Opt. Soc. Am. B **12**, 1628 (1995).

[60] M. D. Iturbe-Castillo, P. A. Marquez-Aguilar, J. J. Sanchez-Mondragon, S. Stepanov, and V. Vysloukh, Appl. Phys. Lett. **64**, 408 (1994).

[61] M. Shih, M. Segev, G. C. Valley, G. Salamo, B. Crosignani, and P. Diporto, Electron. Lett. **31**, 826 (1995).

[62] M. Shih, M. Segev, G. C. Valley, G. Salamo, B. Crosignani, and P. Diporto, Opt. Lett. **21**, 324 (1996).

[63] G. C. Valley, M. Segev, B. Crosignani, A. Yariv, M.M. Fejer, and M. Bashaw, Phys. Rev. A **50**, R4457 (1994).

[64] M. Segev, G. C. Valley, M. Bashaw, M. Taya, and M. M. Fejer, J. Opt. Soc. Am. B **14**, 1772 (1997).

[65] M. Taya, B. Bashaw, M.M. Fejer, M. Segev, and G. C. Valley, Phys. Rev. A **52**, 3095 (1995).

[66] M. Taya, B. Bashaw, M.M. Fejer, M. Segev, and G. C. Valley, Opt. Lett. **21**, 943 (1996).

[67] M. Chauvet, S. A. Hawkins, G. Salamo, M. Segev, D. F. Bliss, and G. Bryant, Opt. Lett. **21**, 1333 (1996).

[68] M. Chauvet, S. A. Hawkins, G. Salamo, M. Segev, D. F. Bliss, and G. Bryant, Appl. Phys. Lett. **70**, 2499 (1997).

[69] M. Segev, and A. Agranat, Opt. Lett. **22**, 1299 (1997).

[70] E. Delre, B. Crosignani, M. Tamburrini, M. Segev, M. Mitechell, E. Refaeli, and A. J. Agranat, Opt. Lett. **23**, 421 (1988).

[71] M. Morin, G. Duree, G. Salamo, and M. Segev, Opt. Lett. **20**, 2066 (1995).

[72] M. Shih, M. Segev, and G. Salamo, Opt. Lett. **21**, 931 (1996).

[73] Y. N. Karamzin, and A. P. Sukhorukov, Sov. Phys. JETP. **41**, 414 (1976).

[74] W.E. Torruellas, Z. Wang, D.J. Hagan, E.W. VanStryland, G.I. Stegeman, L. Torner, and C.R. Menyuk, Phys. Rev. Lett. **74**, 5036 (1995).

[75] C. Etrich, U. Peschel, and F. Lederer, Phys. Rev. Lett. **79**, 2454 (1997).

[76] G. Leo, G. Assanto, and W. E. Torruella, Opt. Commun. **134**, 223 (1997).

[77] G. Leo, G. Assanto, and W. E. Torruella, J. Opt. Soc. Am. B **14**, 3134 (1997).

[78] R. A. Fuerst, B. L. Lawrence, W. E. Torruellas, and G. I. Stegeman, Opt. Lett. **22**, 19 (1997).

[79] R. A. Fuerst, D. M. Baboiu, B. L. Lawrence, W. E. Torruellas, G. I. Stegeman, S. Trillo, and S. Wabnitz, Phys. Rev. Lett. **78**, 2756 (1997).

[80] D. M. Baboiu, and G. I. Stegeman, Opt. Lett. **23**, 31 (1998).

[81] A. De Rossi, S. Trillo, A. V. Buryak, and Y. S. Kivshar, Opt. Lett. **22**, 868 (1997).

[82] A. D. Boardman, P. Bontemps, and K. Xie, J. Opt. Soc. Am. B **14**, 3119 (1997).

[83] A. S. Davydov, and N. I. Kislukha, Phys. Status. Solidi **59**, 465 (1973).

[84] W. P. Wu, J. R. Schieffer, and A. J. Heeger, Phys. Rev. Lett. **42**, 1968 (1979).

[85] A. Trombettoni, and A. Smerzi, Phys. Rev. Lett. **86**, 2353 (2001).

[86] D.N. Christodoulides and R.I. Joseph, Opt. Lett. **13**, 794 (1988).

[87] N. Efremidis, S. Sears, D.N. Christodoulides, J. Fleischer, and M. Segev, Phys. Rev. E **66**, 046602 (2002).

[88] J. Fleischer, T. Carmon, M. Segev, N. Efremidis, and D.N. Christodoulides, Phys. Rev. Lett. **90**, 023902 (2003).

[89] J. Fleischer, M. Segev, N. Efremidis, and D.N. Christodoulides, Nature (London) **422**, 147 (2003).

[90] D. Neshev, A. A. Sukhorukov, B. Hanna, W. Krolikowski, and Y. S. Kivshar, Phys. Rev. Lett. **93**, 083905 (2004).

[91] J. Yang and Z. Musslimani, Opt. Lett. **28**, 2094 (2003).

[92] Z. Musslimani and J. Yang, J. Opt. Soc. Am. B **21**, 973 (2004).

[93] D. N. Neshev, T. J. Alexander, E. A. Ostrovskaya, and Yu. S. Kivshar, Phys. Rev. Lett. **92**, 123903 (2004).

[94] J. Fleischer, G. Bartal, O. Cohen, O. Manela, M. Segev, J. Hudock, and D. N. Christodoulides, Phys. Rev. Lett. **92**, 123904 (2004).

[95] Y. V. Kartashov, V. A. Vysloukh, and L. Torner, Phys. Rev. Lett. **93**, 093904 (2004).

[96] X. Wang, Z. Chen, and P. G. Kevrekidis, Phys. Rev. Lett. **96**, 083904 (2006).

[97] K. G. Makris, S. Suntsov, D. N. Christodoulides, and G. I. Stegeman, Opt. Lett. **30**, 2466 (2005).

[98] S. Suntsov, K. G. Makris, D. N. Christodoulides, G. I. Stegeman, A. Hache, R. Morandotti, H. Yang, G. Salamo, and M. Sorel, Phys. Rev. Lett. **96**, 063901 (2006).

[99] Y. V. Kartashov, V. A. Vysloukh, and L. Torner, Phys. Rev. Lett. **96**, 073901 (2006).

[100] C. R. Rosberg, D. N. Neshev, W. Krolikowski, A. Mitchell, R. A. Vicencio, M. I. Molina, and Y. S. Kivshar, Phys. Rev. Lett. **97**, 083901 (2006).

[101] X. Wang, A. Bezryadima, Z. Chen, K. G. Makris, D. N. Christodoulides, and G. I. Stegeman, Phys. Rev. Lett. **98**, 123903 (2007).

[102] A. Szameit, Y. V. Kartashov, F. Dreisow, T. Pertsch, S. Nolte, A. Tunnermann, and L. Torner, Phys. Rev. Lett. **98**, 173903 (2007).

[103] Y. S. Kivshar, and B. Luther-Davies, Phys. Rep. **298**, 81 (1998).

[104] M. Mitchell, M. Segev, and D. N. Christodoulides, Phys. Rev. Lett. **80**, 4657 (1998).

[105] E. A. Ostrovskaya, Y. S. Kivshar, D. V. Skyyabin, and W. J. Firth, Phys. Rev. Lett. **83**, 296 (1999).

[106] A. D. Boardman, K. Xie, and A. Sangarpaul, Phys. Rev. A **52**, 4099 (1995).

[107] D. Mihalache, F. Lederer, D. Mazilu, and L.-C. Crasovan, Opt. Eng. **35**, 1616 (1996).

[108] N. I. Nikolov, D. Neshev, O. Bang, and W. Krolikowski, Phys. Rev. E **68**, 036614 (2003).

[109] Z.Y. Xu, Y. V. Kartashov, and L. Torner, Opt. Lett. **30**, 3171 (2005).

[110] Z.Y. Xu, Y. V. Kartashov, and L. Torner, Physical Review E, **73**, 055601(R) (2006).

[111] A. S. Desyatnikov, Yu. S. Kivshar, and L. Torner, Prog Optics, **47**, 291 (2005).

[112] G. A. Swartzlander, and C. T. Law, Phys. Rev. Lett. **69**, 2503 (1992).

[113] Z. Chen, M. Shih, M. Segev, D. W. Wilson, R. E. Muller, and P. D. Maker, Opt. Lett. **22**, 1751 (1997).

[114] Y. S. Kivshar, J. Christou, V. Tikhonenko, B. Luther-Davies, and L. Pismen, Opt. Commun. **152**, 198 (1998).

[115] T. Carmon, R. Uzdin, C. Pigier, Z. H. Musslimani, M. Segev, and A. Nepomnyashchy, Phys. Rev. Lett. **87**, 143901 (2001).

[116] Y. Silberberg, Opt. Lett. **15**, 1282 (1990).

[117] C. Etrich, F. Lederer, B.A. Malomed, T. Peschel, and U. Peschel, Progr. Opt. **41**, 483 (2000).

[118] L. Torner and A. Barthelemy, IEEE J. Quantum. Electron. **39**, 22 (2003).

[119] D.N. Christodoulides, F. Lederer, and Y. Silberberg, Nature **424**, 817 (2003).

[120] F. Lederer, and Y. Silberberg, Optics & Photonics News **13**, 49 (2002).

[121] O. Bang, P.D. Miller, Opt. Lett. **21**, 1105 (1996).

[122] A.A. Sukhorukov, Y.S. Kivshar, O. Bang, and C.M. Soukoulis, Phys. Rev. E **63**, 016615 (2000).

[123] O. Bang, P.L. Christiansen, and C.B. Clausen, Phys. Rev. E **56**, 7257 (1997).

[124] P.D. Miller and O. Bang, Phys. Rev. E **57**, 6038 (1998).

[125] T. Peschel, U. Peschel, and F. Lederer, Phys. Rev. E **57**, 1127 (1998).

[126] A. Kobyakov, S. Darmanyan, T. Pertsch, and F. Lederer, J. Opt. Soc. Am. B **16**, 1737 (1999).

[127] B.A. Malomed, P.G. Kevrekidis, D.J. Frantzeskakis, H.E. Nistazakis, and A.N. Yannacopoulos, Phys. Rev. E **65**, 056606 (2002).

[128] R. Iwanow, R. Schiek, G.I. Stegeman, T. Pertsch, Y. Min, and W. Sohler, Phys. Rev. Lett. **93**, 113902 (2004).

[129] R. Scharf and A.R. Bishop, Phys. Rev. E **47**, 1375 (1992).

[130] O. Cohen, T. Schwartz, J.W. Fleischer, M. Segev, and D.N. Christodoulides, Phys. Rev. Lett. **91**, 113901 (2003).

[131] D. Neshev, E. Ostrovskaya, Y. Kivshar, and W. Krolikowski, Opt. Lett. **28**, 710 (2003).

[132] Y. V. Kartashov, V. A. Vysloukh, and L. Torner, Opt. Express. **12**, 2831 (2004).

[133] B.A. Malomed, D. Mihalache, F. Wise, and L. Torner, J. Opt. B. **7**, R53 (2005).

[134] A.A. Kanashov and A.M. Rubenchik, Physica D **4**, 122 (1981); B.A. Malomed, P. Drummond, H. He, A. Berntson, D. Anderson, and M. Lisak, Phys. Rev. E **56**, 4725 (1997); D.V. Skryabin and W.J. Firth, Opt. Commun. **148**, 79 (1998); D. Mihalache, D. Mazilu, B.A. Malomed, and L. Torner, Opt. Commun. **152**, 365 (1998); D. Mihalache, D. Mazilu, J. Dörring, and L. Torner, Opt. Commun. **159**, 129 (1999); D. Mihalache, D. Mazilu, L.-C. Crasovan, L. Torner, B.A. Malomed, and F. Lederer, Phys. Rev. E **62**, 7340 (2000); L. Torner, S. Carrasco, J.P. Torres, L.-C. Crasovan, and D. Mihalache, Opt. Commun. **199**, 277 (2001).

[135] X. Liu, L.J. Qian, and F.W. Wise, Phys. Rev. Lett. **82**, 4631 (1999).

[136] A.B. Aceves, C. De Angelis, A.M. Rubenchik, and S.K. Turitsyn, Opt. Lett. **19**, 329 (1994).

[137] A.B. Aceves, C. De Angelis, G.G. Luther, and A.M. Rubenchik, Opt. Lett. **19**, 1186 (1994).

[138] A.B. Aceves, G.G. Luther, C. De Angelis, A.M. Rubenchik, and S.K. Turitsyn, Phys. Rev. Lett. **75**, 73 (1995).

[139] E.W. Laedke, K.H. Spatschek, and S.K. Turitsyn, Phys. Rev. Lett. **73**, 1055 (1994).

[140] E.W. Laedke, K.H. Spatschek, S.K. Turitsyn, and V.K. Mezentsev, Phys. Rev. E. **52**, 5549 (1995).

[141] L. Berge, V.K. Mezentsev, J.J. Rasmussen, J. Wyller, Phys. Rev. A **52**, R28 (1995).

[142] F. Lederer, S. Darmanyan, and A. Kobyakov, *Discrete Solitons*, in *Spatial Solitons*, eds.: S. Trillo and W. Torruellas, Springer Series on Optical Sciences (Berlin, New York, 2001).

[143] L. Torner, IEEE Photon. Technol. Lett. **11**, 1268 (1999).

[144] I.N. Towers, B.A. Malomed, and F.W. Wise, Phys. Rev. Lett. **90**, 123902 (2003).

[145] L. Torner, D. Mihalache, D. Mazilu, and N.N. Akhmediev, Opt. Lett. **20**, 2183 (1995); L. Torner, D. Mihalache, D. Mazilu, E.M. Wright, W.E. Torruellas and G.I. Stegeman, Opt. Commun. **121**, 149 (1995).

[146] Yu.S. Kivshar, and D.K. Campbell, Phys. Rev. E **48**, 3077 (1993).

[147] D. Cai, A.R. Bishop, and N. Gronbech-Jensen, Phys. Rev. Lett. **72**, 591 (1994).

[148] D.E. Pelinovsky, A.V. Buryak, Y.S. Kivshar, Phys. Rev. Lett. **75**, 591 (1995).

[149] J.M. Soto-Crespo, D.R. Heatley, E.M. Wright, and N.N. Akhmediev, Phys. Rev. A **44**, 636 (1991); D.V. Skryabin

and W.J. Firth, Phys. Rev. E **58**, 3916 (1998); D. Miha-
lache, D. Mazilu, L.-C. Crasovan, I. Towers, B.A. Malomed,
A.V. Buryak, L. Torner, and F. Lederer, Phys. Rev. E **66**,
016613 (2002).

[150] M.G. Vakhitov and A.A. Kolokolov, Izv. Vyssh. Uch. Zav.
Radiofizika **16**, 1020 (1973) [Radiophys. Quantum. Electron.
16, 783 (1973)].

[151] For a review, see, e.g., M. S. Soskin and M. V. Vasnetsov, in
progress in Optics, edited by E. Wolf (Elsevier, Amsterdam,
2001), Vol. 42.

[152] V. I. Kruglov and R. A. Vlasov, Phys. Lett. A **111**, 401
(1985); L. Torner and D. V. Petrov, Electron. Lett. **33**, 608
(1997); W. J. Firth and D. V. Skryabin, Phys. Rev. Lett.
79, 2450 (1997); J. P. Torres, J. M. Soto-Crespo, L. Torner,
and D. V. Petrov, J. Opt. Soc. Am. B **15**, 625 (1998).

[153] V. Tikhonenko, J. Christou, and B. Luther-Daves, J. Opt.
Soc. Am. B **12**, 2046 (1995); D. V. Petrov, L. Torner, J.
Martorell, R. Vilaseca, J. P. Torres, and C. Cojocaru, Opt.
Lett. **23**, 1444 (1998); M. S. Bigelow, P. Zerom, and R. W.
Boyd, Phys. Rev. Lett. **92**, 083902 (2004).

[154] M. Quiroga-Teixeiro and H. Michinel, J. Opt. Soc. Am. B
14, 2004 (1997); I. Towers, A. V. Buryak, R. A. Sammut, B.
A. Malomed, L.-C. Crasovan, and D. Mihalache, Phys. Lett.
A **288**, 292 (2001); B. A. Malomed, L.-C. Crasovan, and
D. Mihalache, Physica D **161**, 187 (2002); D. Mihalache,
D. Mazilu, L.-C. Crasovan, I. Towers, A. V. Buryak, B. A.
Malomed, L. Torner, J. P. Torres, and F. Lederer, Phys. Rev.
Lett. **88**, 073902 (2002); D. Mihalache, D. Mazilu, I. Towers,
B. A. Malomed, and F. Lederer, Phys. Rev. E **67**, 056608
(2003); D. Mihalache, D. Mazilu, B. A. Malomed, and F.
Lederer, Phys. Rev. E **69**, 066614 (2004); D. Mihalache, D.
Mazilu, B. A. Malomed, and F. Lederer, J. Opt. B: Quantum
Semiclass. Opt. **6**, S341 (2004).

[155] B. A Malomed and P. G. Kevrekidis, Phys. Rev. E **64**, 026601 (2001).

[156] Z. Y. Xu, Y. V. Kartashov, L.-C. Crasovan, D. Mihalache, and L. Torner, Phys. Rev. E **70**, (2004).

[157] Y. V. Kartashov, L. Torner, and V. A. Vysloukh, Opt. Lett. **29**, 1117 (2004); Y. V. Kartashov, V. A. Vysloukh, and L. Torner Opt. Lett. **29**, 1399 (2004).

[158] M. Soljačić, S. Sears, and M. Segev, Phys. Rev. Lett. **81**, 4851 (1998); M. Soljačić and M. Segev, Phys. Rev. E **62**, 2810 (2000); M. Soljačić and M. Segev, Phys. Rev. Lett. **86**, 420 (2001).

[159] A. S. Desyatnikov and Yu. S. Kivshar, Phys. Rev. Lett. **87**, 033901 (2001); **88**, 053901 (2002).

[160] Y. V. Kartashov, G. Molina-Terriza, and L. Torner, J. Opt. Soc. Am. **B19**, 2682 (2002); Y. V. Kartashov, L.-C. Crasovan, D. Mihalache, and L. Torner, Phys. Rev. Lett. **89**, 273902 (2002); L.-C. Crasovan, Y. V. Kartashov, D. Mihalache, L. Torner, Y. S. Kivshar, and V. M. Perez-Garcia, Phys. Rev. E **67**, 046610 (2003); D. Mihalache, D. Mazilu, L.-C. Crasovan, B. A. Malomed, F. Lederer, and L. Torner, Phys. Rev. E **68**, 046612 (2003); D. Mihalache, D. Mazilu, L. C. Crasovan, B. A. Malomed, F. Lederer, and L. Torner, J. Opt. B **6**, S333 (2004).

[161] L. Torner, J. P. Torres, D. V. Petrov, and J. M. Soto-Crespo, Opt. Quantum Electron. **30**, 809 (1998); S. Minardi, G. Molina-Terriza, P. Di Trapani, J. P. Torres, and L. Torner, Opt. Lett. **26**, 1004 (2001)

[162] D. N. Christodoulides and E. D. Eugenieva, Phys. Rev. Lett. **87**, 233901 (2001).

[163] E. D. Eugenieva, N. K. Efremidis, and D. N. Christodoulides, Opt. Lett. **26**, 1978 (2001).

[164] H. Martin, E. D. Eugenieva, Z. Chen, and D. N. Christodoulides, Phys. Rev. Lett. **92**, 123902 (2004).

[165] Z. Chen, H. Martin, E. D. Eugenieva, J. Xu, and A. Bezryadina, Phys. Rev. Lett. **92**, 143902 (2004).

[166] Y. V. Kartashov, A. S. Zelenina, L. Torner, and V. A. Vysloukh, Opt. Lett. **29**, 766 (2004).

[167] Y. V. Kartashov, L. Torner, and V. A. Vysloukh, Opt. Lett. **29**, 1102 (2004).

[168] Y. V. Kartashov, A. A. Egorov. A. Vysloukh, and L. Torner, J. Opt. B: Quantum Semi. Opt. **6**, 444 (2004).

[169] G. E. Torres-Cisneros, J. J. Sánchez-Mondragón, and V. A. Vysloukh, Opt. Lett. **18**, 1299 (1993).

[170] Z. Y. Xu, Y. V. Kartashov, L. Torner, and V. A. Vysloukh, Opt. Lett. **30**, 1180 (2005).

[171] J. Durnin, J. Miceli, and J. H. Eberly, Phys. Rev. Lett. **58**, 1499 (1987).

[172] V. Kettunen, and J. Turunen, Opt. Lett. **23**, 1247 (1998).

[173] S. H. Tao, X-C Yuan. and B. S. Ahluwalia, J. Opt. A: Pure Appl. Opt. **7**, 40 (2005).

[174] A. W. Snyder, and D. J. Mitchell, Science **276**, 1538 (1997).

[175] W. Krolikowski, and O. Bang, Phys. Rev. E **63**, 016610 (2001).

[176] W. Krolikowski, O. Bang, J. J. Rasmussen, and J. Wyller, Phys. Rev. E **64**, 016612 (2001).

[177] J. Wyller, W. Krolikowski, O. Bang, and J. J. Rasmussen, Phys. Rev. E **66**, 066615 (2002).

[178] W. Krolikowski, O. Bang, N. I. Nikolov, J. Wyller, J. J. Rasmussen, and D. Edmundson, J. Opt. B **6**, S288 (2004).

[179] M. Peccianti, C. Conti, and G. Assanto, Phys. Rev. E **68**, 025602(R) (2003).

[180] S. K. Turitsyn, Theor. Math. Phys. (Engl. Transl.) **64**, 797 (1985).

[181] O. Bang, W. Krolikowski, J. Wyller, and J. J. Rasmussen, Phys. Rev. E **66**, 046619 (2002).

[182] D. Neshev, G. McCarthy, W. Krolikowski, E. A. Ostrovskaya, Y. S. Kivshar, G. F. Calvo, and F. Agullo-Lopez, Opt. Lett. **26**, 1185 (2001).

[183] W. Krolikowski, O. Bang, and J. Wyller, Phys. Rev. E **70**, 036617 (2004).

[184] A. I. Yakimenko, Y. A. Zaliznyak, and Y. Kivshar, Phys. Rev. E **71**, 065603(R) (2005).

[185] D. Briedis, D. E. Petersen, D. Edmundson, W. Krolikowski, and O. Bang, opt. Express. **13**, 435 (2005).

[186] A. V. Mamaev, A. A. Zozulya, V. K. Mezentsev, D. Z. Anderson, and M. Saffman, Phys. Rev. A **56**, R1110 (1997).

[187] J. P. Gordon, R. C. C. Leite, R. S. Moore, S.P.S. Porto, and J. R. Whinnery, J. Appl. Phys. **36**, 3 (1965).

[188] A. G. Litvak, V. A. Mironov, G. M. Fraiman, and A. D. Yunakovskii, Sov. J. Plasma Phys. **1**, 31 (1975).

[189] L. Santos, G. V. Shlyapnikov, P. Zoller, and M. Lewenstein, Phys. Rev. Lett. **85**, 1791 (2000).

[190] V. M. Perez-Garcia, V. V. Konotop, and J. J. Garcia-Ripoll, Phys. Rev. E. **62**, 4300 (2000).

[191] D. H. J. O'Dell, S. Giovanazzi, and C. Eberlein, Phys. Rev. Lett. **92**, 250401 (2004).

[192] Y. V. Kartashov, V. Vysloukh, and L. Torner, Phys. Rev. Lett. **93**, 153903 (2004).

[193] D. E. Pelinovsky, A. A. Sukhorukov, and Y. Kivshar, Phys. Rev. E. **70**, 036618 (2004).

[194] Y. V. Kartashov, A. A. Egorov, L. Torner, and D. Christodoulides, Opt. Lett. **29**, 1918 (2004).

[195] Y. S. Kivshar, and D. K. Campbell, Phys. Rev. E. **48**, 3077 (1993).

[196] R. Morandotti, U. Peschel, J. S. Aitchison, H. S. Eisenberg, and Y. Silberberg, Phys. Rev. Lett. **83**, 2726 (1999).

[197] M. Oster, M. Johansson, and A. Eriksson, Phys. Rev. E. **67**, 056606 (2003).

[198] M. Peccianti, C. Conti, and G. Assanto, Opt. Lett. **30**, 415 (2005).

[199] G. Assanto, M. Peccianti, and C. Conti, IEEE J. Sel. Top. Quantum Electron. **10**, 862 (2004).

[200] F. Derrien, J. F. Henninot, M. Warenghem, and G. Abbate, J. Opt. A Pure Appl. Opt **2**, 332 (2000).

[201] J. F. Henninot, M. Debailleul, and M. Warenghem, Mol. Crys. Liq. Crys. **375**, 631 (2002).

[202] A. A. Sukhorukov, Y. Kivshar, H. S. Eisenberg, and Y. Silberberg, IEEE J. Quantum Electron. **39**, 31 (2003).

[203] N. Akozbek and S. John, Phys. Rev. E. **57**, 2287 (1998).

[204] S. F. Mingaleev and Y. S. Kivshar, Phys. Rev. Lett. **86**, 5474 (2001).

[205] B. J. Eggleton, R. E. Slusher, C. M. de Sterke, P. A. Krug, and J. E. Sipe, Phys. Rev. Lett. **76**, 1627 (1996).

[206] B. Eiermann, Th. Anker, M. Taglieber, P. Treutlein, K.-P. Marzlin, and M. K. Oberthaler, Phys. Rev. Lett. **92**, 230401 (2004).

[207] P. J. Y. Louis, E. A. Ostrovskaya, C. M. Savage, and Y. S. Kivshar, Phys. Rev. A. **67**, 013602 (2003).

[208] N. K. Efremidis and D. N. Christodoulides, Phys. Rev. A. **67**, 063608 (2003).

[209] D. Mandelik, R. Morandotti, J. S. Aitchison, and Y. Silberberg, Phys. Rev. Lett. **92**, 093904 (2004).

[210] D. Christodoulides and T. H. Coskun, Opt. Lett. **21**, 1220 (1996).

[211] W. Krolikowski, N. Akhmediev, B. Luther-Davies, and M. Cronin-Golomb, Phys. Rev. E. **54**, 5761 (1996).

[212] S. R. Singh, M. I. Carvalho, and D. N. Christodoulides, Opt. Commun. **130**, 288 (1996).

[213] V. Aleshkevich, Y. V. Kartashov, and V. Vysloukh, Phys. Rev. E. **63**, 016603 (2001).

[214] Z. Xu, Y. V. Kartashov, and L. Torner, Phys. Rev. Lett. **95**, 113901 (2005).

[215] M. Peccianti, K. A. Brzdakiewicz, and G. Assanto, Opt. Lett. **27**, 1460 (2002).

[216] N. I. Nikolov, D. Neshev, W. Krolikowski, O. Bang, J. J. Rasmussen, and P. L. Christiansen, Opt. Lett. **29**, 286 (2004).

[217] I. A. Kolchugina, V. A. Mironov, and A. M. Sergeev, Pis'ma Zh.Eksp. Teor. Fiz. **31**, 333 (1980) [JETP Lett. **31**, 304 (1980)].

[218] V. A. Mironov, A. M. Sergeev, and E. M. Sher, Dokl. Akad. Nauk SSSR **260**, 325 (1981) [Sov. Phys. Dokl. **26**, 861 (1981)].

[219] X. Hutsebaut, C. Cambournac, M. Haelterman, A. Adamski, and K. Neyts, Opt. Commun. **233**, 211 (2004).

[220] A. Dreischuh, D. N. Neshev, D. E. Petersen, O. Bang, and W. Krolikowski, Phys. Rev. Lett. **96**, 043901 (2006).

[221] G. Agez, P. Glorieux, C. Szwaj, and E. Louvergneaux, Opt. Commun. **245**, 243 (2005).

[222] T. Carmon, C. Anastassiou, S. Lan, D. Kip, Z. H. Musslimani, M. Segev, and D. Christodoulides, Opt. Lett. **25**, 1113 (2000).

[223] W. Krolikowski, E. A. Ostrovskaya, C. Weilnau, M. Geisser, G. McCarthy, Y. S. Kivshar, C. Denz, and B. Luther-Davies, Phys. Rev. Lett. **85**, 1423 (2000).

[224] N. Akhmediev and V. V. Afanasjev, Phys. Rev. Lett. **75**, 2320 (1995).

[225] N. N. Rosanov, S. F. Fedorov, and A. N. Shatsev, Phys. Rev. Lett. **95**, 053903 (2005).

[226] W. Krolikowski, M. Saffman, B. Luther-Davies, and C. Denz, Phys. Rev. Lett. **80**, 3240 (1998).

[227] S. Skupin, O. Bang, D. Edmundson, and W. Krolikowski, Phys. Rev. E **73**, 036603 (2006).

[228] A. I. Yakimenko, V. M. Lashkin, and O. O. Prikhodko, Phys. Rev. E **73**, 066605 (2006).

[229] S. Lopez-Aguayo, A. S. Desyatnikov, Y. S. Kivshar, S. Skupin, W. Krolikowski, and O. Bang, Opt. Lett. **31**, 1100 (2006).

[230] M. R. Matthews, B. P. Anderson, P. C. Haljan, D. S. Hall, C. E. Wieman, and E. A. Cornell, Phys. Rev. Lett. **83**, 2498 (1999).

[231] J. Williams and M. Holland, Nature (London) **401**, 568 (1999).

[232] T. Busch and J. R. Anglin, Phys. Rev. A. **60**, R2669 (1999).

[233] J. I. Garcia-Ripoll, J. I. Cirac, J. Anglin, V. M. Perez-Garcia, and P. Zoller, Phys. Rev. A. **61**, 053609 (2000).

[234] S. V. Manakov, Sov. Phys. JETP **38**, 248 (1974).

[235] D. N. Christodoulides and R. I. Joseph, Opt. Lett. **13**, 53 (1988).

[236] J. U. Kang, G. I. Stegeman, J. S. Aitchison, and N. Akhmediev, Phys. Rev. Lett. **76**, 3699 (1996).

[237] N. Akhmediev, W. Krolikowski, and A. W. Snyder, Phys. Rev. Lett. **81**, 4632 (1998).

[238] A. W. Snyder, S. J. Hewlett, and D. J. Mitchell, Phys. Rev. Lett. **72**, 1012 (1994).

[239] G. I. Stegeman and M. Segev, Science. **286**, 1518 (1999).

[240] C. Cambournac, T. Sylvestre, H. Maillotte, B. Vanderlinden, P. Kockaert, Ph. Emplit, and M. Haelterman, Phys. Rev. Lett. **89**, 083901 (2002).

[241] J. Yang, Physica D **108**, 92 (1997).

[242] D. E. Pelinovsky and J. Yang, Stud. Appl. Math. **115**, 109 (2005).

[243] S. Darmanyan, A. Kobyakov, E. Schmidt, and F. Lederer, Phys. Rev. Lett. **57**, 3520 (1998).

[244] A. A. Sukhorukov and Y. S. Kivshar, Phys. Rev. Lett. **91**, 113902 (2005).

[245] Y. V. Kartashov, A. S. Zelenina, V. A. Vysloukh, and L. Torner, Phys. Rev. E **70**, 066623 (2003).

[246] Y. V. Kartashov, F. Ye, V. A. Vysloukh, and L. Torner, Opt. Lett. **32**, 2260 (2007).

[247] A. Barak, C. Rotschild, B. Alfassi, M. Segev, and D. N. Christodoulides, **32**, 2450 (2007).

[248] R. El-Ganainy, D. N. Christodoulides, C. Rotschild, and M. Segev, Opt. Express **15**, 10207 (2007).

List of Figures